Physics Reports 950 (2022) 1–37

Contents lists available at ScienceDirect

Physics Reports

journal homepage: www.elsevier.com/locate/physrep

Kitaev materials

Simon Trebst *, Ciarán Hickey

Institute for Theoretical Physics, University of Cologne, 50937 Cologne, Germany

ARTICLE INFO

Article history:
Received 3 March 2021
Received in revised form 2 November 2021
Accepted 7 November 2021
Available online 3 January 2022
Editor: P. van Loosdrecht

Keywords:
Spin–orbit entangled Mott insulators
Kitaev model
Spin liquids

ABSTRACT

In transition-metal compounds with partially filled 4*d* and 5*d* shells spin–orbit entanglement, electronic correlations, and crystal-field effects conspire to give rise to a variety of novel forms of topological quantum matter. This includes Kitaev materials — a family of spin–orbit assisted Mott insulators, in which local, spin–orbit entangled $j = 1/2$ moments form that are subject to dominant bond-directional Ising exchange interactions. On a conceptual level, Kitaev materials attract much interest for their potential for unconventional forms of magnetism, such as spin liquid physics in two- and three-dimensional lattice geometries or the formation of non-trivial spin textures. Experimentally, a number of Kitaev materials have been synthesized, which includes the honeycomb materials Na_2IrO_3, α-Li_2IrO_3, $H_3LiIr_2O_6$, and, most prominently, α-$RuCl_3$, the triangular materials $Ba_3Ir_xTi_{3-x}O_9$, as well as the three-dimensional hyper-honeycomb and stripy-honeycomb materials β-Li_2IrO_3 and γ-Li_2IrO_3. We provide a short review of the current status of the theoretical and experimental exploration of these Kitaev materials.

Contents

* Corresponding author.
E-mail address: trebst@thp.uni-koeln.de (S. Trebst).

https://doi.org/10.1016/j.physrep.2021.11.003

1. Spin–orbit entangled Mott insulators

Transition-metal oxides with partially filled 4*d* and 5*d* shells exhibit an intricate interplay of electronic, spin, and orbital degrees of freedom arising from a largely accidental balance of electronic correlations, spin–orbit entanglement, and crystal-field effects [1]. With different materials exhibiting slight tilts towards one of the three effects, a remarkably broad variety of novel forms of quantum matter can be explored. On the theoretical side, topology is found to play a crucial role in these systems — an observation which, in the weakly correlated regime, has lead to the discovery of the topological band insulator [2,3] and subsequently its metallic cousin, the Weyl semi-metal [4,5]. Upon increasing electronic correlations, Mott insulators with unusual local moments such as spin–orbit entangled degrees of freedom can form and whose collective behavior gives rise to unconventional types of magnetism including the formation of quadrupolar correlations, topological magnons or the emergence of so-called spin liquid states. A rough guide to these novel types of quantum matter, currently widely explored in materials with substantial spin–orbit coupling, is given by the general phase diagram of Fig. 1, adapted from an early review [6] of this rapidly evolving field at the current forefront of condensed matter physics.

Our focus here will be on the particularly intriguing scenario of the formation of novel types of Mott insulators in which the local moments are spin–orbit entangled $j = 1/2$ Kramers doublets [7–9]. The latter are typically formed for ions in a d^5 electronic configuration – a vast family of such d^5 materials exist that not only includes many iridates with a Ir^{4+} ($5d^5$) valence, but also some Ru-based materials with a Ru^{3+} ($4d^5$) valence along with the (extremely toxic) osmates and (so far largely unexplored) rhenates. The level scheme of such d^5 ionic systems is illustrated in Fig. 2. With the crystal field (e.g. of an octahedral oxygen cage) splitting off the two e_g levels, this puts the five electrons with a total $s = 1/2$ magnetic moment into the t_{2g} orbitals with an effective $\ell = 1$ orbital moment. Strong spin–orbit coupling then results in a system with a fully filled $j = 3/2$ band and a half-filled $j = 1/2$ band. The reduced bandwidth of the latter then allows for the opening of a Mott gap even for the relatively moderate electronic correlations of the 4*d* and 5*d* compounds. This latter point should again be emphasized. The formation of a Mott insulator in these compounds is per se somewhat counterintuitive as the larger atomic radii of their 4*d* and 5*d* constituents give rise to considerable atomic overlap, which results in a large electronic bandwidth and thus an effective suppression of the electronic correlations. As such, conventional wisdom has

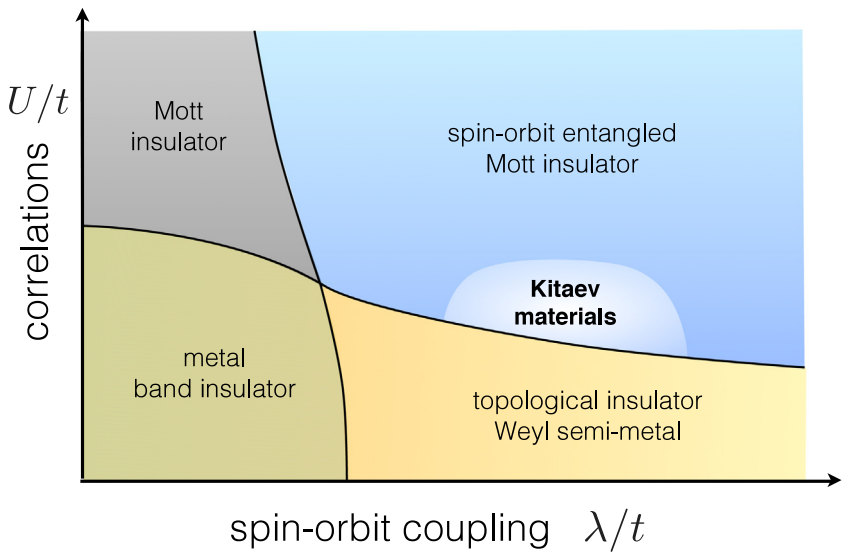

Fig. 1. General form of the phase diagram in the presence of electronic correlations and spin–orbit coupling. *Source:* Figure adapted from the review [6].

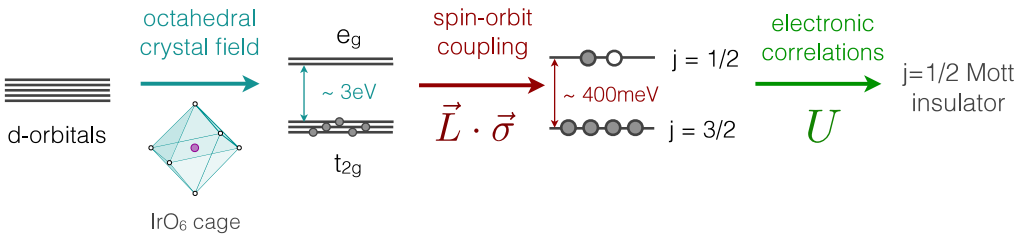

Fig. 2. Formation of spin–orbit entangled $j = 1/2$ moments for ions in a d^5 electronic configuration such as for the iridium valence Ir^{4+} or the ruthenium valence Ru^{3+}.

long considered these "heavy" transition metal compounds to generically form metallic states. It is only because of an enormously enhanced spin–orbit coupling that the effective electronic bandwidth of these materials can be reduced (via the formation of two separate $j = 3/2$ and $j = 1/2$ bands) to a level that the largely suppressed electronic correlations can still drive the system into a Mott insulating state. These $j = 1/2$ Mott materials are therefore sometimes referred to as "spin–orbit assisted Mott insulators" and are located in the proximity of the metal–insulator transition for large spin–orbit coupling in the general phase diagram of Fig. 1.

The formation of such a $j = 1/2$ Mott insulator was first observed experimentally in 2008/2009 [10,11] for the perovskite iridate Sr_2IrO_4 — a $5d$ transition-metal oxide which is an isostructural analogue of La_2CuO_4, the parent compound of the cuprate superconductors. Remarkably, its low-temperature physics indeed shares a striking resemblance to the phenomenology of the cuprate superconductors including the formation of long-range antiferromagnetic order of the $j = 1/2$ pseudospins for the undoped material and the emergence of a pseudogap phase and associated Fermi arcs for electron-doped systems [12–14]. There is an intense ongoing search [15,16] for superconductivity in doped Sr_2IrO_4 and other perovskite iridates.

In parallel, much attention has been drawn towards $j = 1/2$ Mott insulators that exhibit dominant bond-directional Ising-type exchange interactions and are thought to exhibit unconventional forms of magnetism, such as the emergence of spin liquids [17,18] or the formation of non-trivial spin textures. We refer to these systems as *Kitaev materials*. Of particular interest here are the sister compounds Na_2IrO_3 and α-Li_2IrO_3 and, most prominently, α-$RuCl_3$ that form Mott insulators, in which local $j = 1/2$ moments are aligned in (almost decoupled) hexagonal layers. As such they are perfect candidate materials for a solid-state realization of the Kitaev honeycomb model [19] as envisioned by Jackeli and Khaliullin in 2009 [9]. More recently, a "second generation" of iridate compounds such as $H_3LiIr_2O_6$, $Cu_3LiIr_2O_6$, or $Cu_3NaIr_2O_6$ have come into view, which expand the family of honeycomb-based Kitaev materials. Over the last decade, materials synthesis of novel $j = 1/2$ Mott insulators has been thriving at a remarkable pace and has further broadened our view on Kitaev materials beyond the original honeycomb structure. As will be outlined in the remainder of this review, $j = 1/2$ Mott insulators with strong bond-directional exchange interactions have also been synthesized with triangular lattice geometries, e.g. in the family of hexagonal perovskites $Ba_3Ir_xTi_{3-x}O_9$, with three-dimensional, tricoordinated lattice generalizations of the honeycomb lattice (dubbed the hyper-honeycomb and stripy-honeycomb) in polymorphs of α-Li_2IrO_3, i.e. the iridates β-Li_2IrO_3 and γ-Li_2IrO_3, respectively. In addition, theoretical progress has been made in comprehensively classifying the gapless spin liquid ground states of the three-dimensional, tricoordinated Kitaev models. It will be the purpose of this review to provide what is hopefully a concise review of the current status of these Kitaev materials and their conceptual understanding.

Though they do not feature in this review, we should also briefly point out that there is a plethora of fascinating phenomena also to be found in spin–orbit entangled Mott insulators with $j \neq 1/2$. For example, there have been theoretical proposals for realizing non-magnetic states in materials with d^1 ions and $j = 3/2$ moments [20], e.g. spin–orbital liquids [21] and dimer singlet states [22], as well as a platform for realizing SU(4)-symmetric spin–orbital models [23,24]. On the materials side, there have also been potential candidate materials identified, e.g. Ba_2BMoO_6 (B = Y, Lu) [22] and α-$ZrCl_3$ [23]. There have even been theoretical studies suggesting that materials with d^4 ions and Van Vleck-type $j = 0$ moments, which might naively seem like a rather trivial situation, could host excitonic magnetism and emergent one-dimensional excitations [25]. There is still much to be explored within this wider world of spin–orbit entangled materials.

1.1. Bond-directional interactions

At the heart of all Kitaev materials are bond-directional Ising-type interactions, i.e. interactions where the exchange easy axis depends on the spatial orientation of an exchange bond, and which dominate in coupling strength over all other exchange types. The microscopic origin of such bond-directional interactions in d^5 transition metal compounds has been worked out in a pioneering 2005 paper by Khaliullin [7] and later refined to the context of Kitaev-type interactions in the joint work of Jackeli and Khaliullin [9]. These papers have undoubtedly shaped the formation of what is now a burgeoning field of experimental and theoretical exploration of Kitaev materials.

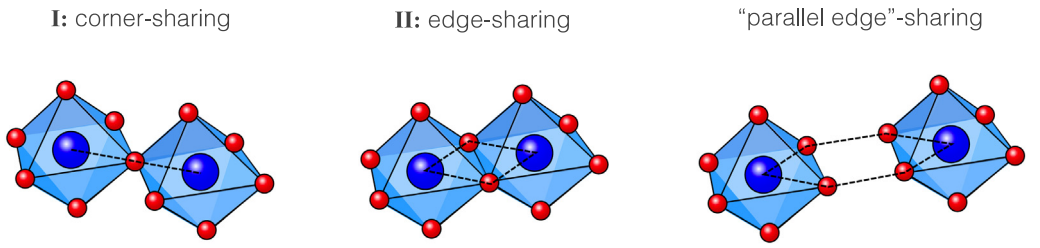

Fig. 3. Illustration of possible geometric orientations of neighboring IrO_6 octahedra that give rise to different types of (dominant) exchange interactions between the magnetic moments located on the iridium ion at the center of these octahedra. For the corner-sharing geometry (I) one finds a dominant symmetric Heisenberg exchange, while for the edge-sharing geometries (II) one finds a dominant bond-directional, Kitaev-type exchange.

What Khaliullin and Jackeli have realized is that the geometric orientation of neighboring IrO_6 octahedra plays a crucial role in determining the microscopic exchange of the magnetic moments located on the iridium ion at the center of these octahedra. They distinguish two elementary scenarios, which are illustrated (along with an extension) in Fig. 3. First, for perovskite iridates such as Sr_2IrO_4 two neighboring IrO_6 octahedra share a *corner*. For the coupling between the two neighboring iridium ions this means that there is a single Ir–O–Ir exchange path, which is also referred to as 180° bond. The dominant coupling along this type of bond is – despite the presence of a strong spin–orbit coupling – a symmetric Heisenberg exchange between the spin–orbit entangled $j = 1/2$ moments. The second scenario plays out in materials in which two neighboring IrO_6 octahedra share an *edge*. Here there are two Ir–O–Ir exchange paths, which exhibit a 90° bonding geometry. The fact that there are *two* exchange paths turns out to be crucial, as the two alternative paths lead to a destructive interference of the symmetric Heisenberg exchange when restricting the coupling to arise exclusively from the $j = 1/2$ bands, or alternatively to a significant suppression to some residual Heisenberg exchange when considering the full multi-orbital model also including the (virtual) $j = 3/2$ bands. In lieu of the highly suppressed isotropic exchange, it is a bond-directional coupling, stemming from Hund's coupling and mediated through the multiplet structure of the excited levels, that takes center stage and becomes the dominant coupling. The bond-directionality of the coupling arises since the pair of d-orbitals linked for two neighboring octahedra depends on the type of edge shared at their intersection. This in turn gives rise to a spatially oriented Ising-type coupling between the spin–orbit entangled $j = 1/2$ moments where the magnetic easy-axis is perpendicular to the plane spanned by the two exchange paths [7,9]. The strength of this bond-directional coupling is given by

$$-\frac{8t^2 J_H}{3U^2} S_1^\gamma S_2^\gamma \,, \tag{1}$$

where t is the effective interorbital hopping mediated by the oxygen ions, J_H is the Hund's coupling and U the electronic correlation strength. The two spin–orbit entangled $j = 1/2$ moments, represented by the usual vectors of SU(2) spin-1/2 Pauli matrices $\mathbf{S}_1$ and $\mathbf{S}_2$, are ferromagnetically coupled only via a single spin component $\gamma = x, y, z$. As such the edge-sharing 90° bond geometry naturally gives rise to a quantum *compass model* [26], originally introduced by Kugel and Khomskii for the orbital degrees of freedom in Jahn-Teller systems [27] and realized here for the first time in a truly *magnetic* variant. It is precisely this edge-sharing exchange coupling, which has been envisioned [9] to lead to a realization of Kitaev couplings in the honeycomb iridates Na_2IrO_3, α-Li_2IrO_3, $H_3LiIr_2O_6$, and α-$RuCl_3$ and which has later also been found to be realized in the 3D hyper-honeycomb and strip-honeycomb materials β-$Li_2IrO_3$and γ-Li_2IrO_3. This second scenario of edge-sharing exchange can be further expanded by considering octahedral geometries where neighboring IrO_6 octahedra do not share an edge, but have two parallel edges as illustrated in the right-most panel of Fig. 3. Following a similar line of arguments, one also arrives at a destructive interference for the isotropic Heisenberg exchange in this setting and the emergence of a bond-directional exchange. This latter geometry is realized in triangular Kitaev materials such as $Ba_3IrTi_2O_9$.

Beyond the traditional Jackeli–Khaliullin mechanism discussed above, there have also been more recent proposals to realize similar Kitaev couplings amongst $j = 1/2$ spin–orbit entangled moments in materials with a high-spin d^7 electron configuration [28,29], such as in Co^{2+} and Ni^{3+}, or with an f^1 configuration [30,31], such as in Pr^{4+}. While the d^7-based proposal also leads to a ferromagnetic Kitaev coupling, the latter f^1 proposal is expected to generate an *antiferromagnetic* coupling. Concerning the d^7 proposal, there were also promising candidate materials identified, including the Co-based $Na_2Co_2TeO_6$ and $Na_3Co_2SbO_6$ [28], both discussed later in Section 2.5. See Ref. [32] for a recent review of such proposals. Beyond $j = 1/2$, there has also been a proposal to generate Kitaev couplings amongst effective spin-one moments, with the necessary ingredients including strong Hund's coupling between cation e_g electrons and strong spin–orbit coupling for the anion electrons [33]. Proposed candidate materials here include $A_3Ni_2XO_6$ with X = Bi, Sb, and A = Li, Na. Unlike the Jackeli–Khaliullin mechanism or d^7 proposal, this is predicted to generate an *antiferromagnetic* coupling. Finally, recent ab-initio calculations have also suggested the possibility of spin-3/2 Kitaev materials [34].

In passing we note that recently also the microscopics of *face-sharing* octahedra [35] has been discussed, which is relevant, for instance, to the quantum magnetism of $Ba_5AlIr_2O_{11}$ [36].

Going beyond these geometry-guided considerations and performing a symmetry analysis of the most generally allowed microscopic interactions [37,38], one finds that the generic Hamiltonian describing the interactions between $j = 1/2$ spin–orbit entangled moments of spin–orbit assisted Mott insulators takes the general form

$$H = \sum_{\gamma-\text{bonds}} J\ \mathbf{S}_i\mathbf{S}_j + K\ S_i^\gamma S_j^\gamma + \Gamma\left(S_i^\alpha S_j^\beta + S_i^\beta S_j^\alpha\right), \tag{2}$$

where the sum runs over nearest-neighbor spins at sites coupled by a bond $\langle i,j\rangle$ along the $\gamma = (x,y,z)$ direction. The strength of the isotropic Heisenberg coupling is given by J, and the bond-directional couplings include (i) a Kitaev term of strength K that couples the component γ of the spins along a γ-bond and (ii) a symmetric off-diagonal exchange Γ that couples the two orthogonal spin components $\alpha, \beta \perp \gamma$ for a bond along the $\gamma = x, y, z$ direction. The relative strength and sign of the various couplings can in principle vary from material to material, but a common thread in all Kitaev materials is that the Kitaev coupling is the dominant exchange coupling, i.e. $K > J, \Gamma$. In the case of non-ideal octahedra, as occurs in materials with trigonal distortion, there is also a fourth symmetry allowed interaction, Γ', which couples the γ-component of the spin with the two orthogonal $\alpha, \beta \perp \gamma$ components for a γ-bond [39]. The microscopic model (2), which is also referred to as the $JK\Gamma$ model, is often simplified to the Heisenberg–Kitaev model ($\Gamma = 0$), which has first been conceptualized and studied in the context of the honeycomb iridates by Chaloupka, Jackeli, and Khaliullin [40]. We will return to this model after a discussion of the pure Kitaev model ($J, \Gamma = 0$) in the next section.

It is useful to note that the microscopic $JK\Gamma$ model (2) can also be recast via an alternate choice of spin quantization axes [39,41,42]. By performing a spin rotation such that the spin axes align with the crystallographic axes, i.e. the x, y, z axes lie parallel to the a, b, c crystallographic axes, the Hamiltonian for a γ-bond can be rewritten as

$$\begin{aligned} H_{\langle i,j\rangle\in\gamma} = {} & J_{xy}\left(S_i^x S_j^x + S_i^y S_j^y\right) + J_z S_i^z S_j^z \\ & + J_{\pm\pm}\left[c_\gamma\left(S_i^x S_j^x - S_i^y S_j^y\right) - s_\gamma\left(S_i^x S_j^y + S_i^y S_j^x\right)\right] \\ & - \sqrt{2}J_{z\pm}\left[c_\gamma\left(S_i^x S_j^z + S_i^z S_j^x\right) + s_\gamma\left(S_i^y S_j^z + S_i^z S_j^y\right)\right], \end{aligned} \tag{3}$$

where $c_\gamma = \cos\phi_\gamma$, $s_\gamma = \sin\phi_\gamma$ and $\phi_\gamma = 0, 2\pi/3, 4\pi/3$ for the z, x, y bonds. The new parameters are related to the original parameters, J, K and Γ, by the following relations

$$\begin{aligned} J_{xy} &= J + K/3 - \Gamma/3 \ , \ J_{\pm\pm} = K/3 + 2\Gamma/3 \\ J_z &= J + K/3 + 2\Gamma/3 \ , \ J_{z\pm} = K/3 - \Gamma/3 \end{aligned} \tag{4}$$

This alternate form is more familiar in the context of spin–orbit coupled rare-earth magnets such as $YbMgGaO_4$ [43,44] and the pyrochlore spin ice compounds [45–48]. The underlying physics is of course independent of the choice of convention but, depending on the material and the values of its various exchange couplings, it may be possible to gain additional insight or intuition by casting the Hamiltonian in this different light [49].

1.2. Kitaev model

The pure Kitaev model, which couples SU(2) spin-1/2 degrees of freedom with bond-directional interactions — Ising-like couplings with a magnetic easy axis sensitive to the spatial orientation γ of the bond (see Figs. 4 and 5 for an illustration)

$$H_{\text{Kitaev}} = -\sum_{\gamma-\text{bonds}} K_\gamma\ S_i^\gamma S_j^\gamma \ , \tag{5}$$

is of central interest in condensed matter physics (and beyond). The effect of bond-directional interactions is a strong exchange frustration arising from the simple fact that these interactions cannot be simultaneously minimized, as illustrated in Fig. 4. Like geometric frustration, its more widely known counterpart that arises when the lattice geometry gives rise to constraints that cannot be simultaneously satisfied, the effect of exchange frustration is to inhibit magnetic ordering and give rise to a residual ground-state entropy. This is true already on the *classical* level. For instance, the classical Kitaev honeycomb model does not exhibit a finite-temperature phase transition [50,51], but undergoes a thermal crossover to an extensively degenerate Coulomb phase [52] at zero temperature.

The model is of course most famously known for harboring both gapped and gapless quantum spin-liquid ground states. At the same time, it is one of the rare microscopic models that can be solved exactly, as demonstrated in seminal work [19] by Alexei Kitaev in 2006. This analytical tractability allows one to precisely describe and track the fractionalization of the original spin–orbit entangled degrees of freedom $\mathbf{S}_i$ into a fermionic degree of freedom, a so-called Majorana fermion, and a Z_2 gauge field as illustrated in Fig. 5. The flux of the Z_2 gauge field is locally conserved, rendering the gauge field static. It is ordered at zero temperature and its elementary vison excitations are found to be massive. This unique situation leads to, amongst other things, purely nearest-neighbor spin–spin correlations. The Majorana fermions, on the other hand, remain itinerant and form a gapless state – a *Majorana metal* – around the point of equal coupling $K_x = K_y = K_z$. For the honeycomb lattice, this Majorana metal is a semi-metal with a Dirac cone dispersion (well known from the analogous calculation of free complex fermions for graphene-like electron systems). If one of the three couplings dominates, the

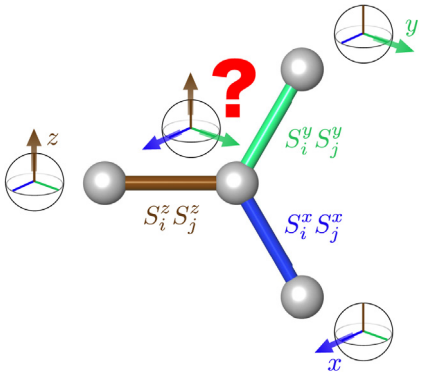

Fig. 4. Exchange frustration arising from spin–orbit induced bond-directional interactions, i.e. Ising-like couplings where the exchange easy axis depends on the spatial orientation of an exchange bond. Spins subject to these bond-directional interactions cannot simultaneously minimize all couplings, which holds both for quantum and classical moments.

system undergoes a phase transition (e.g. for dominant K_z coupling along the line $K_z = K_x + K_y$) into a gapped spin liquid. This latter state exhibits Abelian (Z_2) topological order akin to the well-known toric code model [53] and macroscopic entanglement.

A perturbative calculation reveals that applying a magnetic field along the 111-direction, i.e. coupling the magnetic field to all three spin components, gaps out the gapless spin liquid into an even more exotic (chiral) spin liquid with non-Abelian topological order [19]. Note that though the bulk is gapped, on the edge there is a chiral current of Majorana fermions. The non-Abelian character of the phase is identical to that of a $p_x + ip_y$ superconductor [54], the Moore–Read state [55] proposed for the $\nu = 5/2$ fractional quantum Hall state, heterostructures of superconductors and topological band insulators [56] or semiconductors [57], as well as that of a network [58] of Majorana wires [59,60] – all physical systems, which have gathered considerable interest in the context of proposals for fault-tolerant topological quantum computation [53,61]. Despite this similarity, the search for Kitaev materials and a solid-state realization of the Kitaev model is probably less driven by a potential application in quantum computing technologies, but deeply inspired by the fundamental pursuit of (i) the synthesis of spin liquid materials, (ii) the experimental discovery of Majorana fermions, and (iii) a direct experimental probe of the underlying (Z_2) gauge physics — such experimental evidence for gauge physics in a condensed-matter context has long been lacking, despite theorists using the concept of Z_2 gauge theories in the classical statistical mechanics of nematics [62] and to capture the physics of fractionalization in quantum many-body systems [63–65] for decades.

The conceptual understanding of the physics of the Kitaev model has been steadily growing since its initial description and analytical solution [66,67]. This includes the fundamental role of vacancies [68,69], depletion [70], and impurities [71],

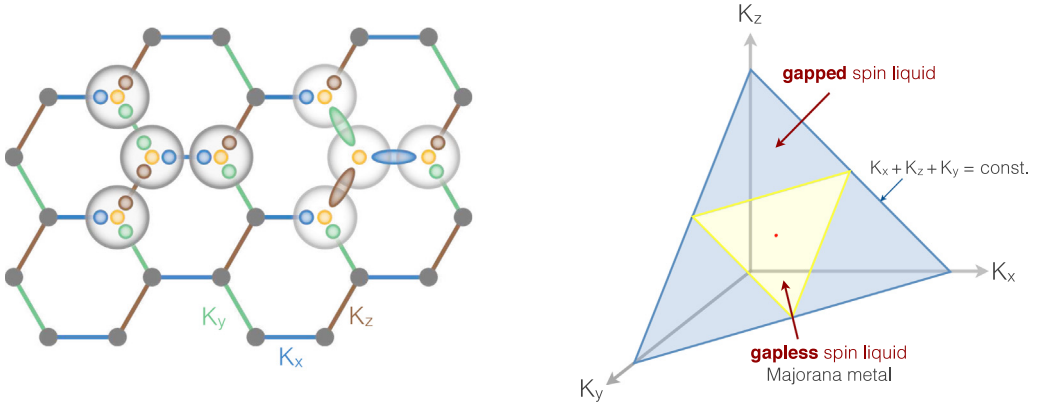

Fig. 5. Left: The honeycomb Kitaev model with bond-directional couplings K_x, K_y and K_z. The model can be analytically solved by introducing four flavors of Majorana fermions (indicated by the yellow, blue, green and brown circles) and recombining them into a static Z_2 gauge field (indicated by the blue, green and brown ovals) and a remaining itinerant Majorana fermion (yellow circle). Right: Phase diagram of the Kitaev model plotted for a plane $K_x + K_y + K_z = \text{const}$. If one of the three couplings dominates, the system forms a gapped spin liquid indicated by the blue shading. Around the point of isotropic coupling strengths $K_x = K_y = K_z$ (indicated by the red dot) a gapless spin liquid emerges, which can be best characterized as a (semi-)metal of the Majorana fermions.

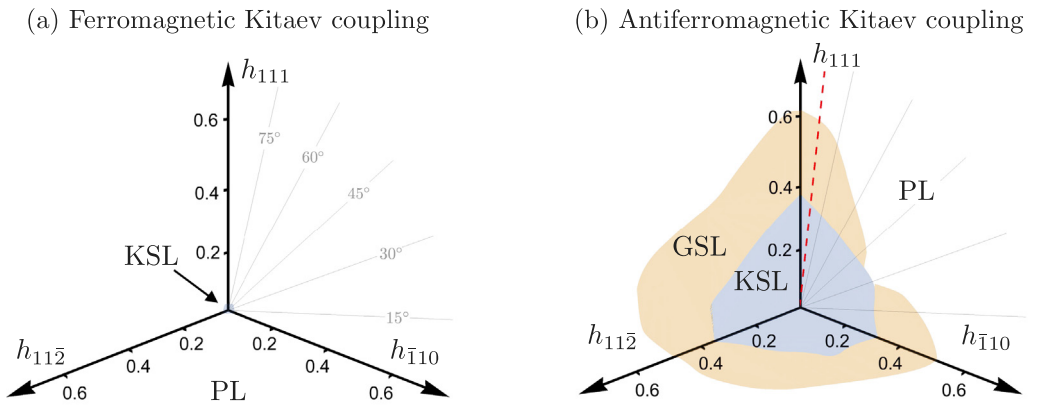

Fig. 6. Phase diagram of the (a) ferromagnetic and (b) antiferromagnetic Kitaev model in a magnetic field. The blue shaded region indicates the gapped Kitaev spin liquid (with non-Abelian Ising topological order), while the orange region indicates a gapless spin liquid that appears only for antiferromagnetic couplings.
Source: Figure adapted from Ref. [108].

disorder effects [68,72–75], the physics of the semiclassical limit [76,77], alternative solutions [78–80], and more exotic phenomena such as the strain-induced formation of Landau levels [81,82] or topological liquid nucleation [83,84] arising form vortex–vortex interactions in the non-Abelian phase [85]. The emergence of p-wave superconductivity upon doping has been discussed [86–89]. Theoretical studies of the higher-spin generalizations of the model, which defy an exact solution, have shed light on the nature of the disordered ground state for the spin-1 [76,90–94] and spin-3/2 [76,95] models. With an eye towards a material realization of the (pure) Kitaev model several experimental signatures have been discussed including the dynamical response [96–99], whose distinct spectral gap can be probed via inelastic neutron scattering (INS) or electron spin resonance (ESR), the inelastic light scattering response (both resonant and non-resonant Raman scattering) [100–102], the NMR response [98,99,103], the coupling to phonons [104], the thermal transport behavior [105], as well as the resonant inelastic X-ray scattering (RIXS) response [106,107].

1.3. Field-induced physics in the Kitaev model

The impact of a magnetic field, beyond the perturbative regime originally considered by Kitaev and discussed in the previous subsection, has only recently been fully explored. In this case, it turns out one must make a distinction between ferromagnetic (FM) and antiferromagnetic (AFM) Kitaev couplings. In the absence of a field, these two cases share all of the same relevant physics, and in fact can be mapped one to the other via a four-sublattice spin transformation. However, in the presence of a field, their behavior is strikingly different.

The FM Kitaev model exhibits a single transition with increasing magnetic field, from the non-Abelian spin liquid phase to the high-field partially polarized phase at a critical field $h_c \sim 0.02K$ [109], independent of the direction of the field as shown in the left panel of Fig. 6 (assuming a simple magnetic field term of the form $-\sum_i \vec{h} \cdot \vec{S}_i$, i.e. neglecting g-factor anisotropy). Note that the fully polarized state, with a fully saturated magnetization, is not an eigenstate of the model at any finite field. Rather, at high fields, a trivial *partially* polarized phase is reached. Interestingly, the critical field for the FM case is smaller than the zero-field gap for the vison excitations, $\Delta_v = 0.07K$.

On the other hand, in the AFM model, the non-Abelian phase is significantly more stable, surviving up to a critical field an order of magnitude larger, $h_c \sim 0.3K$ [108,110–115], as shown in the right panel of Fig. 6. Surprisingly, there then appears an intermediate phase, between the low-field non-Abelian spin liquid and the high-field partially polarized phase, e.g. within the region $h \sim 0.3$–0.6 for a 111-field [111]. Numerical calculations suggest that this phase is not ordered and harbors gapless excitations [108,114,115], with Fig. 7 showing the energy spectrum, specific heat, and dynamical spin structure factor from exact diagonalization.[1]

It has been proposed that the intermediate phase may in fact be a U(1) quantum spin liquid with a neutral Fermi surface [108,115,117]. Such a sequence of phases can be more easily conceptualized by switching to a more conventional (complex) fermionic parton picture of the Kitaev model. From such a vantage, the non-Abelian phase corresponds to a topological superconductor of partons [118]. Increasing magnetic field destroys the superconducting order, liberating the fermions to form a metallic state via an Anderson–Higgs transition, which simultaneously triggers a change in the underlying gauge structure from $\mathbb{Z}_2$ to U(1) [108].

[1] One arrives at very similar results when one considers the field-driven physics of the spin-1 version of the AFM Kitaev model [116].

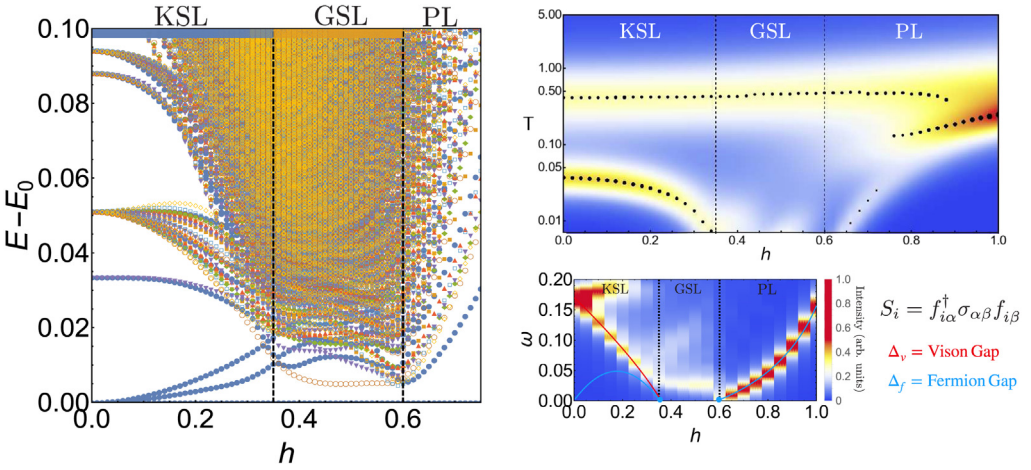

Fig. 7. Antiferromagnetic Kitaev model in a magnetic field. The three phases as a function of increasing field are the Kitaev spin liquid (KSL), a gapless spin liquid (GSL) and the partially polarized state (PL). (a) Energy spectrum from exact diagonalization, different markers represent different momentum sectors. (b) Specific heat calculated using the method of thermal pure quantum states. (c) Total dynamical spin structure factor at the Γ' point, $S(\Gamma', \omega)$, with interpretation in terms of the vison/fermion gap overlaid on top. All data is for a 24-site honeycomb cluster with an external magnetic field tilted $\pi/24$ away from the [111] direction towards the [$\bar{1}$10] direction (ensuring that $h_x \neq h_y \neq h_z$).
Source: Figure adapted from Ref. [108].

1.4. Beyond the pure Kitaev model

Going beyond the pure Kitaev model, some effort has been made to explore the full phase diagram of the $JK\Gamma$ model (2). A comprehensive overview, based on exact diagonalization calculations, is shown in Fig. 8, with the parameterization $J = \sin\theta\cos\phi$, $K = \sin\theta\sin\phi$, and $\Gamma = \cos\theta$. The vast majority of the phase diagram consists of conventional magnetically ordered states, examples of which are given in Fig. 8(b), with the Kitaev spin liquid restricted to small pockets around the exactly solvable points.

In particular, considerable attention has been devoted to the Heisenberg–Kitaev model. Its principal phase diagram [119] corresponds to the boundary of each disk in Fig. 8, $\theta = \pi/2$, and thus $J = \cos\phi$, $K = \sin\phi$. Besides extended spin liquid phases around the pure Kitaev limit (with either ferro- or antiferromagnetic coupling) there are four magnetically ordered phases. This includes conventional ferromagnetic and Néel ordering around the pure Heisenberg limits, as well as a stripy and a zig-zag ordered phases. The origin of the latter can be readily understood by a duality [7] (sometimes referred to as Klein duality [120]) of these phases to the two conventionally ordered ones. In particular, the Klein duality allows to map the left- and right-hand sides of the circular phase diagram onto one another by the relation

$$J \to -J \qquad \text{and} \qquad K \to 2J + K\,, \tag{6}$$

and a concurrent four-sublattice rotation [7]. This duality thereby connects the ferromagnet to the stripy phase, and the Néel ordered state to the zig-zag ordered phase (as well as the spin liquid phases onto themselves).

The conceptual understanding of the extended Heisenberg–Kitaev model has been furthered by a discussion of its finite-temperature physics [121] and dynamical response [122] along with the effects of an applied magnetic field [109], lattice distortions [51], as well as the inclusion of further neighbor Heisenberg [123] and Kitaev [124] interactions. The potentially multicritical point at the phase transition between the spin liquid and the magnetically ordered phases has been investigated both numerically [109] and analytically [125]. The dynamical spin structure factor beyond the Kitaev limit has recently been discussed [126–128] as have been liquid–liquid transitions upon introducing an additional Ising coupling [129]. Extensions including charge fluctuations have also been discussed [130]. Finally, a classical variant of the Heisenberg–Kitaev model has also been explored [51,131,132], including the formation of spin textures in a magnetic field [133,134]. The formation of topological magnons [135] due to Kitaev interactions in magnetically ordered regimes, e.g. for strong (ferromagnetic) Heisenberg interactions has been elucidated [136], fueled by recent experimental observations of topological spin excitations in the spin–orbit coupled material CrI_3 [137].

In addition to the Heisenberg interaction, the generic Hamiltonian (2) also contains the symmetric off-diagonal exchange interaction Γ. The effects of finite Γ can be readily observed in Fig. 8, bringing with it the appearance of 120° and spiral order, joining the already mentioned ordered phases. However, it is important to note that the region containing FM Kitaev, $K < 0$, and AFM Γ, $\Gamma > 0$, of particular importance for current materials, is still not fully understood. What is not apparent from the phase diagrams is that a finite-Γ also has the important consequence of breaking some of the symmetries present in the Kitaev–Heisenberg model, such as two-fold spin rotations.

Besides being an integral part of the full microscopic model for Kitaev materials, the pure off-diagonal exchange model has proven to be a rich source of interesting physics in its own right. In the classical limit it forms a classical

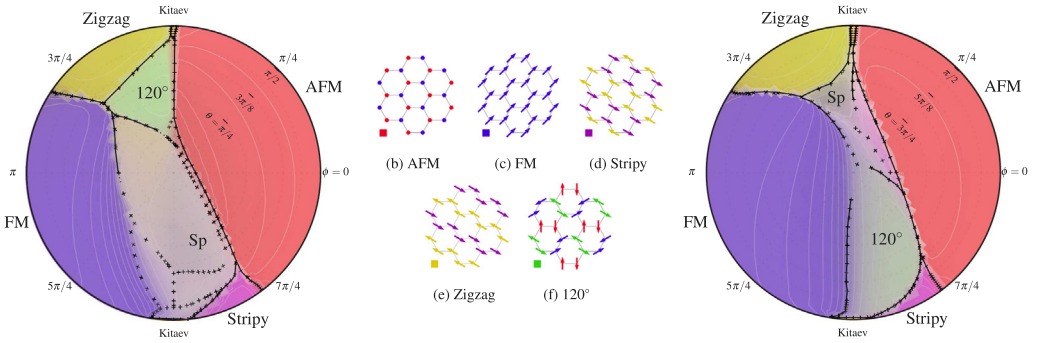

Fig. 8. Phase diagram of the $JK\Gamma$ model from exact diagonalization of a 24-site honeycomb cluster. (a) Phase diagram for $\Gamma > 0$. (b)–(f) Classical configurations of the commensurate magnetic orders that appear. (g) Phase diagram for $\Gamma < 0$.
Source: Figure adapted from Ref. [37].

spin liquid at zero temperature [138], and features an order-by-disorder driven transition at finite temperature in which certain plaquette degrees of freedom spontaneously order [139]. In the quantum spin-1/2 limit, there is still debate as to the true ground state of the model, though a number of numerical studies have suggested that it is a quantum spin liquid [140–142], potentially related to the spin liquid at the FM Kitaev point [140,141].

Though the spin liquid occupies only a small fraction of the relevant parameter space for Kitaev materials, remnants of spin liquid physics may still be found at finite temperatures and energies, despite the trivial nature of the ground state. This is similar to, for example, studies of one dimensional spin chain compounds where dynamical signatures of fractionalization have been observed at energies larger than the weak interchain coupling, ultimately responsible for the appearance of 3d long-range order at low temperatures [143–145]. In the context of the Kitaev materials, the scenario in mind is sketched in Fig. 9. Above the magnetic ordering temperature, a so-called *proximate spin liquid regime* is entered (a terminology first introduced in two experimental papers [146,147], which we will discuss below). This proximate spin liquid regime smoothly connects to the intermediate temperature regime of the pure Kitaev model, described by itinerant Majorana fermions in a disordered flux background, and separated from the high-temperature trivial paramagnet and the low-temperature quantum spin liquid via finite temperature crossovers. It is important to note though that there is no strict definition of proximate spin liquid behavior in the literature, nor is there a sharp transition as one crosses from the proximate spin liquid regime in Fig. 9 to the featureless paramagnetic region above the magnetically ordered state.

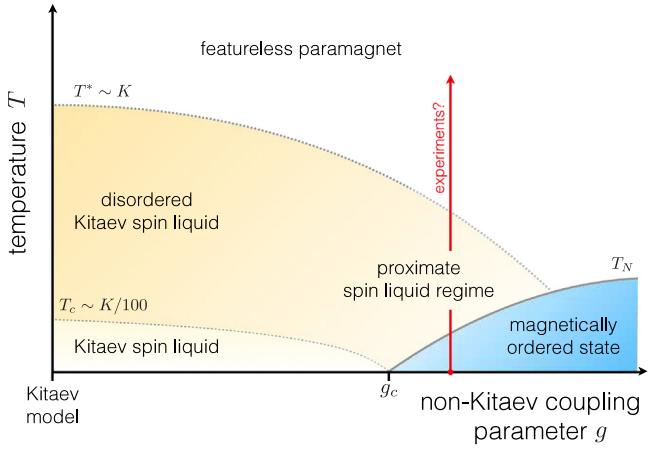

Fig. 9. Proximate spin-liquid regime in a hypothesized phase diagram of the Kitaev model in the presence of additional non-Kitaev interactions. In the pure Kitaev model (left), the ordered $\mathbb{Z}_2$ quantum-spin-liquid ground state is separated from the featureless, high-temperature paramagnet by a disordered $\mathbb{Z}_2$ spin liquid (dashed lines denote crossovers). Long-range magnetic order is expected for sufficiently large strength of additional exchange terms (right). Above the magnetic-ordering transition, an intermediate-temperature regime might persist, in which the system resides in a "proximate spin-liquid regime", where it exhibits fingerprints of Kitaev physics up to temperatures at most of the order of the Kitaev coupling K.

2. Honeycomb Kitaev materials

The quest to synthesize and explore Kitaev materials was kick-started in 2009 by the profound theoretical vision of Jackeli and Khaliullin [9] that laid out in remarkably precise terms what the elementary ingredients (in its literal sense) for a successful material search strategy are. In particular, they not only explained the microscopic origin of Kitaev-type bond-directional exchange interactions in certain (edge sharing) $4d^5$ and $5d^5$ transition metal compounds (as reviewed in the previous section). They also laid out a detailed proposal for a material realization of the honeycomb Kitaev model in the iridate α-Li_2IrO_3 and, more generally, iridates of the form A_2IrO_3 with a crystal structure as illustrated in Fig. 10 — a proposal that was quickly refined [40] to also include Na_2IrO_3 which, at the time, had already been synthesized [148,149] and scrutinized as a potential topological insulator [150].

2.1. Na_2IrO_3

Na_2IrO_3 was independently synthesized to explore its potential for Kitaev physics in 2009/2010 by the groups of Takagi [148] and Gegenwart [149]. Since then samples have been grown in a number of labs around the world, including large single crystals of diameters up to 10 mm in the group of Cao [151]. With samples readily available, numerous experimental probes have been taken that have revealed that Na_2IrO_3 is indeed a Mott insulator with an insulating gap of $\Delta = 340$ meV (opening at around 300 K) measured in optical transmission experiments [152]. Fits of the magnetic susceptibility confirm the predominant $j = 1/2$ nature of the local moments indicating magnetic moments of $1.79(2)\mu_B$ [149,153], rather close to the value of $1.74\mu_B$ expected for spin 1/2 moments, while X-ray absorption spectroscopy [154] points to a small admixture of $j = 1/2$ and $j = 3/2$ states. Resonant inelastic X-ray scattering (RIXS) [155,156] finds evidence for a trigonal distortion of the IrO_6 octahedra resulting in a crystal field splitting of the $j = 3/2$ states of about 110 meV, which, however, is smaller than the typical strength of the spin–orbit coupling of the iridates $\lambda \approx 400 - -500$ meV [157,158].

The system, however, does not exhibit the sought after spin liquid ground state, but is found to magnetically order at around $T_N = 15$ K, a temperature significantly below the Curie–Weiss temperature of $\Theta_{CW} = -125$ K [153]. The suppression of the ordering temperature with regard to the Curie–Weiss temperature indicates magnetic frustration which, quantified by the ratio $f = |\Theta_{CW}|/T_N \approx 8$, is unusually high for a quantum magnet on a bipartite lattice. It has been rationalized [121,153] to arise from geometric frustration arising from next-nearest neighbor couplings within the elementary hexagons of the honeycomb structure and is not indicative of a close proximity to the Kitaev spin liquid. The exact form of the magnetic ordering was subsequently determined to be of zig-zag type by resonant X-ray magnetic scattering [159] and inelastic neutron scattering [151,160]. The microscopic origin of this zig-zag ordering has been scrutinized in light of the Heisenberg–Kitaev model [119] supplemented with next-nearest neighbor Heisenberg [153] and Kitaev [161,162] couplings along with a flurry of ab initio calculations [154,163–165] and, most recently, dynamical mean-field studies [166].

Probably the best experimental evidence that Na_2IrO_3 should indeed be considered to be the first Kitaev material to be synthesized comes from diffuse magnetic X-ray scattering [167], which has provided a direct experimental observation of bond-directional exchange and a dominant Kitaev coupling. This is clearly seen in Fig. 11, where the individual components of the equal-time spin structure factor were extracted above the magnetic ordering temperature. Resonant inelastic X-ray scattering (RIXS) measurements suggest that short-range spin–spin correlations persist to high temperatures, far above T_N, a potential sign for a proximate spin liquid regime [168,169].

Several ideas have been put forward to bring Na_2IrO_3 closer to the Kitaev spin liquid regime, such as the making of thin films [170] or heterostructures [171], but probably the most practical scheme has been to replace the Na atoms by the smaller Li atoms and instead explore the physics of Li_2IrO_3.

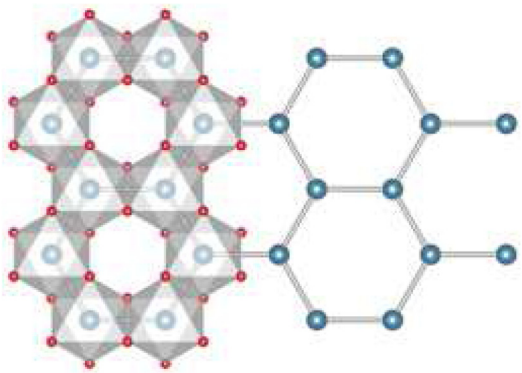

Fig. 10. Crystal structure of the honeycomb Kitaev materials A_2IrO_3 such as Na_2IrO_3 and α-Li_2IrO_3.

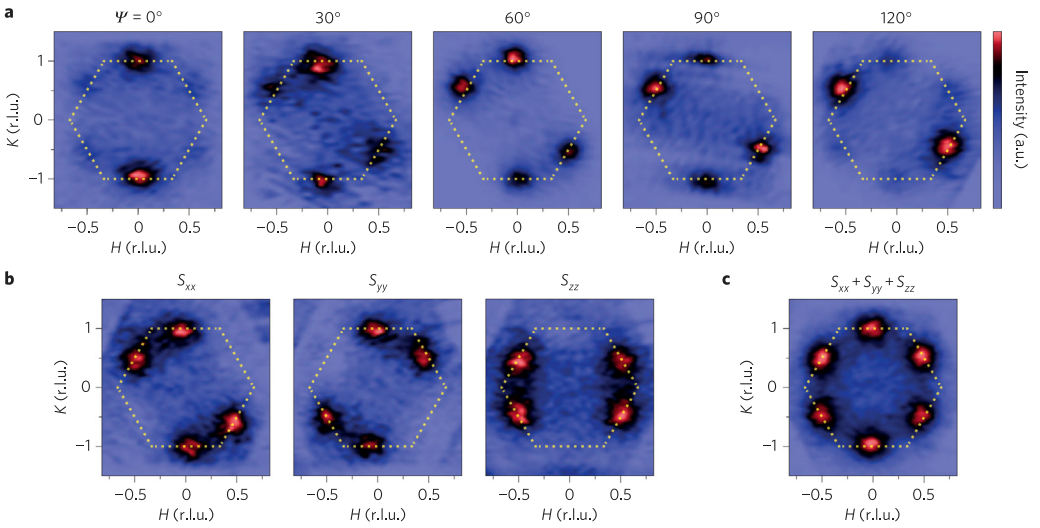

Fig. 11. Diffuse magnetic X-ray scattering on Na_2IrO_3 at $T = 17$ K, above the magnetic ordering temperature. (a) Intensity plots within the honeycomb planes for a range of angles Ψ between the a-axis and the scattering plane. Dashed hexagon corresponds to the first Brillouin zone. (b) Extracted equal-time spin–spin correlations $S_{\alpha\alpha}$ and (c) their sum. Clear evidence for locking between certain spin components and certain crystallographic directions, emblematic of bond-directional interactions.
Source: Reproduced from Ref. [167].

2.2. α-Li_2IrO_3

The exploration of Li_2IrO_3 as a candidate Kitaev material has indeed lent further impetus to the field. Probably the biggest surprise came when its synthesis lead to the discovery of several polymorphs [153,172,173] which have been dubbed α-Li_2IrO_3, β-Li_2IrO_3, and γ-Li_2IrO_3 in the sequence of their discovery. Only α-Li_2IrO_3 is isostructural to Na_2IrO_3 and exhibits iridium honeycomb layers (as depicted in Fig. 10), while the other two polymorphs, β-Li_2IrO_3 and γ-Li_2IrO_3, have been found to exhibit three-dimensional, tricoordinated networks of the iridium ions. We will discuss the latter in the context of three-dimensional Kitaev materials below.

The first high-quality samples of α-Li_2IrO_3 have been synthesized by the Gegenwart group [153] in 2012. Magnetic susceptibility fits reveal magnetic moment of $1.83(5)\mu_B$, a value slightly larger than expected for spin-1/2 degrees of freedom [153]. Like its sister compound Na_2IrO_3, α-Li_2IrO_3 undergoes a magnetic ordering transition at $T_N = 15$ K with a Curie–Weiss temperature of $\Theta = -33$ K. Thin films of Li_2IrO_3 created by pulsed laser deposition on ZrO_2:Y (001) single crystalline substrates reveal [174] a small optical gap of 300 meV indicative of a Mott gap of similar size as in its sister compound Na_2IrO_3.

The further experimental analysis of α-Li_2IrO_3 has been largely hampered by the fact that (in contrast to Na_2IrO_3) it has remained extremely challenging to synthesize bulk single crystals — an essential ingredient e.g. for neutron scattering studies, in particular to compensate for the large neutron absorption cross-section of the iridium ions. The early powder samples were found to exhibit single crystalline ordering only on length scales smaller than 10 μm. Recent experimental progress, however, has pushed this boundary to about a millimeter [175]. These single crystals have been sufficiently large to allow resonant magnetic X-ray diffraction combined with powder magnetic neutron diffraction to reveal an incommensurate magnetic ordering where the magnetic moments in iridium honeycomb layers are *counter-rotating* on nearest-neighbor sites [176], as shown in Fig. 12(c). Prior to its experimental observation a number of theoretical proposals [37,42,177,178] for spiral or other forms of incommensurate magnetic ordering in this honeycomb material have been put forward, none of which envisioned counter-rotating spirals. However, a very similar magnetic ordering is observed in the three-dimensional β-Li_2IrO_3 and γ-Li_2IrO_3 polymorphs where subsequent theoretical analysis has lead to a unifying theory [179–181] of counter-rotating spiral magnetism in all three compounds. The minimal model to explain the occurrence of counter-rotating spirals appears to be a Kitaev model supplemented with small Heisenberg and Ising interactions [176] with theoretical estimates indicating that the Kitaev interaction might be up to a factor of 20 larger than the Heisenberg exchange [179,181].

Taking a step back, α-Li_2IrO_3 remains somewhat less explored than its sister compound Na_2IrO_3 despite its more unconventional magnetism, whose origin in a vastly enhanced Kitaev coupling puts α-Li_2IrO_3 probably much closer to the sought-after Kitaev spin liquid than Na_2IrO_3. This leads to the tempting observation that replacing the Na atoms by Li atoms indeed pushed the system closer to the Kitaev regime and that the next logical step would be to replace Li by an even smaller atom, i.e. hydrogen. While this has been a small step for a theorist to contemplate, taking such a step in the lab amounts to a big leap for material synthesis. But it is precisely this leap which the Takagi group has taken

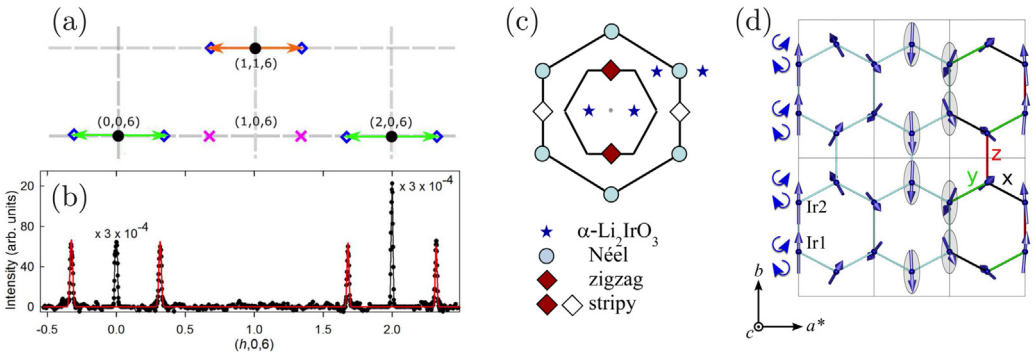

Fig. 12. Magnetic structure of α-Li_2IrO_3. (a) Schematic of the honeycomb lattice reciprocal plane with filled circles, diamonds, and magenta crosses indicating positions of structural peaks, measured magnetic peaks, and the absence of peaks, respectively. (b) Scan across reciprocal space with structural and magnetic peaks clearly visible. The solid (red) line is the calculated magnetic scattering intensity for the structure shown in (d). (c) Positions of the magnetic Bragg peaks found in Li_2IrO_3 and those expected for other potential magnetic orders. (d) Classical spin configuration for the spiral magnetic structure found in α-Li_2IrO_3.
Source: Reproduced from Ref. [176].

by successfully synthesizing $H_3LiIr_2O_6$, which we will discuss with some other "second-generation" Kitaev materials in Section 2.4 below.

2.3. α-$RuCl_3$

In parallel, another material has taken center stage in the search for Kitaev materials — the 4*d* compound α-$RuCl_3$. The material consists of very weakly bounded layers of edge-sharing $RuCl_6$ octahedra (of almost perfect cubic symmetry) with the central Ru^{3+} ($4d^5$) ions forming an almost ideal honeycomb lattice. Originally thought to be a conventional semiconductor in early 1970's transport measurements [182], spectroscopic measurements in the mid 1990s pointed towards the formation of a Mott insulator [183]. It was only in 2014 that the group of Young-June Kim realized that α-$RuCl_3$ is in fact a spin–orbit assisted $j = 1/2$ Mott insulator [184]. Direct evidence for Mott physics in α-$RuCl_3$ comes from optical spectroscopy [184] measuring an optical gap of 200 meV and angle-resolved photoemission spectroscopy (ARPES) [185] observing a charge gap of 1.2 eV at temperatures of 200 K. The strength of the spin–orbit coupling has been determined from optical spectroscopy [186] to be $\lambda \approx 100$ meV and from neutron scattering experiments on polycrystalline samples [146] to be $\lambda \approx 130$ meV, both estimates somewhat smaller than the atomic spin–orbit coupling $\lambda \approx 150$ meV for ruthenium [187]. While the strength of the spin–orbit coupling in this 4*d* compound is thus considerably smaller than for the heavier 5*d* iridates, it has been argued on the basis of ab initio calculations [184] that the *ratio* of the spin–orbit coupling and the electronic bandwidth is only slightly smaller than in the iridates and still suffices to induce the formation of spin–orbit entangled $j = 1/2$ and $j = 3/2$ bands. The formation of $j = 1/2$ local moments is further supported by Curie–Weiss fits [188,189] of the magnetic susceptibility yielding a magnetic moment of $2.2\mu_B$ (somewhat above the expected value of $1.74\mu_B$ for a spin-1/2) and by angle-resolved photoemission, X-ray photoemission, and electron energy loss spectroscopy [190,191]. Scanning transmission electron and scanning tunneling microscopies [192] on exfoliated/cleaved α-$RuCl_3$ samples report a Mott gap of 250 meV in the measured density of states, slightly larger than the value obtained for bulk samples in optical spectroscopy, and a subtle charge ordering pattern originating from anisotropy in the charge distribution along Ru–Cl–Ru hopping pathways.

In exploring the magnetism of α-$RuCl_3$, susceptibility measurements on powder samples [188,189] indicate a Curie–Weiss temperature of around 23–40 K consistent with single crystal measurements [193] of the in-plane susceptibility yielding a value of $\Theta_{CW} = 37$ K, while the out-of-plane susceptibility reveals a value of $\Theta_{CW} = -150$ K. At first two successive ordering transitions at 7 K and 15 K have been reported, both in specific heat and susceptibility measurements on powder samples [193] as well as in single crystal inelastic neutron scattering experiments [146], with the higher transition later attributed to the presence of stacking faults in less pristine samples of α-$RuCl_3$ and entirely absent in high-quality single crystals probed by X-ray diffraction [194] and inelastic neutron scattering [147] experiments. Below $T_N = 7$ K pristine α-$RuCl_3$ exhibits zig-zag magnetic ordering (similar to that of Na_2IrO_3) confirmed in various experimental probes including neutron [195,196] and X-ray [194,197] diffraction experiments, inelastic neutron scattering on polycrystalline [146] and single crystal [147] samples along with muon spin rotation measurements [198]. The emergence of zig-zag magnetic ordering in α-$RuCl_3$ is also consistent with ab initio calculations [197,199–201] and microscopic calculations for the $JK\Gamma$ model (2) [162] and variations thereof [202]. Estimates of the magnitude of the Kitaev coupling in α-$RuCl_3$ vary considerably, with the majority lying within the range 60-120 K. For example, on the one hand, a combination of ab-initio calculations and theoretical analysis of the magnon spectrum suggests a coupling of 60 K [203], whereas, on the other hand, fitting to the in-field magnetization suggests a coupling of 120 K [204]. For more details, see the tables and associated references in Refs. [49,205].

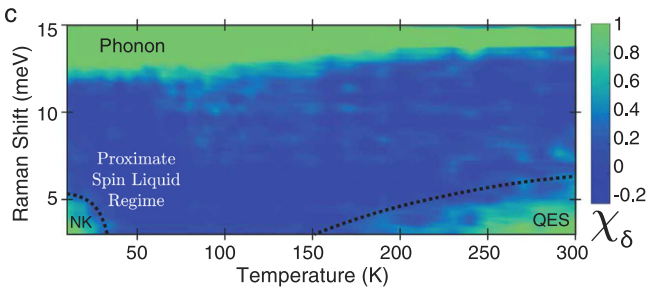

Fig. 13. Comparison of the Raman scattering data of α-$RuCl_3$ with theoretical predictions for the pure Kitaev model. The color represents the difference in the extracted Raman susceptibility for α-$RuCl_3$ with the Raman susceptibility computed for the pure Kitaev model using quantum Monte Carlo techniques, $\chi_\delta = \chi_{\text{exp}} - \chi_{\text{QMC}}$. The NK region at low temperatures and energies is dominated by non-Kitaev interactions, and shows poor agreement with the theoretical predictions. At high energies, $>$ 12 meV, the deviation is due to a nearby phonon line and at high temperatures, $>$ 150 K, the deviation is due to quasi-elastic scattering due to thermal fluctuations. The remaining area, indicated by the blue color, shows good agreement with the Kitaev model prediction, suggestive of proximate spin liquid behavior.
Source: Figure reproduced from Ref. [206].

2.3.1. Proximate spin liquid behavior

In the absence of a magnetic field, what sets α-$RuCl_3$ apart from the honeycomb iridates Na_2IrO_3 and α-Li_2IrO_3 is that several unusual features *above* the magnetic ordering transition have been interpreted as arising from close proximity to a Kitaev spin liquid. Here we want to highlight two such features of this proximate spin liquid regime, found in Raman scattering and inelastic neutron scattering experiments of α-$RuCl_3$.

We start with the Raman scattering experiments by K. Burch and collaborators [186,206,207]. It has been argued that the observed Raman susceptibility exhibits evidence of *fermionic* excitations across a broad energy and temperature range. This is an extraordinary observation, since the excitations of ordinary magnetic insulators, magnons and phonons, obey bosonic statistics. In the context of Kitaev spin liquids, however, fermionic excitations arise naturally, as one of the defining aspects of these spin liquids is the fractionalization of the original spin degrees of freedom into a Z_2 gauge field and a Majorana *fermion*. Conventional Raman response, dominated by Fleury–Loudon processes, naturally couples to just the fermionic degrees of freedom [100]. This should also hold for systems in close proximity to such a Kitaev spin liquid, which is precisely what they argue to be the case for α-$RuCl_3$ [208].

The experimental evidence that is considered in their argument is the temperature dependence of the Raman susceptibility, $\text{Im}[\chi(\omega, T)]$ [206]. By measuring both the energy loss and gain intensities the Raman susceptibility can be extracted, it simply corresponds to the difference between the two. To remove contributions from high temperature quasi-elastic scattering and phonons they focus on the difference in susceptibility between temperatures $T < 150$ K and $T = 150$ K. The resulting data is found to be well-approximated by Fermi functions with half the scattering energy, suggesting pairs of fractional fermionic excitations. An analysis of the spectral weight, for a given polarization, shows similar agreement with the prediction for pairs of fermionic excitations. Fig. 13 shows the difference between the experimentally determined Raman susceptibility and that obtained via quantum Monte Carlo simulations of the pure

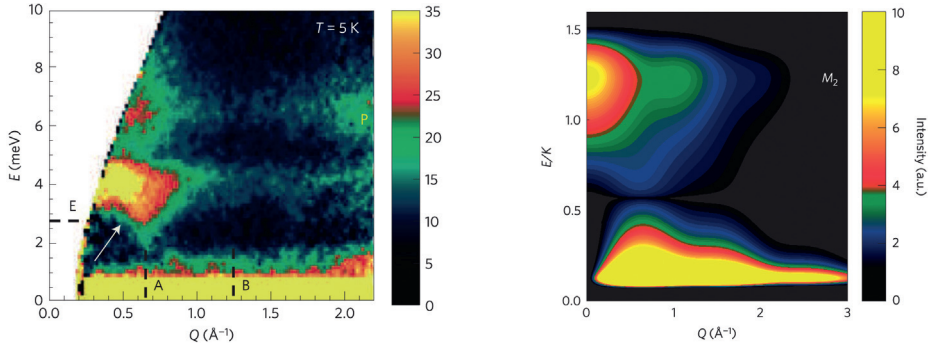

Fig. 14. Left: False color plot of the inelastic neutron scattering data of α-$RuCl_3$. Two magnetic modes with band centers around $E = 4$ and 6 meV are identified. While the lower one is attributed to the concave spin wave dispersion on a zig-zag ordered background (indicated by the white arrow), the upper feature resembles the broad, non-dispersive high-energy response expected of a Kitaev spin liquid. Right: Analytical calculation of the dynamical response of the Kitaev spin liquid. Above a low-energy band a broad feature is found that is strongest at $Q = 0$ and decreases with increasing Q.
Source: Figures adapted from Ref. [146].

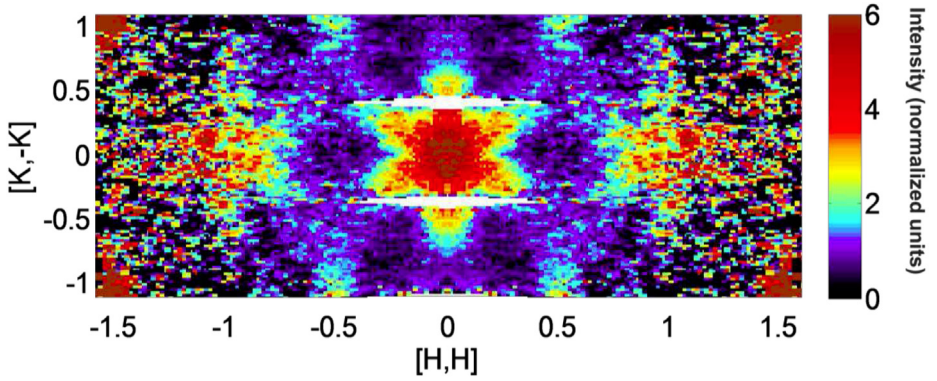

Fig. 15. Extended zone picture of neutron scattering data of α-$RuCl_3$ integrated over the energy window [4.5, 7.5] meV and symmetrized along the $(H, H, 0)$-direction taken at $T = 10$ K, i.e. well above the magnetic ordering transition at $T_N = 7$ K. The star-like feature at the zone center arises from the interplay of spin wave and spin liquid physics in this temperature regime and can be rationalized within the context of the Heisenberg–Kitaev model [122].
Source: Figure reproduced from Ref. [147].

Kitaev model. At low temperatures and energies, $T < 40$ K and $E < 6$ meV, there is significant deviation while at higher temperatures and energies there is good agreement suggestive of a proximate spin liquid regime. Taken together, these are intriguing results — taken at face value, they constitute experimental indication for the emergence of (Majorana) fermion excitations in a bulk magnetic insulator.

Another experimental feature that strongly supports the idea that α-$RuCl_3$ is indeed in close proximity to a Kitaev spin liquid is found in the magnetic scattering observed in inelastic neutron scattering experiments [146,147]. Unlike the Ir based compounds, Ru is much more amenable to neutron scattering techniques due to its smaller neutron-absorption cross section, one of the keys to its popularity. While at low energies the scattering is consistent with spin waves on a zig-zag ordered background, a broad scattering continuum is found at higher energies. It is this continuum that resembles the broad, non-dispersive high-energy response expected of a Kitaev spin liquid [146]. A comparison of the experimental neutron scattering data with exact analytical calculations of the dynamical response of the Kitaev model are given in Fig. 14. At intermediate energy scales there are star-like features (reproduced in Fig. 15 from Ref. [147]), which arise from the interplay of spin wave and spin liquid physics in this regime. While the dynamical response of the pure Kitaev model does not show this star-like feature, it can be explained by the small admixture of additional neighbor correlations as induced, for instance, by the inclusion of a Heisenberg exchange and experimentally observed in optical spectroscopy [209]. Indeed, recent numerical studies [122] of the dynamical response of the Heisenberg–Kitaev model have quantitatively reproduced the star-like feature.

It must be noted that alternate explanations for the unusual magnetic excitation spectrum observed by neutron scattering, which do not rely on spin liquid physics, have also been proposed. Within spin-wave theory, the low symmetry of the magnetic Hamiltonian for α-$RuCl_3$, and indeed any Kitaev material, permits additional interaction and decay channels not allowed in conventional Heisenberg magnets. This can lead to the destruction of well-defined magnons throughout much of reciprocal space and the concomitant appearance of continuum like features [49,203].

In total, the mounting experimental data on α-$RuCl_3$ in zero-field support the proposal that, although α-$RuCl_3$ magnetically orders, it is in such close proximity to a Kitaev spin liquid that remnants of decisive spin-liquid features can still be probed *above* the magnetic ordering transition. This includes experimental evidence for fermionic quasiparticles in Raman scattering [207,208], and a broad magnetic continuum at high energies [146] preceded by a star-like feature at intermediate energies [122,147] above the magnetic ordering transition in inelastic neutron scattering.

2.3.2. Field-driven phenomena

In the presence of an external magnetic field, the magnetic order of α-$RuCl_3$ can be destroyed, with a number of intriguing experimental results in the resulting field-induced phase diagram. The most spectacular of these is the reported observation of a half-integer quantized thermal Hall effect which, if true, represents a striking feature of the existence of a chiral Majorana edge mode.

Two potential scenarios for the field-induced phase diagram of α-$RuCl_3$ are sketched in Fig. 16. In Fig. 16(a) there is long-range magnetic order below a critical field B_c^{MO}, and a trivial partially polarized state above. The partially polarized state is gapped, does not spontaneously break any symmetry and does not exhibit a finite temperature phase transition. It is also sometimes referred to as a "quantum disordered state" or "quantum paramagnet", in analogy to the trivial high-field state of the transverse-field Ising model. However, to avoid any confusion with the physics of quantum spin liquids, we will avoid such terms. In the second potential scenario, sketched in Fig. 16(b), there is a quantum spin liquid between the low-field magnetic order, ending at B_c^{MO}, and the high-field trivial state, starting at B_c^{QSL}. Distinguishing between these

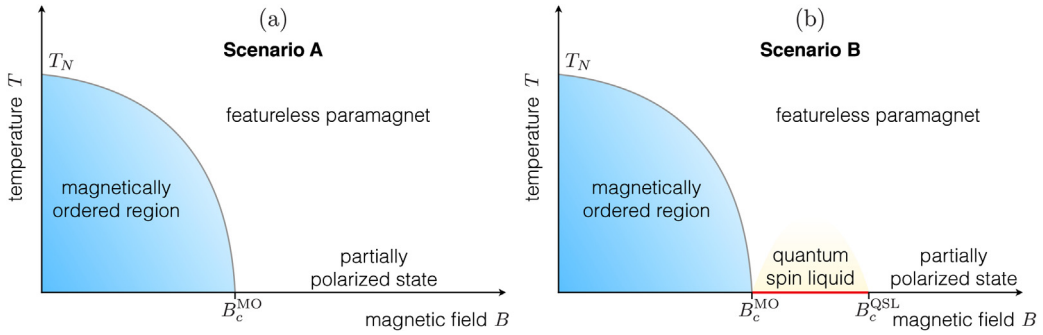

Fig. 16. Two possibilities for the phase diagram of α-$RuCl_3$ in a magnetic field. In (a), the trivial partially polarized state is immediately entered once magnetic order is destroyed at B_c^{MO}. In (b) there is an intermediate quantum spin liquid state between the magnetic order at low fields and the partially polarized state at high fields, resulting in an additional quantum phase transition at B_c^{QSL}. In both scenarios, once magnetic order is destroyed there are no further finite temperature transitions. Finite temperature destroys both the quantum spin liquid and partially polarized state and smoothly connect to the high-temperature featureless paramagnet. Note that, for simplicity, we neglect transitions within the magnetically ordered region.

scenarios is difficult as a spin liquid can share many of the same properties as the partially polarized state, e.g. exhibit partial magnetization, an energy gap, no spontaneous symmetry breaking and no finite temperature phase transition.

Concerning the stability of the ordered state, early magnetic field studies of α-$RuCl_3$ revealed that an in-plane magnetic field of $B \sim 8$ T was enough to destroy the zigzag magnetic order, as seen for example by tracking the peak in specific heat [193,197,210–212]. On the other hand, for an out-of-plane field, along the c-axis, the magnetic order was seen to survive up to 60 T, indicating an enormous anisotropic response of the zigzag ordered state [197]. More recent studies, at even higher fields, have shown that an out-of-plane field of 70 T is needed to fully destroy the zigzag order, and have furthermore mapped out the full extent of the zigzag state from purely in-plane to out-of-plane fields [213]. Within the zigzag ordered region itself, there is in fact a field-driven first-order transition in which the stacking periodicity in the out-of-plane direction changes, but the in-plane zigzag order remains the same [214].

What precisely happens once the magnetic order is destroyed has been hotly debated, with a wide variety of experimental probes applied to the region beyond the break-down of magnetic order. So far, the majority of these studies do not observe evidence for any further transitions, i.e. they observe a *single* field-induced state within their accessible field range [211,212,215–224]. Evidence for a gap opening once the transition is crossed has been observed in specific heat [212,215], thermal conductivity [216–218], electron spin resonance [219], THz spectroscopy [220], Raman spectroscopy [221,225], NMR [211] and inelastic neutron scattering [222]. On the other hand, there have also been some studies reporting evidence for gapless excitations in the field-induced state, for example using NMR [226,227]. Added to this, there have been conflicting descriptions of the observed field-induced state in the literature, with some claiming it as a field-induced QSL and others the trivial partially polarized state. Recent Raman studies with in-plane fields of up to 30 T have clearly demonstrated that, at least at high fields $B > 15$ T, α-$RuCl_3$ has certainly entered the trivial partially polarized phase, with a linearly increasing spin gap whose slope approaches the g-factor value expected for the simple $|\Delta S| = 1$ spin-flip excitation [221,225]. We note, however, that, despite the apparent trivial nature of the high-field state, an interesting scale invariant magnetic response has been reported up to very high fields of 64T [213].

The neutron scattering response of the high-field disordered state bears striking similarity to the high-temperature response at zero-field [222]. The broad magnetic continuum observed at zero-field, above the magnetic ordering temperature, is qualitatively similar to the response observed at finite field, at low temperatures above the critical field. This suggests that proximate Kitaev spin liquid behavior may be accessed by destroying the zigzag order either via temperature or magnetic fields.

The most spectacular experimental results for α-$RuCl_3$ in field are the thermal Hall measurements of Yuji Matsuda's group in Kyoto [228] that claim a half-integer quantized plateau within a field range of $B \sim 7$–10 T. In particular, for fields tilted 45° and 60° away from the c-axis, a plateau was reported in κ_{xy}/T for fields $B \sim 7$–10 T and temperatures $T \sim 4$–6 K, with the 2-d value, obtained by dividing by the number of honeycomb layers, given by $\kappa_{xy}^{2d}/T = (1/2)(\pi k_B^2/6\hbar)$, as shown in Fig. 17. This is a remarkable experiment, not only for its observation of a quantized thermal Hall state but the actual *half-quantization* that is reported. For a conventional electronic mode the thermal conductance is quantized in integer multiples of $(\pi k_B^2/6\hbar)$, the quantum of thermal conductance. On the other hand, a half-integer value is evidence for a Majorana mode (one can think of a Majorana as "half an electron"). It can be directly related to the chiral central charge that characterizes the conformal field theory description of the edge states. Observation of a clear and robust half-integer

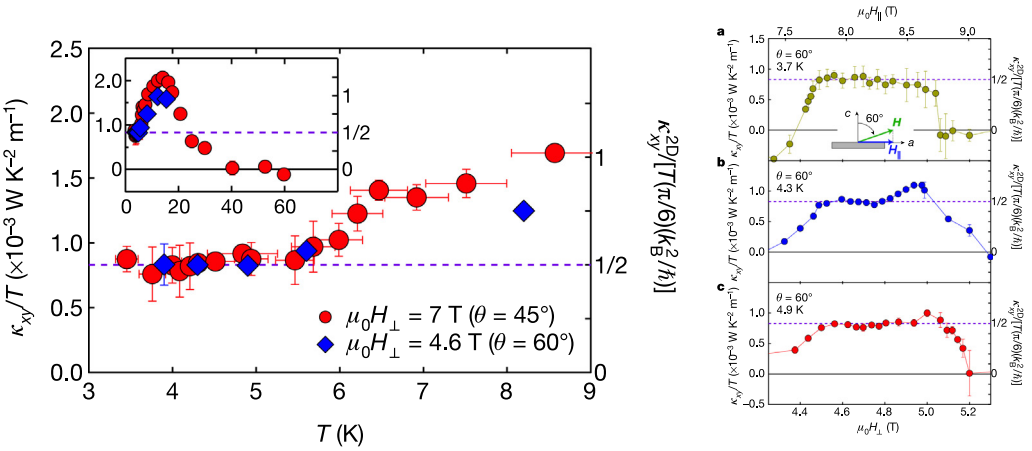

Fig. 17. Thermal Hall conductivity of α-$RuCl_3$ in a tilted magnetic field. In the left panel κ_{xy}/T is shown as a function of temperature for two fixed tilted magnetic field configurations. As shown in the inset, it starts to increase below ∼40 K, overshooting the 1/2-quantized value and reaching a maximum at ∼ 14 K before decreasing and plateauing at the 1/2-quantized value within a temperature range of 4–6 K. In the right panel the thermal Hall conductivity as a function of increasing magnetic field, at a fixed angle of 60° away from the c-axis, is shown at fixed temperatures of (a) 3.7 K, (b) 4.3 K and (c) 4.9 K. The plateau is stable over an extended field and temperature range.
Source: Figure adapted from Ref. [228].

plateau thus serves as smoking-gun evidence for the existence of emergent non-Abelian anyons in the form of Majorana fermions.[2]

Follow-up measurements by the Kyoto group have reported that even a purely *in-plane* magnetic field can support a half-integer quantized plateau, and that the sign of the signal can be reversed without changing the out-of-plane component of the field [230] — two traits that do not occur in the usual electronic quantum Hall effect arising from the formation of Landau levels. Rather, the correct analogy here is to a quantum anomalous Hall insulator, in which the non-trivial edge states arise due to the topology of the band structure, rather than Landau level physics. The thermal Hall results are indicative of the scenario sketched in Fig. 16(b) in which an intermediate QSL occurs between low-field magnetic order and the high-field trivial state.

Despite the spectacular nature and potential far-reaching implications of the thermal Hall results it is important to keep in mind a number of caveats. At the time of writing, no other experimental group has fully independently reproduced a robust quantized plateau in α-$RuCl_3$. There is also a tremendous sample dependence to the data, and, due to the particulars of the thermometers used, the measurements were restricted to temperatures $T > 4$ K, with quantization only observed in a narrow range $T \sim$ 4–6 K. Observation of a robust quantized plateau, however, is key as the appearance of a non-quantized thermal Hall conductivity can simply be explained by topological magnon bands in the partially polarized state [128,231–233].

It should also be pointed out that, apart from the thermal Hall measurements themselves, the scenario in Fig. 16(b), which the measurements imply, should result in an additional quantum phase transition beyond the zigzag magnetic order. No clear evidence for such a transition has so far been found. It remains an ongoing puzzle, both for experimentalists and theorists, to resolve these apparent inconsistencies between the thermal Hall measurements, and the intermediate QSL state they imply, and a number of other magnetic field studies of α-$RuCl_3$ to come to a conclusive picture of the in-field physics of this particularly intriguing Kitaev material.

On the theoretical side, beautiful conceptual work [234,235] has shown why the thermal Hall conductance of α-$RuCl_3$ can remain almost perfectly quantized, at least within a certain temperature window, despite the presence of gapless phonon modes in the bulk (which is a striking difference from the electronic quantum Hall states whose bulk is fully gapped). There have also been theoretical studies exploring the non-quantized thermal Hall effect that can arise from topological magnons and its field dependence [128,231–233], finite temperature signatures of the quantum phase transition to the purported spin liquid [236], evolution of the magnetization and spin dynamics in field [201,237], the dynamics of visons and their potential contribution to the thermal Hall signal [238], and the field-induced behavior in the classical limit [133,239].

Let us finally mention that also α-$RuCl_3$ has a polymorph, β-$RuCl_3$, in which face-sharing $RuCl_6$ octahedra are arranged in chains. β-$RuCl_3$ is found to show no magnetic ordering down to 5 K [188] and awaits further experimental analysis.

[2] We note in passing, that in the same volume of *Nature* that reported the half-quantized thermal Hall effect reported by Matsuda's group for the Kitaev material α-$RuCl_3$, there was also the report of Heiblum's group at the Weizmann Institute observing a half-quantized thermal Hall effect in the $\nu = 5/2$ quantum Hall state [229].

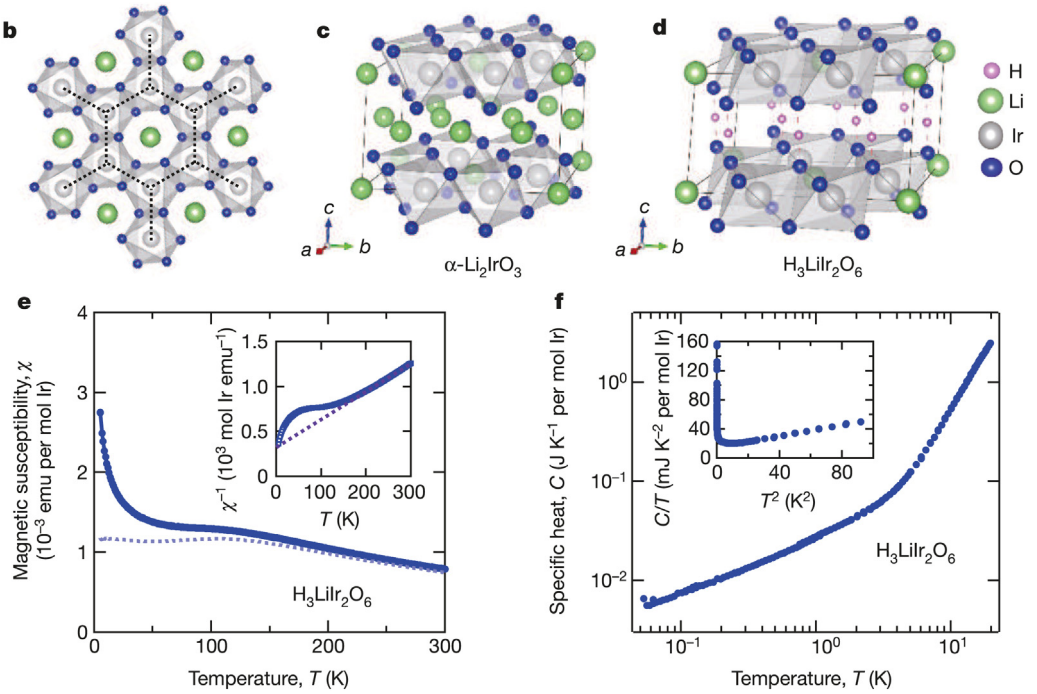

Fig. 18. Structural and magnetic properties of $H_3LiIr_2O_6$. (a)–(c) show the structure of the edge-shared network of IrO_6 octahedra within the planes, the stacking of Li_2IrO_3, and $H_3LiIr_2O_6$ respectively. (d) is the magnetic susceptibility at 1 T, with its inverse given in the inset. (e) is the specific heat as a function of temperature, with C/T against T^2 in the inset. Neither measurement displays any signatures of a phase transition, down to a temperature of 0.05 K.
Source: Figure reproduced from Ref. [240].

2.4. Second-generation Kitaev materials

Over the last three years a "second-generation" of Kitaev materials has seen the light of day by modifying the alkali atoms of α-A_2IrO_3. Starting from Li_2IrO_3, the interlayer Li^+ ions can be replaced by either H, Ag or Cu, using a soft-chemical ion-exchange reaction, to create $H_3LiIr_2O_6$ [240], $Ag_3LiIr_2O_6$ [241] and $Cu_3LiIr_2O_6$ [242]. On the other hand, starting from Na_2IrO_3, it is possible to fully replace the Na^+ ions with Cu^+ to create Cu_2IrO_3 [243], or to replace just the interlayer ions to form $Cu_3NaIr_2O_6$ [242]. All of these materials share a similar structural motif, with the same IrO_6 honeycomb planes as their parent compounds, but connected by linear O-*A*-O dumbbells (A = H, Ag or Cu). They also share a similar propensity to disorder, which has added a new dimension of complexity to the realm of Kitaev materials and spurred a number of theoretical studies on disorder in the Kitaev model. So far, these materials only exist in polycrystalline form, with single crystal studies still to be carried out.

2.4.1. $H_3LiIr_2O_6$, $Ag_3LiIr_2O_6$ and $Cu_3LiIr_2O_6$

By successfully replacing the interlayer Li^+ ions of α-Li_2IrO_3 with H^+ ions, the group of Takagi synthesized powder samples of a new layered honeycomb iridate, $H_3LiIr_2O_6$, in 2018 [240]. This hydrogen intercalated compound shares the same $LiIr_2O_6$ honeycomb planes as α-Li_2IrO_3 but has a reduced interlayer spacing, from 5.12 Å to 4.87 Å, due to the smaller ionic radius of H^+. Measurements of the resistivity confirm that the material is an insulator, with an activation gap of 0.12 eV, and the magnetic susceptibility exhibits Curie–Weiss behavior, with effective magnetic moments of $1.60\mu_B$ per Ir atom (very close to the ideal spin-1/2 value of $1.73\mu_B$). X-ray diffraction studies indicate the presence of substantial stacking faults between the planes [240,244].

Unlike Na_2IrO_3 and α-Li_2IrO_3 and its polymorphs, no evidence of magnetic ordering is seen down to 50 mK, despite a Curie–Weiss temperature of -105 K. There are no anomalies present in either specific heat nor magnetic susceptibility, as seen in Fig. 18, and both ^{7}Li and ^{1}H NMR spectra exhibit no significant broadening down to 1 K. There are indications of low-energy excitations present, from the weak power-law behavior of the low-temperature specific heat $C/T \sim T^{-1/2}$ as well as the NMR spin relaxation rate T_1^{-1}. However, these excitations account for a small fraction of the total entropy of the system, only 1-2% of $k_B \ln 2$ [240]. Nevertheless, taken together, these are tantalizing indicators that this material may lie closer to the idealized Kitaev model and may even realize a quantum spin liquid ground state.

However, the material is expected to exhibit a significant amount of disorder. Alongside the stacking faults previously mentioned, there is also predicted to be significant disorder associated with the positions of the interlayer H^+ ions, due

to their low mass [245–247]. The interlayer O–H–O bonds can form a double-well potential for the H ion. A dielectric spectroscopy study indicates that at high temperatures the H ion exhibits thermally activated hopping between the two well minima, while at low temperatures it exhibits quantum mechanical tunneling between the minima. However, the observed low temperature time scale for tunneling is rather high, compared to magnetic time scales, in the region of 1–100 s. Thus the magnetic system effectively experiences static disorder in the positions of the interlayer H ions [248]. A related deuterated compound, $D_3LiIr_2O_6$, was examined in the same study and was found to have an even longer tunneling time scale, consistent with the larger mass of the D ion [248]. Ab-initio studies suggest that the magnetic interactions are highly sensitive to the location of the interlayer H^+ ions, and that the Kitaev interaction may be boosted [245–247]. The physics of $H_3LiIr_2O_6$ may thus be closer to that of a bond-disordered Kitaev model, as opposed to the idealized, clean case considered by Kitaev. Indeed, a theoretical study of such a bond-disordered model seems to capture much of the relevant physics [249,250]. Decisively disentangling the role of disorder and true spin liquid physics remains a challenge.

The related compound $Ag_3LiIr_2O_6$ also shows promising signatures of potential spin liquid physics [251]. In this case, the interlayer Li^+ is replaced by Ag^+ cations, leading to a significant 30% enhancement of the interlayer spacing [241]. Again, unlike its parent compound Li_2IrO_3 there is no 15 K peak in magnetic susceptibility to indicate a transition to long-range magnetic order, despite a similar magnetic moment and a larger Curie–Weiss temperature of -142 K. Measurements of the ac magnetic susceptibility obey the scaling form expected in the presence of random singlets, suggesting either a valence-bond or spin liquid state. The magnetic specific heat, obtained by subtracting the contribution from $Ag_3LiSn_2O_6$, exhibits a two-step structure, with an extremely broad hump centered at ~ 75 K followed by a peak at 13 K [251]. This kind of two-step behavior is consistent with expectations for the pure Kitaev model.

It has been suggested, based on ab-initio calculations, that the absence of order can be attributed to a finite weight of Ag 4*d* orbitals at the Fermi level. This leads to an enhancement of the Kitaev coupling due to stronger spin–orbit coupling mediated via the O–Ag–O bonds between the layers [251]. It is also important to note that, similar to $H_3LiIr_2O_6$, there are significant stacking faults present in the material, with a recent X-ray study suggesting the stacking is almost completely random from one plane to the next [252].

Finally, $Cu_3LiIr_2O_6$ has been realized by replacing the interlayer Li^+ ions with non-magnetic d^{10} Cu^+ cations [242]. Like its parent compound, magnetic susceptibility measurements point towards a magnetic transition at 15 K and a Curie–Weiss fit indicates it shares an almost identical value for the magnetic moment. However, it has a much larger Curie–Weiss temperature of -145 K, as compared to -61 K for Li_2IrO_3. This indicates an enhanced frustration parameter, i.e. a larger ratio of the Curie–Weiss temperature to the ordering temperature [242]. There is still much to be explored regarding the physics of this compound.

2.4.2. Cu_2IrO_3 and $Cu_3NaIr_2O_6$

In 2017, the Tafti group was able to successfully substitute Cu^+ ions into the Na^+ sites of Na_2IrO_3, resulting in the first synthesis of Cu_2IrO_3 [243]. The new compound has the same space group as Na_2IrO_3 but with an increased interlayer spacing and bond angles that are closer to the ideal 120° honeycomb geometry. Above 30 K, it also exhibits a nearly identical magnetic susceptibility, with a similar Curie–Weiss temperature and magnetic moment.

Unlike Na_2IrO_3 it does not exhibit signatures of long-range magnetic order at low temperatures. Rather, there is evidence for only short-range correlations with specific heat exhibiting a broad hump [243,253], μSR measurements indicating persistent spin dynamics and concomitant absence of bulk static magnetism [253,254], and nuclear quadrupole/magnetic resonance measurements suggesting a paramagnetic state with activated behavior for $1/T_1$ [255]. A recent Raman study has also observed an anomalous shift and broadening of the Raman active phonons, which they attribute to phonon decay into itinerant Majorana modes [256].

However, there are reported issues of disorder that prevent a clear attribution of the lack of long-range order to spin liquid physics. A significant fraction of the Cu ions within the honeycomb planes are Cu^{2+}, rather than the desired Cu^+, which can result in the nearby Ir ions becoming nonmagnetic Ir^{3+} [254]. This means that a significant fraction of the honeycomb lattice sites are nonmagnetic, rather than $j = 1/2$, and that there are also additional magnetic $S = 1/2$ Cu^{2+} spins within the planes, see Fig. 19. The resulting combination of site dilution and bond disorder complicates the interpretation of the experimental data in terms of the physics of the pure Kitaev model.

Finally, we note that it has also been possible to grow $Cu_3NaIr_2O_6$ [242]. This compound can be synthesized via an ion exchange reaction in which the interlayer Na^+ ions are replaced by non-magnetic d^{10} Cu^+ cations, just as in the case of $Cu_3LiIr_2O_6$ but with Na_2IrO_3 as the parent compound. The high-temperature portion of the magnetic susceptibility is almost identical to Na_2IrO_3, resulting in a similar Curie–Weiss temperature and magnetic moment. However, at low temperatures, there is a dramatic difference, with a strong enhancement and peak at 10 K indicative of a magnetic transition. On the other hand, specific heat does not exhibit any sharp features down to 2 K. No new magnetic Bragg reflections can be seen at 5 K, as compared to 295 K. This would seem to suggest a spin glass ground state, yet ac susceptibility measurements do not exhibit the expected behavior for a spin-glass transition [242]. The true nature of the 10 K transition and the ground state physics remains to be resolved.

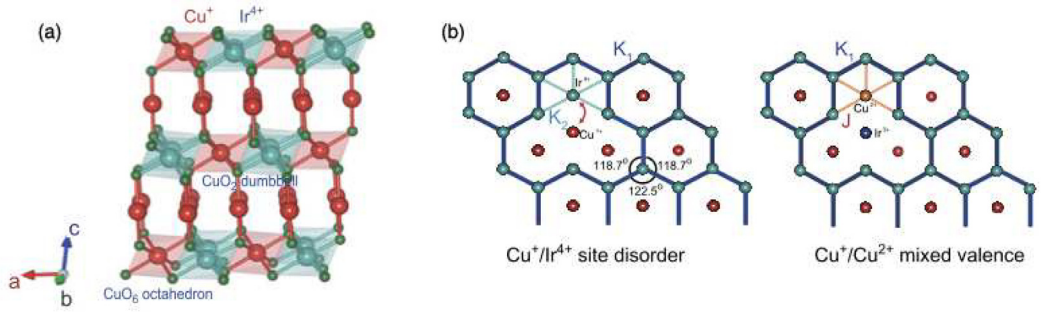

Fig. 19. Disorder in Cu_2IrO_3. (a) Crystal structure. (b) Schematic of the Cu disorder, with Cu^+/Ir^{4+} site disorder and appearance of Cu^{2+}, resulting in magnetic Cu^{2+} state in the centers of the hexagon and nearby nonmagnetic Ir^{3+} on the honeycomb lattice.
Source: Reproduced from Ref. [253].

2.5. Other materials

So far, the honeycomb Kitaev materials that have been discussed all fall under the Jackeli–Khaliullin mechanism, outlined in Section 1.1. However, as was briefly noted in that same section, there have recently been alternative proposals for generating Kitaev interactions amongst spin–orbit entangled $j = 1/2$ moments. The Co-based compounds $Na_2Co_2TeO_6$ [257,258] and $Na_3Co_2SbO_6$ [257] have both received attention recently as Kitaev material candidates based on $j = 1/2$ moments forming from the d^7 configuration of the Co^{2+} ions [28]. Both materials exhibit zigzag magnetic order at low temperatures, with $T_N \approx 27$ K [145,259] and 8 K [260] respectively. Inelastic neutron scattering measurements of their magnetic excitation spectrum seem to fit well with the predictions of a magnetic Hamiltonian that includes dominant Kitaev exchange interactions [261,262], though this is still under debate. Application of a magnetic field to $Na_2Co_2TeO_6$ hints at a field-induced disordered state that could potentially harbor spin liquid physics [263,264]. Though a clear connection to Kitaev physics remains to be fully explored, both compounds represent promising examples of a new set of Kitaev materials beyond the d^5 based compounds focused on so far.

3. Three-dimensional honeycomb Kitaev materials

The exploration of three-dimensional Kitaev materials was kick-started with the independent, but almost concurrent synthesis of two Li_2IrO_3 polymorphs in 2013 – β-Li_2IrO_3 in Takagi's group [172] and γ-Li_2IrO_3 in the group of Analytis [173]. Both polymorphs realize truly three-dimensional, but still tricoordinated sublattices of the iridium $5d^5$ ions, dubbed the hyper-honeycomb and stripy-honeycomb, respectively. As such, these compounds are candidate materials for the realization of three-dimensional Kitaev physics, which we will briefly review in the following before returning to the materials.

3.1. Conceptual overview

On a conceptual level, it has been realized early on that the original honeycomb Kitaev model [19] can be generalized to other lattice structures and retain its analytical tractability if one preserves one essential feature of the honeycomb lattice — the *tricoordination* of its vertices. This idea has been exploited, for instance, by Yao and Kivelson [265] in designing a decorated honeycomb lattice for which the Kitaev model exhibits a *chiral spin liquid* — a distinct gapped spin liquid originally proposed by Kalmeyer and Laughlin in 1987 [266] as a bosonic analogue of the fractional quantum Hall effect.[3] The potential for *three-dimensional* generalizations of the Kitaev model[4] has first been explored by Mandal and Surendran [274] by considering a site-depleted cubic lattice, a tricoordinated lattice structure which turns out to be isomorphic to the hyper-honeycomb lattice later identified in the context of the iridium sublattice in β-Li_2IrO_3. This first three-dimensional generalization of a Kitaev model illustrates that much of the physics of the two-dimensional honeycomb Kitaev models carries over to higher dimensions: The original spin degrees of freedom again fractionalize into Majorana fermions coupled to a Z_2 gauge field. As in the two-dimensional case, the gauge field remains static, which again allows to analytically track the model by (i) solving a basically classical problem identifying the ground state of the Z_2 gauge field and (ii) subsequently diagonalizing a free fermion Hamiltonian describing the physics of the

[3] Microscopic realizations of this long sought-after spin liquid in SU(2) invariant quantum magnets have more recently been established in certain kagome systems [267–270].

[4] Alternative approaches to generalize the Kitaev model to three spatial dimensions also include higher spin generalizations such as a spin-3/2 Kitaev-type model on the diamond lattice [271] as well as initial work [272,273] identifying spin-1/2 Kitaev models on certain three-dimensional, tricoordinated helix lattices.

Table 1
Overview of tricoordinated lattices in two and three spatial dimensions. Each lattice is described by its Schläfli symbol (p, c) identifying the length of the elementary loops (or polygonality) p and tricoordination ($c = 3$). Along with alternative names used in the literature (second column) some basic lattice information is provided: the number of sites in the unit cell (third column), lattice symmetries (fourth and fifth column) and its space group information (last two columns).

Lattice	Alternate names	Sites in unit cell	Inversion symmetry	Non symmorphic	Space group	
					Symbol	No.
(10,3)a	hyperoctagon	4	chiral	✓	$I4_132$	214
(10,3)b	hyperhoneycomb	4	✓	✓	Fddd	70
(10,3)c		6	chiral	✓	$P3_112$	151
(10,3)d		8	✓	✓	Pnna	52
(9,3)a	hypernonagon	12	✓	–	$R\bar{3}m$	166
(8,3)a		6	chiral	✓	$P6_222$	180
(8,3)b	hyperhexagon	6	✓	–	$R\bar{3}m$	166
(8,3)c		8	✓	✓	$P6_3/mmc$	194
(8,3)n		16	✓	–	I4/mmm	139
(6,3)	honeycomb	2	✓	–		

remaining itinerant Majorana fermions (coupled to a fixed gauge field configuration). The result is a gapless spin liquid whose nodal structure is no longer a pair of Dirac cones (as for the two-dimensional honeycomb model), but in fact a *line* of Dirac cones [274]. This result has foreshadowed a more systematic understanding of three-dimensional Kitaev models [275,276] obtained from a systematic classification of the gapless spin liquids in Kitaev models on the most elementary tricoordinated lattices in three spatial dimensions.

In fact, tricoordinated lattices in three spatial dimensions have been exhaustively classified by Wells in the 1970s [277]. The most elementary ones are lattice structures where all plaquettes (i.e. shortest loops within the lattice) have the *same* length (which is also referred to as the polygonality p of the lattice). While for two spatial dimensions there is only one such elementary tricoordinated lattice — the honeycomb lattice of polygonality 6, there are multiple elementary lattices of higher polygonality 8, 9, 10 and higher, which are all three-dimensional. An overview of these elementary tricoordinated lattices is given in Table 1, where each lattice is labeled by its Schläfli symbol $(p, 3)$ and a letter that simply enumerates the lattices for a given Schläfli symbol (the 3 indicates its tricoordination). Fig. 20 illustrates these lattice structures with some of their basic features color-coded (such as the handedness of spirals). For each of these lattice structures there is precisely one assignment of bond-directional Kitaev-type couplings that respects all symmetries of the lattice (up to a trivial permutation among the couplings). The so-defined Kitaev models can all be solved analytically[5] and for all but one lattice, (8,3)n, the ground state is found to be a gapless spin liquid. This state is best described as a *Majorana metal* formed by the itinerant Majorana fermions, while the elementary excitations of the (static) Z_2 gauge field – the visons – are gapped. The precise nature of these Majorana (semi)metals turns out to depend on the underlying lattice geometry and can be captured, e.g. by its nodal manifold [275]. As described for the hyper-honeycomb (corresponding to the (10,3)b lattice in the above classification) considered by Mandal and Surendran [274], this nodal manifold can be a nodal line. Other possibilities for the nodal structure include the formation of Majorana Fermi surfaces [279], nodal chains (in the presence of nonsymmorphic symmetries) [280], or even topologically protected[6] Weyl nodes [281]. Table 2 provides a complete classification of the Majorana metals of all elementary three-dimensional lattices, which notably contains multiple examples each for the emergence of Fermi surfaces, nodal lines, or Weyl nodes for the various lattice structures. For a given lattice, the precise nature of these Majorana metals can in fact be deduced from an elementary symmetry analysis of the projective time-reversal and inversion symmetries as discussed in detail in Ref. [275]. Going beyond these most elementary lattices one might consider, for instance, higher harmonics of a given elementary lattice by systematically enlarging some plaquettes while simultaneously shortening others, see Ref. [173] for further details and showcasing that the stripy-honeycomb lattice is in fact a higher harmonic of the elementary (10,3)b hyper-honeycomb

[5] In all fairness, it should be noted that this is not entirely true in a rigorous sense. While for the two-dimensional honeycomb model the ground state of the Z_2 gauge field can be readily inferred from a theorem of Lieb [278], this is not generically true for the three-dimensional lattices. In fact, only one of the lattices, (8,3)b, strictly allows for the application of the theorem, while for all other lattices one has to resort to alternative means such as Monte Carlo simulations [276]. Thus, in a more rigorous sense, only the Kitaev model on lattice (8,3)b can be solved exactly.

[6] The topological nature of the bulk band structure is also reflected in gapless surface states [275,281,282] such as Fermi arcs for the Weyl spin liquids.

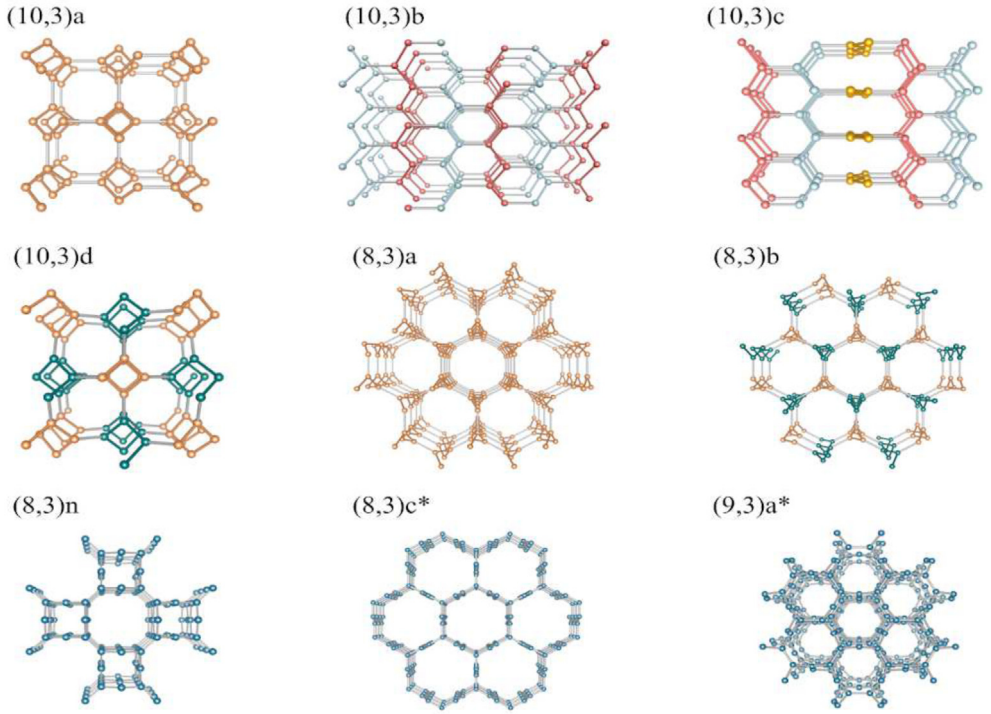

Fig. 20. Illustration of the elementary tricoordinated lattices. Recurring geometric motifs such as spirals and zig-zag chains are color-coded. Further information on these lattices is provided in Table 1.

Table 2
Overview of Majorana metals characterizing the gapless spin liquids in three-dimensional Kitaev models. Depending on the underlying lattice geometry, different Majorana (semi)metals are formed by the itinerant Majorana fermions, which are characterized here via their nodal structures. Results for the pure Kitaev model (5) are given in the second column, while the third column provides information on how the metallic nature (and its nodal structure) changes when time-reversal symmetry (TRS) is broken, e.g. by augmenting the Kitaev model by a magnetic field term (pointing along the 111-direction). The last column indicates whether the metallic state is susceptible to a spin-Peierls instability [283].
Source: Table adapted from Refs. [275] and [276].

Lattice	Majorna metal	Time-reversal symmetry breaking	Peierls instability	Ground-state flux sector	Lieb theorem
(10,3)a	Fermi surface	Fermi surface	✓	0	–
(10,3)b	nodal line	Weyl nodes	–	0	–
(10,3)c	nodal line	Fermi surface	–	0	–
(10,3)d	nodal chain	Weyl nodes	–	0	–
(9,3)a	Weyl nodes	Weyl nodes	–	$\pm\pi/2$	–
(8,3)a	Fermi surface	Fermi surface	✓	π	–
(8,3)b	Weyl nodes	Weyl nodes	✓	π	✓
(8,3)c	nodal line	Weyl nodes	–	frustrated	–
(8,3)n	gapped	gapped	–	π	–
(6,3)	Dirac nodes	gapped	–	0	✓

lattice. The classification scheme described above covers all these higher harmonics as well, as the nature of the emergent Majorana metal remains unchanged going from an elementary lattice to any of its higher harmonics.[7]

[7] This excludes the limiting case of the "infinite harmonic", which in fact is a two-dimensional lattice, e.g. the square-octagon lattice for lattice (10,3)a or the honeycomb lattice for the hyper-honeycomb lattice (10,3)b.

What does change the nature of the Majorana metal for a given lattice though is the application of a magnetic field or, more generally, the breaking of time-reversal symmetry. For the two-dimensional honeycomb lattice a particularly interesting scenario occurs — the Dirac spin liquid gaps out into a massive non-Abelian topological phase when applying a magnetic field along the 111 direction, i.e. a magnetic field that couples to all three spin components

$$H = -\sum_{\gamma-\text{bonds}} K_\gamma \; S_i^\gamma S_j^\gamma - \sum_j \mathbf{h}\cdot\mathbf{S}_j \,, \tag{7}$$

with $\mathbf{h} = h\,(1,\,1,\,1)^t$. Keeping in mind that the Kitaev model reduces to a free (Majorana) fermion model, this scenario can be rationalized by considering the classification of topological insulators [284–286] rooted in the symmetry classification of free-fermion systems [287]. While the unperturbed Kitaev model resides in symmetry class *BDI*, the model with broken time-reversal symmetry is in symmetry class *D* for which the classification scheme of topological insulators indeed points to the possibility of a topologically non-trivial band insulator in two spatial dimensions. For three spatial dimensions, in contrast, this scenario of driving the (non-interacting) Majorana metal into a topologically non-trivial gapped phase is not possible. Instead, it is found that in the presence of a time-reversal symmetry breaking field (again pointing along the 111-direction), the three-dimensional Kitaev models remain gapless, but the nature of the Majorana metal might change. This is, for instance, the case for the nodal line metals, which in the presence of a magnetic field turn either into Weyl semimetals or Weyl metals, i.e. the energy spectrum acquires Weyl nodes in both cases sitting right at the Fermi energy in the first case and above/below the Fermi energy in the second case [275]. The effect of time-reversal symmetry breaking for all Majorana metals is provided in the third column of Table 2.

Three-dimensional Kitaev models distinguish themselves from their two-dimensional counterparts not only with regard to the variety of possible Majorana metals, but also with regard to the physics of their underlying Z_2 gauge theory. One striking difference between two and three spatial dimensions arises when considering the effect of thermal fluctuations on the order of the Z_2 gauge field. In two spatial dimensions such thermal fluctuations immediately melt the zero-temperature order of the Z_2 gauge field, while for three spatial dimensions it takes a critical strength of the thermal fluctuations to destroy the Z_2 order, i.e. there is a *finite-temperature* transition separating a low-temperature Z_2 ordered state from a high-temperature disordered state. The origin for the absence/occurrence of such a finite-temperature transition in two/three spatial dimensions can readily be understood when considering the nature of defects in the low-temperature Z_2 gauge order. In two spatial dimensions, e.g. for the honeycomb lattice, the elementary excitations are point-like vison excitations (associated with the plaquettes of the honeycomb lattice) that can freely move through the lattice (at no additional energy cost) and thereby thread a flux line through the system which destroys the long-range order of the Z_2 gauge field. For three spatial dimensions, the elementary vison excitations form closed flux *loops*, which leads to a competition between their excitation energy and configurational entropy. As a consequence, it takes a finite temperature to drive the system out of a regime of short flux loops into a regime of extended flux lines, which is connected to the paramagnetic high-temperature regime. In the context of the Kitaev model, this Z_2 gauge physics has been nicely demonstrated [276,288–292] via numerically exact quantum Monte Carlo simulations [288] (in the sign-problem free Majorana basis) of the Kitaev model for the entire family of three-dimensional tricoordinated lattices mentioned above. These finite-temperature simulations in fact reveal not only the Z_2 gauge transition at a temperature scale of about

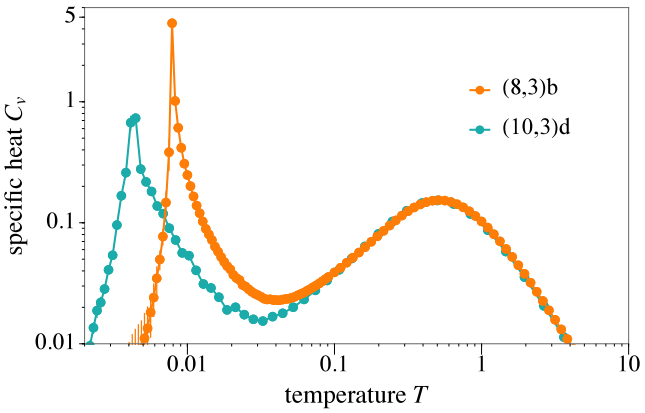

Fig. 21. Typical two-peak signature of the specific heat in three-dimensional Kitaev models, indicating both spin fractionalization (upper crossover peak) and a subsequent Z_2 gauge transition (lower peak), for two representative lattices. A thermal cross-over indicated by a system-size invariant peak at temperature $T \approx 0.6\ K$ (where K is the strength of the Kitaev coupling) reveals the temperature scale at which the original spin degrees of freedom fractionalize into Majorana fermions and a Z_2 gauge field. The latter undergoes an ordering transition indicated by the (diverging) lower-temperature peak at about $T \approx 0.004\ K$. Results shown have been obtained using numerically exact quantum Monte Carlo simulations [288]. *Source:* Figure adapted from Ref. [289].

$T \approx K/1000 - K/100$ (where K is the strength of the Kitaev coupling), but also a thermal cross-over at around $T \approx 0.6\,K$ (i.e. on the bare scale of the Kitaev coupling), which indicates the actual spin fractionalization into Majorana fermions and a Z_2 gauge field, see the two specific heat traces illustrated for two typical 3D lattices in Fig. 21. Some lattices show more peculiar effects with regard to their low-temperature Z_2 gauge structure. Lattice (8,3)c exhibits the phenomenon of "gauge frustration" [291], where an extensive number of Z_2 gauge configurations form a degenerate low-temperature manifold (which is split in an intricate interplay with the collective Majorana fermion state). Lattice (9,3)a stands out as the only three-dimensional lattice with an *odd* number of sites in its elementary loop. As a result, the elementary plaquette flux must be $\pm\pi/2$ for the Majorana fermions (which by the virtue of their complex hopping amplitude pick up a phase of $\pm\pi/2$ per bond when traversing an elementary loop). This in turn implies a spontaneous breaking of time-reversal symmetry in the ground state – akin to the physics of the Yao–Kivelson model on the decorated honeycomb model [265] – with the effect that a three-dimensional chiral spin liquid forms as ground state [292].

The conceptual understanding of three-dimensional Kitaev models has been further expanded by analytical calculations of the dynamical structure factor for the hyper-honeycomb Kitaev model [293] relevant to neutron scattering experiments and the Raman response for both the hyper-honeycomb and stripy-honeycomb Kitaev model [294]. It has been pointed out that signatures of fractionalization of three-dimensional Kitaev spin liquids, with regard to both the gauge and Majorana fermion excitations, can be probed experimentally in resonant inelastic X-ray scattering (RIXS) [295]. The effects of disorder [296] and interactions [283] have been discussed for some of these lattices with the latter allowing for the possibility of a spin-Peierls instability. For the hyper-honeycomb lattice, extensions of the Kitaev model such as a three-dimensional Heisenberg–Kitaev model [120,297–299] and the $JK\Gamma$-model of Eq. (2) have been considered [180]. Finally, we note that beyond the analytically tractable 3D Kitaev models on tricoordinated lattices other 3D Kitaev generalizations for arbitrary lattice geometries [120] have been considered.

Before we turn to candidate Kitaev materials with three-dimensional lattice geometries, we want to close this conceptual overview of 3D Kitaev spin liquids with a few words on their experimental viability. In general, one might argue that the emergence of quantum spin liquid behavior in truly three-dimensional settings is even less likely to occur than in two dimensional systems as quantum fluctuations are less potent in three spatial dimensions than in two or one dimensional lattice geometries. While this is indisputably right, it remains an open question whether the effect of magnetic frustration might still tip the balance to the formation of 3D quantum spin liquids as it is broadly discussed, e.g., in the context of geometric frustration in pyrochlore spin ice systems [300,301]. Whether this also holds for the exchange frustration present in 3D Kitaev materials remains to be seen. On the upside, some signatures of spin liquid physics are *more* pronounced in three spatial dimensions than in two — for instance, the Z_2 lattice gauge structure in Kitaev spin liquids will lead to a true thermodynamic phase transition (with a clear experimental signature in the specific heat) as opposed to two dimensional geometries (as discussed above).

3.2. β-Li_2IrO_3 and γ-Li_2IrO_3

The two Li_2IrO_3 polymorphs β-Li_2IrO_3 [172] and γ-Li_2IrO_3 [173] are the first truly three-dimensional Kitaev materials — realizing as illustrated in Fig. 22 a hyper-honeycomb and stripy-honeycomb lattice of edge-sharing IrO_6 octahedra, respectively. Independently synthesized almost at the same time, they are found to exhibit rather similar physics. Both systems are spin–orbit entangled Mott insulators with effective moments of 1.6(1) μ_B close to the value of 1.73 μ_B for an ideal $j = 1/2$ moment. Susceptibility fits indicate strong ferromagnetic interactions with estimates of the Curie–Weiss temperature found to be $\Theta_{\mathrm{CW}} \sim 40$ K (β) and $\Theta_{\mathrm{CW}} \sim 75$ K (γ), respectively. They both order at around $T_N \sim 38$ K into non-collinear magnetic order. Resonant magnetic X-ray diffraction experiments [302,303] on about 17–100 μm wide single crystals identify this non-collinear magnetic ordering with non-coplanar, counter-rotating long range spin spirals with an incommensurate ordering wave vector $q = (0.57, 0, 0)$ along the orthorhombic a axis in both materials. This unusual *counter-rotating* spiral order in these three-dimensional Li_2IrO_3-polymorphs is thus very similar to the one (subsequently) observed in the original honeycomb material α-Li_2IrO_3.

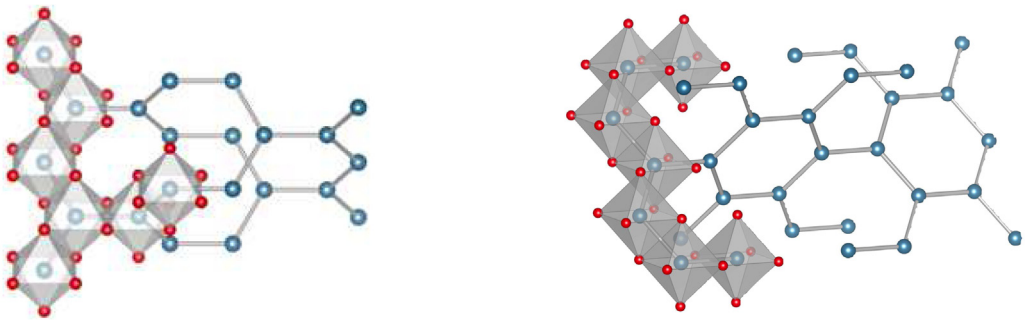

Fig. 22. Crystal structure of the hyper-honeycomb Kitaev material β-Li_2IrO_3 (left) and stripy-honeycomb Kitaev material γ-Li_2IrO_3 (right).

From a theoretical perspective, the two three-dimensional Li_2IrO_3 polymorphs have been investigated via ab initio calculations supporting the $j = 1/2$ picture and dominant Kitaev-type bond-directional coupling [304,305], which for the case of γ-Li_2IrO_3, further argue [306] for a reduced symmetry of the local Ir–O–Ir environment (possibly giving rise to rather complex magnetic interactions) to explain the anisotropic behavior observed in optical conductivity measurements [307] for different polarizations. The origin of the magnetic ordering has been scrutinized based on a Heisenberg–Kitaev–Ising model [179,298] and $JK\Gamma$-model [180,181,297] leading to a unifying theoretical framework [179,181] for the spiral magnetism in all three Li_2IrO_3 polymorphs and their dynamics [308].

More recent experimental studies have argued for evidence of (Majorana) fermion quasiparticles in the Raman scattering [309], employing similar arguments as presented above in some detail for the Raman signatures of α-$RuCl_3$, and the observation that a magnetic field with a small component along the magnetic easy-axis melts the magnetic long-range order, first argued to reveal a bistable, strongly correlated spin state [310,311]. In further theoretical treatment, the nature of this state was identified with a commensurate spin order with six spin sublattices (and the zero-field incommensurate state as a long-distance twisting of this nearby commensurate order), which can be captured within the framework of the $JK\Gamma$ model [312,313]. Follow-up magnetic-field experiments [314–316] have revealed that the elementary magnons of the zero-field incommensurately ordered state β-Li_2IrO_3 are gapless (and not gapped as, e.g., the zero-field zig-zag order in α-$RuCl_3$). Beyond a critical field strength of $H_c \approx 2.8$ T, the commensurate state exhibits massive magnons with the magnon gap increasing linearly with magnetic field strength [315].

High-pressure experiments, theoretically argued to drive the three-dimensional Kitaev material closer to the spin liquid regime [317], have revealed that a strong dimerization [318] (induced by pressure) breaks up the local spin–orbit entangled $j = 1/2$ moments and stabilizes a bonding molecular-orbital state of neighboring d orbitals in the Ir-O_2-Ir bond plane, experimentally observed both in resonant inelastic X-ray scattering (RIXS) [319,320] as well as Raman spectroscopy experiments [321].

3.3. Other 3D materials

We close by mentioning other materials scrutinized as three-dimensional Kitaev materials. Spin–orbit entangled Mott insulators where the local $j = 1/2$ moments form a face-centered cubic (fcc) lattice geometry have been scrutinized first in La_2BIrO_6 (B=Mg,Zn) [323,324] and, more recently, in K_2IrCl_6 [325] and Ba_2CeIrO_6 [322,326]. Based on resonant inelastic X-ray scattering (RIXS) experiments, the latter material has been argued to be an almost ideal $j = 1/2$ system (with less than 1% admixture of other spin–orbital states to the ground-state wavefunction) [322], which shows an unexpectedly strong magnetoelastic effect, see Fig. 23. The microscopic interplay of these pristine $j = 1/2$ moments in Ba_2CeIrO_6 is characterized by competing nearest and next-nearest Heisenberg coupling (J_1 and J_2), which on the underlying fcc lattice leads to geometric frustration that manifests itself, for certain parameters and on the classical level, in(subextensive) ground-state manifolds of spin spiral states, see Fig. 24. Interestingly, an additional bond-directional Kitaev interaction is found to counteract this frustration and induce magnetic ordering commensurate with the experimental observation of antiferromagnetic order below $T_N = 14$ K. In passing, we mention the sister material $Ba_3CeIr_2O_9$, where the Iridium ions form a quasi-molecular electronic structure that has been probed in "double split" experiments using resonant inelastic X-ray scattering (RIXS) experiments [327].

On a more theoretical footing, it has been suggested [328] to synthesize metal–organic compounds such as honeycomb Ru-oxalate frameworks that might realize tricoordinated lattice structures in three spatial dimensions beyond the hyper-honeycomb (and its higher harmonics) such as the (10,3)a hyper-octagon lattice [279]. Finally, also the hyperkagome material $Na_4Ir_3O_8$ [329] has attracted some renewed interest [330,331] exploring the role of Kitaev-type interactions.

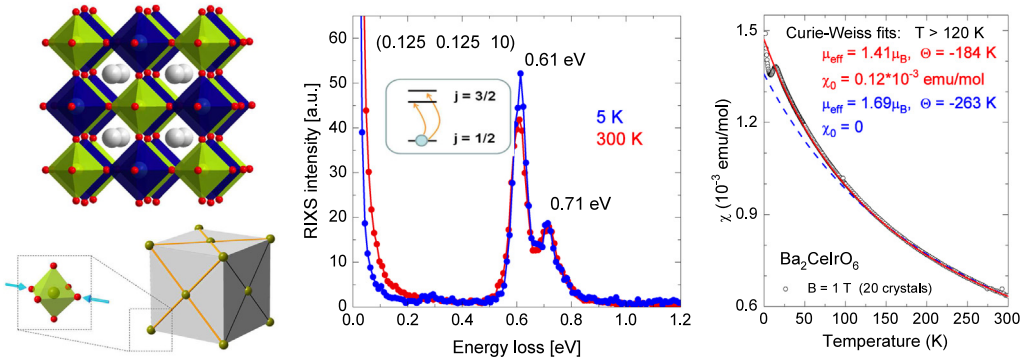

Fig. 23. In the spin–orbit entangled Mott insulator Ba_2CeIrO_6 the local $j = 1/2$ moments form a face-centered cubic (fcc) lattice (left panel). The pristine nature of these $j = 1/2$ moments (with very low admixture from other spin–orbit entangled moments) has been revealed resonant inelastic X-ray scattering (RIXS) experiments (middle panel). Below $T_N = 14$ K these moments order antiferromagnetically, as seen in the susceptibility trace (right panel). Unusual for a $j = 1/2$ system Ba_2CeIrO_6 exhibits a strong magnetoelastic effect (illustrated on the lower left).
Source: Figure adopted from Ref. [322].

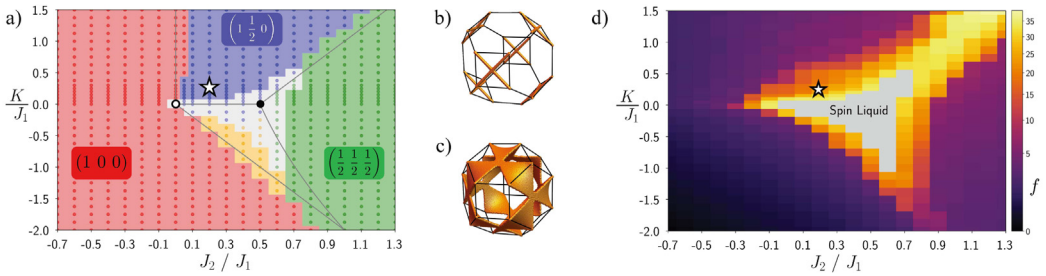

Fig. 24. Competing nearest and next-nearest Heisenberg coupling (J_1 and J_2) on the face-centered cubic (fcc) lattice gives rise to geometric frustration, which for certain parameters can lead to (subextensive) ground-state manifolds of spin spiral states (b–c). Interestingly, an additional bond-directional Kitaev interaction is found to counteract this frustration and induce magnetic ordering as indicated in the phase diagram (a) of the left panel. The central spin liquid region (gray area) is identified via a maximal suppression of the magnetic ordering as illustrated by a color coding of the frustration parameter $f = T_N/\Theta_{\rm CW}$ in the right panel (d).
Source: Figure adopted from Ref. [322].

4. Other lattice geometries

4.1. Triangular Kitaev materials

Beyond the search for spin liquids, Kitaev materials also provide ample opportunity to study other unconventional forms of magnetism. A particularly interesting class might be materials in which $j = 1/2$ moments form quasi-two-dimensional *triangular* lattice structures. Such a scenario has been proposed [332] for the family of hexagonal perovskites $Ba_3Ir_xTi_{3-x}O_9$, in particular the sister compounds $Ba_3IrTi_2O_9$ ($x = 1$) [333] and $Ba_3TiIr_2O_9$ ($x = 2$) [334]. This has drawn interest to the triangular Heisenberg–Kitaev model, for which the interplay of geometric and exchange frustration leads to the formation of non-trivial spin textures [332,335], such as the formation of a Z_2-vortex crystal induced by the Kitaev couplings that destabilize the 120° order of the (antiferromagnetic) quantum Heisenberg model. Extensions to a full $J-K-\Gamma$ model on the triangular lattice have recently been explored in Ref. [336]

4.1.1. $Ba_3Ir_xTi_{3-x}O_9$

The 2012 synthesis of $Ba_3IrTi_2O_9$ ($x = 1$) by the group of Mahajan [333] marks the discovery of what might be the first triangular $j = 1/2$ Mott insulator. It is now recognized as the first representative of a family of hexagonal $j = 1/2$ iridium perovskite-like structures of the form $Ba_3Ir_xTi_{3-x}O_9$, of which various members with $1 \leq x \leq 2$ have been synthesized over the last years [337]. The crystal structure of these compounds – which are found to exhibit hexagonal space group symmetries $P6_3mc$ ($x = 1$) [333] or $P6_3/mmc$ ($x = 2$) [334], respectively – is illustrated in Fig. 25. Generically, the structure is composed of three layers of [Ir/TiO_6] octahedra, two of which form a double-layer of face-sharing Ir_2O_9 bioctahedra (indicated by the blue octahedra) and a single layer (indicated by the light brown octahedra). The occupation of the octahedral sites in the different layers with Ir^{4+} and Ti^{4+} ions is complicated by the fact that the two ions have rather similar radii and the same valence. For $Ba_3Ir_2TiO_9$, it is found that the iridium ions fill all octahedral sites in the double-layer [334], which are then well separated by a single layer of (non-magnetic) titanium ions. For $Ba_3IrTi_2O_9$ a more complicated picture emerges with the iridium ions still preferably occupying octahedral sites in one of two double-layers, but a significant amount of site inversion ($37 \pm 10\%$) with the titanium ions from the other double-layer has been reported [333].

Magnetic susceptibility, heat capacity data [333] and muon spin relaxation data [338] for $Ba_3IrTi_2O_9$ show no magnetic ordering down to 23 *mK* in spite of a strong antiferromagnetic coupling as evidenced by a large Curie–Weiss temperature $\Theta_{CW} \sim -130\ K$. The effective moment is theoretically argued to be a spin–orbit entangled $j = 1/2$ moment (on the basis of ab initio calculations [339]), despite the considerable suppression of the experimentally determined magnetic moment of $1.09\ \mu_B$ [333].

The unconventional magnetism of spin–orbit entangled $j = 1/2$ moments on a triangular lattice again arises from the presence of bond-directional exchange couplings. On a microscopic level, it has been argued [332] that the arrangement of the IrO_6 octahedra within the layers, depicted in Fig. 26, fulfills the two necessary ingredients for Kitaev-type interactions. First, neighboring octahedra exhibit parallel edges, which gives rise to two separate exchange paths for every pair of iridium ions. As in the case of edge-sharing IrO_6 octahedra, this leads to a destructive interference and subsequent suppression of the isotropic Heisenberg exchange [7,9,40]. Second, there are three distinct exchange paths for the three principal bond directions of the triangular lattice, with each cutting through *different* edges of the IrO_6 octahedra. This results in a distinct locking of the exchange easy axis [7,9,40] along the three principal lattice directions as illustrated in Fig. 26. Since the Ir layer is normal to the 111 direction (see the left panel in Fig. 26), the strength of the bond-directional coupling is equivalent in all three directions. Ultimately, this gives rise to the bond-directional exchange of a triangular Kitaev model. In total, these microscopic considerations lead to a triangular Heisenberg–Kitaev model as a very

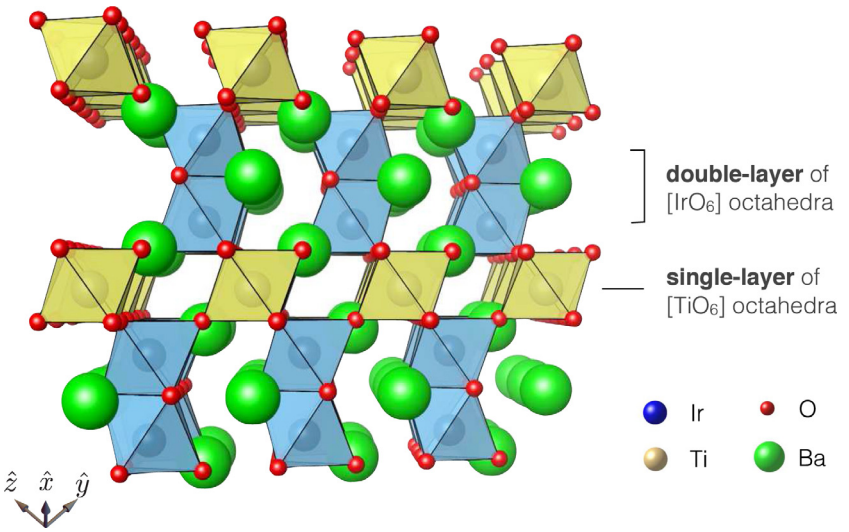

Fig. 25. Crystal structure of $Ba_3Ir_2TiO_9$ [334], a candidate material for the realization of a triangular Kitaev material.

promising candidate for the description of the magnetism in $Ba_3IrTi_2O_9$. Ab initio calculations [339] complete this picture by arguing that in addition a symmetric off-diagonal exchange Γ should be considered along with the possible emergence of a Dzyaloshinskii–Moriya (DM) exchange term arising from distortions in the oxygen octahedra, which break inversion symmetry about the Ir–Ir bond center.

One of the prevalent features of the magnetism of the triangular Heisenberg–Kitaev model is the emergence of non-trivial spin textures [332,335]. The Kitaev exchange destabilizes the 120° order of the Heisenberg antiferromagnet and induces a lattice of Z_2-vortices [335] whose spatial separation is inversely proportional to the strength of the Kitaev coupling (independent of its sign). The resulting phase diagram of the Heisenberg–Kitaev model has been explored both in its classical [335,340] and quantum [43,332,341–344] variants using a combination of analytical and numerical techniques. A summary, based on the comprehensive density matrix renormalization group (DMRG) work of Ref. [343] is given in Fig. 27. We note that these DMRG calculations have revealed that an extended nematic phase, argued for and informed by a semiclassical perspective in Refs. [332,335,339,342,345], is in fact not present in the quantum variant of the triangular Heisenberg–Kitaev model, but reduces to the phase boundary between two magnetically ordered phases. In addition, these DMRG studies argue for an extended spin liquid regime between the spin textured phase of the (antiferromagnetic) Heisenberg model with weak Kitaev interactions and the stripe phase around the (antiferromagnetic) Kitaev model (and their duals), see the phase diagram of Fig. 27.

Finally, we note that other non-trivial spin textures beyond the Z_2-vortex crystal can be stabilized by spin–orbit coupling effects. For instance, a Dzyaloshinskii–Moriya (DM) exchange also destabilizes the 120° order of the Heisenberg antiferromagnet and instead favors the formation of a skyrmion crystal in the presence of a magnetic field [346–348].

Returning to the family of $Ba_3Ir_xTi_{3-x}O_9$ materials, it would be most intriguing to experimentally establish the emergence of non-trivial spin textures in $Ba_3IrTi_2O_9$. This, however, requires high-quality single crystals (without the aforementioned Ir/Ti site inversion) that would allow for inelastic neutron scattering experiments. The magnetism of the sister compound $Ba_3TiIr_2O_9$ is probably dominated by the formation of dimers in the Iridium double-layer and is currently being explored both theoretically and experimentally.

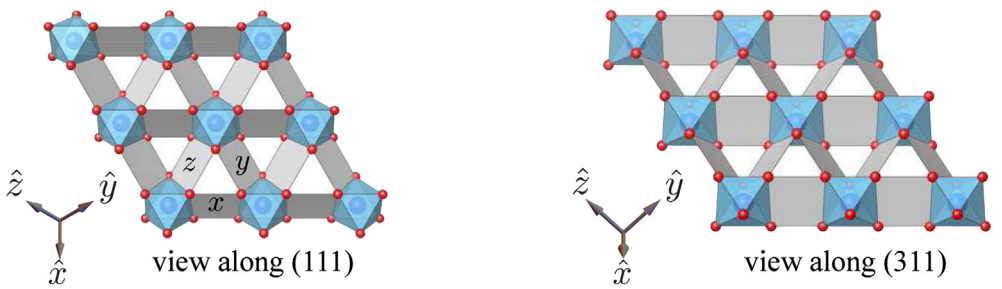

Fig. 26. Views of the triangular layer of IrO_6 octahedra from two different perspectives.

Fig. 27. The phase diagram of the triangular Heisenberg–Kitaev model, obtained from large-scale density matrix renormalization group (DMRG) calculations [343] exhibits distinct types of magnetic order. Around the 120° order of the Heisenberg antiferromagnet, one finds spin textures that can be described as three-sublattice intertwined crystals of Z_2-vortices (as illustrated for one sublattice in the right panel). Around the antiferromagnetic Kitaev point an extended region of stripe order forms. Between these two magnetically ordered phase an extended spin liquid (SL) regime opens up. The dashed lines indicate Klein-dual points in the phase diagram, thereby connecting all phases on the right-hand side with their duals on the left-hand side.
Source: The left panel is reproduced from Ref. [343], the right panel from Ref. [332].

4.2. Other materials

Recently, a new family of hexagonal $j = 1/2$ iridium perovskites of the form $Ba_3MIr_2O_9$ with $M = (Sc, Y)$ has been experimentally explored [349,350]. In contrast to the $Ba_3Ir_xTi_{3-x}O_9$ compounds, the (average) iridium valence here is $Ir^{4.5+}$. This possibly leads to a scenario where in each double-layer one has one effective spin–orbit entangled $j = 1/2$ moment per face-sharing Ir_2O_9 bioctahedra [35]. As argued above, the latter are coupled via three distinct parallel (bi)octahedral edges and as such the effective $j = 1/2$ moments are likely subject to a bond-directional exchange. While both $Ba_3ScIr_2O_9$ and $Ba_3YIr_2O_9$ have been reported to exhibit magnetic ordering at around 10 K (Sc) and 4.5 K (Y), respectively, the closely related $Ir^{4.5+}$-compound $Ba_3InIr_2O_9$ [334] does not exhibit any sign of magnetic ordering down to 250 mK [351] and, thus, is a potential $j = 1/2$ spin liquid candidate system.

Another related spin liquid candidate material is the recently synthesized ruthenate $Ba_3ZnRu_2O_9$ [352], in which a hexagonal lattice of Ru^{5+} dimers (with $S = 3/2$) forms in the double-layer of face-sharing Ru_2O_9 bioctahedra. The absence of long-range magnetic order down to 37 mK along with a linear specific heat [352] indicate the possible formation of a spin liquid in this material, which would be remarkable given the rather large effective magnetic moment of $S = 3/2$.

5. Outlook

Before taking a look at the road ahead, it is very much worthwhile to note that in the years since the original 2009 proposal for Kitaev physics in the $4d^5$ and $5d^5$ transition metals [9] experimental progress has been made at an incredible pace. Not only have several Kitaev materials with different two- and three-dimensional lattice geometries been synthesized and firmly established as $j = 1/2$ spin–orbit entangled Mott insulators, but there has also been a streak of impressive experimental findings that most notably have provided direct evidence for bond-directional Kitaev-type interactions [167] in the first Kitaev material Na_2IrO_3, and, in the case of α-$RuCl_3$, have established the notion of a "proximate spin liquid" regime and have even suggested the emergence of a true quantum spin liquid state under application of a magnetic field. This includes experimental evidence of fermionic excitations in Raman scattering of a magnetic insulator [206–208], a number of highly unusual signatures in inelastic neutron scattering (above the magnetic ordering transition) that have been attributed to the proximity of spin liquid physics [146,147], and the reported observation of a half-integer quantized thermal Hall conductance [228]. On the way, the unconventional magnetism of spin–orbit entangled $j = 1/2$ moments in the Li_2IrO_3 polymorphs has been elucidated as a rare example of counter-rotating spin spirals [176].

As the field keeps moving with unflagging momentum, many novel materials are expected to take center stage in the coming years. Within the family of iridates, the hydrogen-intercalated honeycomb material $H_3LiIr_2O_6$ [353] will undoubtedly receive much attention for its apparent spin liquid behavior. Other members of the so-called "second-generation" of Kitaev materials also await a full experimental and theoretical understanding. Beyond the iridates, other $5d^5$ oxides await experimental scrutiny such as the recently synthesized honeycomb rhodate Li_2RhO_3 [354–358]. One of the most exciting recent developments has been the new proposals for realizing Kitaev interactions beyond the original Jackeli–Khaliullin d^5-based mechanism. This allows for a welcome expansion of the materials search, including d^7-based transition metal compounds such as $Na_2Co_2TeO_6$ and $Na_3Co_2SbO_6$. Higher-spin versions of the Kitaev model may even be accessible within d^8-based compounds. In further broadening the search for Kitaev materials, it may also be worthwhile to look beyond $4d$ and $5d$ transition metals and consider rare-earth magnets [359] whose $4f$ electrons are much more

localized than the 5*d* or 4*d* electrons in iridates and ruthenates and at the same time experience a considerably stronger spin–orbit coupling — thus potentially providing another path to Kitaev materials in the future. New materials which realize antiferromagnetic Kitaev interactions, in contrast to the ferromagnetic interactions believed to occur in the current set of known Kitaev materials, will be particularly welcome both as a means to explore a new area of the extended phase diagrams and for their distinct in-field properties. At the level of materials synthesis, the search for Kitaev materials readily continues unabated. Further impetus for the field might come from *engineering* novel materials, such as the recent synthesis of $RuCl_3$ / graphene heterostructures [360–362]. The interplay of a Dirac semimetal and Kitaev magnetism is expected [363–365] to drive novel quantum many-body phenomena — either by enhancing the formation of spin liquid physics in $RuCl_3$ through spatial proximity to a semimetal or, vice versa, by imprinting the electronic state of the Dirac metal with the physics of fractionalized degrees of freedom in a proximate spin liquid.

On a conceptual level, interest in Kitaev materials is spurred by their promise to realize what is a truly dichotomous state – a spin–orbit entangled *Mott insulator*, in which the emergent degrees of freedom are Majorana fermions that form an (almost) conventional *metal*. These emergent Majorana metals exhibit distinct (topological) band structures [19,275] including the formation of Fermi surfaces, nodal lines, and Weyl nodes in three-dimensional settings along with the Dirac nodes of the originally proposed honeycomb system. Outside of the potential for fractionalization, the study of Kitaev materials, with their inherent bond-directional interactions and concomitant absence of spin-rotational symmetry, also provides a platform for studying the more conventional physics of quantum magnets, such as magnon dynamics or spin–phonon coupling, in an unconventional setting. It forces one to reevaluate intuition and results based on more familiar Heisenberg interacting systems and thus expands the horizon of the whole field.

Declaration of competing interest

The authors declare that they have no known competing financial interests or personal relationships that could have appeared to influence the work reported in this paper.

Acknowledgments

S.T. thanks his various collaborators on Kitaev physics over the years, first and foremost M. Hermanns along with B. Bauer, M. Becker, C. Berke, F. L. Buessen, G. Chen, T. Disselkamp, V. Dwivedi, T. Eschmann, K. O'Brien, M. Garst, M. Gerlach, M. Gohlke, M. Grüninger, Z.-C. Gu, H.-C. Jiang, Y. Kasahara, Y. Kato, H.Y. Kee, D. Kiese, V. Lahtinen, A. W. W. Ludwig, Y. Matsuda, Y. Motome, J. K. Pachos, X.-L. Qi, A. Rivelli, J. Reuther, A. Rosch, E. Sela, and R. Thomale, as well as P. Gegenwart along with experimental collaborators T. Berlijn, W. Ku, S. Manni, Y. Singh, and P. van Loosdrecht. C.H. would like to thank C. Berke, G. Chen, V. Dwivedi, M. Gohlke, M. Grüninger, Y. Kasahara, H.Y. Kee, Y.B. Kim, Y. Matsuda, J.G. Rau, A. Revelli, R. Schaffer, J.A. Sears, P. van Loosdrecht, and S.M. Winter for fruitful discussions and collaborations on Kitaev physics. We gratefully acknowledge support by the DFG, Germany – project number 277146847 – within the CRC 1238 (projects C02, C03).

References

[1] D. Pesin, L. Balents, Mott physics and band topology in materials with strong spin-orbit interaction, Nat. Phys. 6 (2010) 376–381.
[2] M.Z. Hasan, C.L. Kane, *Colloquium* : Topological insulators, Rev. Modern Phys. 82 (2010) 3045–3067.
[3] X.-L. Qi, S.-C. Zhang, Topological insulators and superconductors, Rev. Modern Phys. 83 (2011) 1057–1110.
[4] X. Wan, A.M. Turner, A. Vishwanath, S.Y. Savrasov, Topological semimetal and Fermi-arc surface states in the electronic structure of pyrochlore iridates, Phys. Rev. B 83 (2011) 205101.
[5] B. Yan, C. Felser, Topological materials: Weyl semimetals, Ann. Rev. Condens. Matter Phys. 8 (2017) 11.1.
[6] W. Witczak-Krempa, G. Chen, Y.B. Kim, L. Balents, Correlated quantum phenomena in the strong spin-orbit regime, Ann. Rev. Condens. Matter Phys. 5 (2014) 57–82.
[7] G. Khaliullin, Orbital order and fluctuations in mott insulators, Progr. Theoret. Phys. Suppl. 160 (2005) 155–202.
[8] G. Chen, L. Balents, Spin-orbit effects in $Na_4Ir_3O_8$: A hyper-kagome lattice antiferromagnet, Phys. Rev. B 78 (2008) 094403.
[9] G. Jackeli, G. Khaliullin, Mott insulators in the strong spin-orbit coupling limit: From heisenberg to a quantum compass and Kitaev models, Phys. Rev. Lett. 102 (2009) 017205.
[10] B.J. Kim, H. Jin, S.J. Moon, J.-Y. Kim, B.-G. Park, C.S. Leem, J. Yu, T.W. Noh, C. Kim, S.-J. Oh, J.-H. Park, V. Durairaj, G. Cao, E. Rotenberg, Novel $J_{\text{eff}} = 1/2$ mott state induced by relativistic spin-orbit coupling in Sr_2IrO_4, Phys. Rev. Lett. 101 (2008) 076402.
[11] B.J. Kim, H. Ohsumi, T. Komesu, S. Sakai, T. Morita, H. Takagi, T. Arima, Phase-sensitive observation of a spin-orbital mott state in Sr2IrO4, Science 323 (2009) 1329–1332.
[12] Y.K. Kim, O. Krupin, J.D. Denlinger, A. Bostwick, E. Rotenberg, Q. Zhao, J.F. Mitchell, J.W. Allen, B.J. Kim, Fermi arcs in a doped pseudospin-1/2 heisenberg antiferromagnet, Science 345 (2014) 187–190.
[13] A. de la Torre, S. McKeown Walker, F.Y. Bruno, S. Riccó, Z. Wang, I. Gutierrez Lezama, G. Scheerer, G. Giriat, D. Jaccard, C. Berthod, T.K. Kim, M. Hoesch, E.C. Hunter, R.S. Perry, A. Tamai, F. Baumberger, Collapse of the mott gap and emergence of a nodal liquid in lightly doped Sr_2IrO_4, Phys. Rev. Lett. 115 (2015) 176402.
[14] Y. Cao, Q. Wang, J.A. Waugh, T.J. Reber, H. Li, X. Zhou, S. Parham, S.R. Park, N.C. Plumb, E. Rotenberg, A. Bostwick, J.D. Denlinger, T. Qi, M.A. Hermele, G. Cao, D.S. Dessau, Hallmarks of the mott-metal crossover in the hole-doped pseudospin-1/2 mott insulator Sr2IrO4, Nature Commun. 7 (2016) 11367.
[15] Y.K. Kim, N.H. Sung, J.D. Denlinger, B.J. Kim, Observation of a d-wave gap in electron-doped Sr2IrO4, Nat. Phys. 12 (2016) 37–41.
[16] Y.J. Yan, M.Q. Ren, H.C. Xu, B.P. Xie, R. Tao, H.Y. Choi, N. Lee, Y.J. Choi, T. Zhang, D.L. Feng, Electron-doped Sr_2IrO_4: An analogue of hole-doped cuprate superconductors demonstrated by scanning tunneling microscopy, Phys. Rev. X 5 (2015) 041018.

[17] L. Balents, Spin liquids in frustrated magnets, Nature 464 (2010) 199.
[18] L. Savary, L. Balents, Quantum spin liquids: a review, Rep. Progr. Phys. 80 (2017) 016502.
[19] A. Kitaev, Anyons in an exactly solved model and beyond, Ann. Physics 321 (2006) 2–111.
[20] G. Chen, R. Pereira, L. Balents, Exotic phases induced by strong spin-orbit coupling in ordered double perovskites, Phys. Rev. B 82 (2010) 174440.
[21] W.M.H. Natori, E.C. Andrade, E. Miranda, R.G. Pereira, Chiral spin-orbital liquids with nodal lines, Phys. Rev. Lett. 117 (2016) 017204.
[22] J. Romhányi, L. Balents, G. Jackeli, Spin-orbit dimers and noncollinear phases in d^1 cubic double perovskites, Phys. Rev. Lett. 118 (2017) 217202.
[23] M.G. Yamada, M. Oshikawa, G. Jackeli, Emergent SU(4) symmetry in $\alpha-ZrCl_3$ and crystalline spin-orbital liquids, Phys. Rev. Lett. 121 (2018) 097201.
[24] W.M.H. Natori, E.C. Andrade, R.G. Pereira, Su(4)-symmetric spin-orbital liquids on the hyperhoneycomb lattice, Phys. Rev. B 98 (2018) 195113.
[25] G. Khaliullin, Excitonic magnetism in van vleck–type d^4 mott insulators, Phys. Rev. Lett. 111 (2013) 197201.
[26] Z. Nussinov, J. van den Brink, Compass models: Theory and physical motivations, Rev. Modern Phys. 87 (2015) 1–59.
[27] K.I. Kugel', D.I. Khomskii, The Jahn-Teller effect and magnetism: transition metal compounds, Sov. Phys. Uspekhi 25 (1982) 231.
[28] H. Liu, G. Khaliullin, Pseudospin exchange interactions in d^7 cobalt compounds: Possible realization of the Kitaev model, Phys. Rev. B 97 (2018) 014407.
[29] R. Sano, Y. Kato, Y. Motome, Kitaev-Heisenberg Hamiltonian for high-spin d^7 mott insulators, Phys. Rev. B 97 (2018) 014408.
[30] S.-H. Jang, R. Sano, Y. Kato, Y. Motome, Antiferromagnetic Kitaev interaction in f-electron based honeycomb magnets, Phys. Rev. B 99 (2019) 241106.
[31] S.-H. Jang, R. Sano, Y. Kato, Y. Motome, Computational design of f-electron Kitaev magnets: Honeycomb and hyperhoneycomb compounds A_2PrO_3 ($A =$ alkali metals), Phys. Rev. Mater. 4 (2020) 104420.
[32] Y. Motome, R. Sano, S. Jang, Y. Sugita, Y. Kato, Materials design of Kitaev spin liquids beyond the Jackeli–Khaliullin mechanism, J. Phys.: Condens. Matter 32 (40) (2020) 404001.
[33] P.P. Stavropoulos, D. Pereira, H.-Y. Kee, Microscopic mechanism for a higher-spin Kitaev model, Phys. Rev. Lett. 123 (2019) 037203.
[34] C. Xu, J. Feng, M. Kawamura, Y. Yamaji, Y. Nahas, S. Prokhorenko, Y. Qi, H. Xiang, L. Bellaiche, Possible Kitaev quantum spin liquid state in 2D materials with $S = 3/2$, Phys. Rev. Lett. 124 (2020) 087205.
[35] S.V. Streltsov, D.I. Khomskii, Covalent bonds against magnetism in transition metal compounds, Proc. Natl. Acad. Sci. 113 (2016) 10491–10496.
[36] J. Terzic, J.C. Wang, F. Ye, W.H. Song, S.J. Yuan, S. Aswartham, L.E. DeLong, S.V. Streltsov, D.I. Khomskii, G. Cao, Coexisting charge and magnetic orders in the dimer-chain iridate $Ba_5AlIr_2O_{11}$, Phys. Rev. B 91 (2015) 235147.
[37] J.G. Rau, E.K.-H. Lee, H.-Y. Kee, Generic spin model for the honeycomb iridates beyond the Kitaev limit, Phys. Rev. Lett. 112 (2014) 077204.
[38] J.G. Rau, E.K.-H. Lee, H.-Y. Kee, Spin-orbit physics giving rise to novel phases in correlated systems: Iridates and related materials, Ann. Rev. Condens. Matter Phys. 7 (2016) 195–221.
[39] J.G. Rau, H.-Y. Kee, Trigonal distortion in the honeycomb iridates: Proximity of zigzag and spiral phases in Na2IrO3, 2014, http://arxiv.org/abs/1408.4811.
[40] J. Chaloupka, G. Jackeli, G. Khaliullin, Kitaev-Heisenberg model on a honeycomb lattice: Possible exotic phases in iridium oxides A_2IrO_3, Phys. Rev. Lett. 105 (2010) 027204.
[41] V.M. Katukuri, S. Nishimoto, V. Yushankhai, A. Stoyanova, H. Kandpal, S. Choi, R. Coldea, I. Rousochatzakis, L. Hozoi, J. van den Brink, Kitaev interactions between j=1/2 moments in honeycomb na_2iro_3 are large and ferromagnetic: insights from ab initio quantum chemistry calculations, New J. Phys. 16 (1) (2014) 013056.
[42] J. Chaloupka, G. Khaliullin, Hidden symmetries of the extended Kitaev-Heisenberg model: Implications for the honeycomb-lattice iridates A_2IrO_3, Phys. Rev. B 92 (2015) 024413.
[43] Y. Li, H. Liao, Z. Zhang, S. Li, F. Jin, L. Ling, L. Zhang, Y. Zou, L. Pi, Z. Yang, J. Wang, Z. Wu, Q. Zhang, Gapless quantum spin liquid ground state in the two-dimensional spin-1/2 triangular antiferromagnet YbMgGaO4, Sci. Rep. 5 (1) (2015) 16419.
[44] Y. Li, P. Gegenwart, A.A. Tsirlin, Spin liquids in geometrically perfect triangular antiferromagnets, J. Phys.: Condens. Matter 32 (22) (2020) 224004.
[45] K.A. Ross, L. Savary, B.D. Gaulin, L. Balents, Quantum excitations in quantum spin ice, Phys. Rev. X 1 (2011) 021002.
[46] H. Yan, O. Benton, L. Jaubert, N. Shannon, Theory of multiple-phase competition in pyrochlore magnets with anisotropic exchange with application to $Yb_2Ti_2O_7$, $Er_2Ti_2O_7$, and $Er_2Sn_2O_7$, Phys. Rev. B 95 (2017) 094422.
[47] J.D. Thompson, P.A. McClarty, D. Prabhakaran, I. Cabrera, T. Guidi, R. Coldea, Quasiparticle breakdown and spin Hamiltonian of the frustrated quantum pyrochlore $Yb_2Ti_2O_7$ in a magnetic field, Phys. Rev. Lett. 119 (2017) 057203.
[48] J.G. Rau, M.J. Gingras, Frustrated quantum rare-earth pyrochlores, Annu. Rev. Condens. Matter Phys. 10 (1) (2019) 357–386.
[49] P.A. Maksimov, A.L. Chernyshev, Rethinking $\alpha - RuCl_3$, Phys. Rev. Res. 2 (2020) 033011.
[50] S. Chandra, K. Ramola, D. Dhar, Classical Heisenberg spins on a hexagonal lattice with Kitaev couplings, Phys. Rev. E 82 (2010) 031113.
[51] E. Sela, H.-C. Jiang, M.H. Gerlach, S. Trebst, Order-by-disorder and spin-orbital liquids in a distorted Heisenberg-Kitaev model, Phys. Rev. B 90 (2014) 035113.
[52] C.L. Henley, The "Coulomb phase" in frustrated systems, Ann. Rev. Condens. Matter Phys. 1 (2010) 179.
[53] A.Y. Kitaev, Fault-tolerant quantum computation by anyons, Ann. Physics 303 (2003) 2–30.
[54] N. Read, D. Green, Paired states of fermions in two dimensions with breaking of parity and time-reversal symmetries and the fractional quantum Hall effect, Phys. Rev. B 61 (2000) 10267–10297.
[55] G. Moore, N. Read, Nonabelions in the fractional quantum Hall effect, Nuclear Phys. B 360 (1991) 362–396.
[56] L. Fu, C.L. Kane, Superconducting proximity effect and majorana Fermions at the surface of a topological insulator, Phys. Rev. Lett. 100 (2008) 096407.
[57] J.D. Sau, R.M. Lutchyn, S. Tewari, S. Das Sarma, Generic new platform for topological quantum computation using semiconductor heterostructures, Phys. Rev. Lett. 104 (2010) 040502.
[58] J. Alicea, Y. Oreg, G. Refael, F. von Oppen, M.P.A. Fisher, Non-Abelian statistics and topological quantum information processing in 1D wire networks, Nat Phys 7 (2011) 412–417.
[59] R.M. Lutchyn, J.D. Sau, S. Das Sarma, Majorana Fermions and a topological phase transition in semiconductor-superconductor heterostructures, Phys. Rev. Lett. 105 (2010) 077001.
[60] Y. Oreg, G. Refael, F. von Oppen, Helical liquids and majorana bound states in quantum wires, Phys. Rev. Lett. 105 (2010) 177002.
[61] C. Nayak, S.H. Simon, A. Stern, M. Freedman, S. Das Sarma, Non-abelian anyons and topological quantum computation, Rev. Modern Phys. 80 (2008) 1083–1159.
[62] P.E. Lammert, D.S. Rokhsar, J. Toner, Topology and nematic ordering, Phys. Rev. Lett. 70 (1993) 1650–1653.
[63] N. Read, S. Sachdev, Large-N expansion for frustrated quantum antiferromagnets, Phys. Rev. Lett. 66 (1991) 1773–1776.
[64] T. Senthil, M.P.A. Fisher, Z_2 Gauge theory of electron fractionalization in strongly correlated systems, Phys. Rev. B 62 (2000) 7850–7881.
[65] X.-G. Wen, Quantum orders and symmetric spin liquids, Phys. Rev. B 65 (2002) 165113.

[66] M. Hermanns, I. Kimchi, J. Knolle, Physics of the Kitaev model: Fractionalization, dynamic correlations, and material connections, Ann. Rev. Condens. Matter Phys. 9 (1) (2018) 17–33.
[67] Y. Motome, J. Nasu, Hunting majorana Fermions in Kitaev magnets, J. Phys. Soc. Japan 89 (1) (2020) 012002.
[68] A.J. Willans, J.T. Chalker, R. Moessner, Disorder in a quantum spin liquid: Flux binding and local moment formation, Phys. Rev. Lett. 104 (2010) 237203.
[69] A.J. Willans, J.T. Chalker, R. Moessner, Site dilution in the Kitaev honeycomb model, Phys. Rev. B 84 (2011) 115146.
[70] E.C. Andrade, M. Vojta, Magnetism in spin models for depleted honeycomb-lattice iridates: Spin-glass order towards percolation, Phys. Rev. B 90 (2014) 205112.
[71] M. Vojta, A.K. Mitchell, F. Zschocke, Kondo impurities in the Kitaev spin liquid: Numerical renormalization group solution and gauge-flux-driven screening, Phys. Rev. Lett. 117 (2016) 037202.
[72] V. Lahtinen, A.W.W. Ludwig, S. Trebst, Perturbed vortex lattices and the stability of nucleated topological phases, Phys. Rev. B 89 (2014) 085121.
[73] F. Zschocke, M. Vojta, Physical states and finite-size effects in Kitaev's honeycomb model: Bond disorder, spin excitations, and NMR line shape, Phys. Rev. B 92 (2015) 014403.
[74] J. Nasu, Y. Motome, Thermodynamic and transport properties in disordered Kitaev models, Phys. Rev. B 102 (2020) 054437.
[75] W.-H. Kao, N.B. Perkins, Disorder upon disorder: Localization effects in the Kitaev spin liquid, Annals of Physics 435, Part 2 (2021) 168506.
[76] G. Baskaran, D. Sen, R. Shankar, Spin-*S* Kitaev model: Classical ground states, order from disorder, and exact correlation functions, Phys. Rev. B 78 (2008) 115116.
[77] I. Rousochatzakis, Y. Sizyuk, N.B. Perkins, Quantum spin liquid in the semiclassical regime, Nature Commun. 9 (1) (2018) 1575.
[78] X.-Y. Feng, G.-M. Zhang, T. Xiang, Topological characterization of quantum phase transitions in a spin-1/2 model, Phys. Rev. Lett. 98 (2007) 087204.
[79] S. Mandal, R. Shankar, G. Baskaran, RVB gauge theory and the topological degeneracy in the honeycomb Kitaev model, J. Phys. A 45 (33) (2012) 335304.
[80] J. Fu, J. Knolle, N.B. Perkins, Three types of representation of spin in terms of Majorana fermions and an alternative solution of the Kitaev honeycomb model, Phys. Rev. B 97 (2018) 115142.
[81] S. Rachel, L. Fritz, M. Vojta, Landau levels of majorana Fermions in a spin liquid, Phys. Rev. Lett. 116 (2016) 167201.
[82] A. Agarwala, S. Bhattacharjee, J. Knolle, R. Moessner, Gapless state of interacting Majorana fermions in a strain-induced Landau level, Phys. Rev. B 103 (2021) 134427.
[83] C. Gils, E. Ardonne, S. Trebst, A.W.W. Ludwig, M. Troyer, Z. Wang, Collective states of interacting anyons, edge states, and the nucleation of topological liquids, Phys. Rev. Lett. 103 (2009) 070401.
[84] A.W.W. Ludwig, D. Poilblanc, S. Trebst, M. Troyer, Two-dimensional quantum liquids from interacting non-Abelian anyons, New J. Phys. 13 (2011) 045014.
[85] V. Lahtinen, A.W.W. Ludwig, J.K. Pachos, S. Trebst, Topological liquid nucleation induced by vortex-vortex interactions in Kitaev's honeycomb model, Phys. Rev. B 86 (2012) 075115.
[86] T. Hyart, A.R. Wright, G. Khaliullin, B. Rosenow, Competition between *d*-wave and topological *p*-wave superconducting phases in the doped Kitaev-Heisenberg model, Phys. Rev. B 85 (2012) 140510.
[87] Y.-Z. You, I. Kimchi, A. Vishwanath, Doping a spin-orbit Mott insulator: Topological superconductivity from the Kitaev-Heisenberg model and possible application to $(Na_2/Li_2)IrO_3$, Phys. Rev. B 86 (2012) 085145.
[88] F. Trousselet, P. Horsch, A.M. Oleś, W.-L. You, Hole propagation in the Kitaev-Heisenberg model: From quasiparticles in quantum Néel states to non-Fermi liquid in the Kitaev phase, Phys. Rev. B 90 (2014) 024404.
[89] G.B. Halász, J.T. Chalker, R. Moessner, Doping a topological quantum spin liquid: Slow holes in the Kitaev honeycomb model, Phys. Rev. B 90 (2014) 035145.
[90] A. Koga, H. Tomishige, J. Nasu, Ground-state and thermodynamic properties of an S=1 Kitaev model, J. Phys. Soc. Japan 87 (6) (2018) 063703.
[91] H.-Y. Lee, N. Kawashima, Y.B. Kim, Tensor network wave function of $S = 1$ Kitaev spin liquids, Phys. Rev. Res. 2 (2020) 033318.
[92] I. Khait, P.P. Stavropoulos, H.-Y. Kee, Y.B. Kim, Characterizing spin-one Kitaev quantum spin liquids, Phys. Rev. Res. 3 (2021) 013160.
[93] X.-Y. Dong, D.N. Sheng, Spin-1 Kitaev-Heisenberg model on a honeycomb lattice, Phys. Rev. B 102 (2020) 121102.
[94] O. Bradley, R.R.P. Singh, Instabilities of spin-one Kitaev Spin Liquid phase in presence of single-ion anisotropies, 2021, http://arxiv.org/abs/2108.05040.
[95] H.-K. Jin, W.M.H. Natori, F. Pollmann, J. Knolle, Unveiling the S=3/2 Kitaev honeycomb spin liquids, 2021, http://arxiv.org/abs/2107.13364.
[96] J. Knolle, D.L. Kovrizhin, J.T. Chalker, R. Moessner, Dynamics of a two-dimensional quantum spin liquid: Signatures of emergent majorana Fermions and fluxes, Phys. Rev. Lett. 112 (2014) 207203.
[97] J. Knolle, D.L. Kovrizhin, J.T. Chalker, R. Moessner, Dynamics of fractionalization in quantum spin liquids, Phys. Rev. B 92 (2015) 115127.
[98] J. Yoshitake, J. Nasu, Y. Kato, Y. Motome, Majorana dynamical mean-field study of spin dynamics at finite temperatures in the honeycomb Kitaev model, Phys. Rev. B 96 (2017) 024438.
[99] J. Yoshitake, J. Nasu, Y. Motome, Temperature evolution of spin dynamics in two- and three-dimensional Kitaev models: Influence of fluctuating Z_2 flux, Phys. Rev. B 96 (2017) 064433.
[100] J. Knolle, G.-W. Chern, D.L. Kovrizhin, R. Moessner, N.B. Perkins, Raman scattering signatures of Kitaev spin liquids in A_2IrO_3 iridates with A=Na or li, Phys. Rev. Lett. 113 (2014) 187201.
[101] B. Perreault, S. Rachel, F.J. Burnell, J. Knolle, Majorana Landau-level Raman spectroscopy, Phys. Rev. B 95 (2017) 184429.
[102] B. Perreault, J. Knolle, N.B. Perkins, F.J. Burnell, Resonant Raman scattering theory for Kitaev models and their majorana fermion boundary modes, Phys. Rev. B 94 (2016) 104427.
[103] J. Yoshitake, J. Nasu, Y. Motome, Fractional spin fluctuations as a precursor of quantum spin liquids: Majorana dynamical mean-field study for the Kitaev model, Phys. Rev. Lett. 117 (2016) 157203.
[104] M. Ye, R.M. Fernandes, N.B. Perkins, Phonon dynamics in the Kitaev spin liquid, Phys. Rev. Res. 2 (2020) 033180.
[105] J. Nasu, J. Yoshitake, Y. Motome, Thermal transport in the Kitaev model, Phys. Rev. Lett. 119 (2017) 127204.
[106] G.B. Halász, N.B. Perkins, J. van den Brink, Resonant inelastic X-Ray scattering response of the Kitaev honeycomb model, Phys. Rev. Lett. 117 (2016) 127203.
[107] G.B. Halász, S. Kourtis, J. Knolle, N.B. Perkins, Observing spin fractionalization in the Kitaev spin liquid via temperature evolution of indirect resonant inelastic x-ray scattering, Phys. Rev. B 99 (2019) 184417.
[108] C. Hickey, S. Trebst, Emergence of a field-driven U(1) spin liquid in the Kitaev honeycomb model, Nature Commun. 10 (1) (2019) 530.
[109] H.-C. Jiang, Z.-C. Gu, X.-L. Qi, S. Trebst, Possible proximity of the mott insulating iridate Na_2IrO_3 to a topological phase: Phase diagram of the Heisenberg-Kitaev model in a magnetic field, Phys. Rev. B 83 (2011) 245104.
[110] S. Fey, Field-driven instabilities of the non-abelian topological phase in the Kitaev model, (MSc Thesis), Technische UniversitÄT Dortmund, 2013.

[111] Z. Zhu, I. Kimchi, D.N. Sheng, L. Fu, Robust non-Abelian spin liquid and a possible intermediate phase in the antiferromagnetic Kitaev model with magnetic field, Phys. Rev. B 97 (2018) 241110.
[112] J. Nasu, Y. Kato, Y. Kamiya, Y. Motome, Successive Majorana topological transitions driven by a magnetic field in the Kitaev model, Phys. Rev. B 98 (2018) 060416.
[113] S. Liang, M.-H. Jiang, W. Chen, J.-X. Li, Q.-H. Wang, Intermediate gapless phase and topological phase transition of the Kitaev model in a uniform magnetic field, Phys. Rev. B 98 (2018) 054433.
[114] M. Gohlke, R. Moessner, F. Pollmann, Dynamical and topological properties of the Kitaev model in a [111] magnetic field, Phys. Rev. B 98 (2018) 014418.
[115] H.-C. Jiang, C.-Y. Wang, B. Huang, Y.-M. Lu, Field induced quantum spin liquid with spinon Fermi surfaces in the Kitaev model, 2018, preprint at https://arxiv.org/abs/1809.08247.
[116] C. Hickey, C. Berke, P.P. Stavropoulos, H.-Y. Kee, S. Trebst, Field-driven gapless spin liquid in the spin-1 Kitaev honeycomb model, Phys. Rev. Res. 2 (2020) 023361.
[117] N.D. Patel, N. Trivedi, Magnetic field-induced intermediate quantum spin liquid with a spinon Fermi surface, Proc. Natl. Acad. Sci. 116 (25) (2019) 12199–12203.
[118] F.J. Burnell, C. Nayak, Su(2) slave fermion solution of the Kitaev honeycomb lattice model, Phys. Rev. B 84 (2011) 125125.
[119] J. Chaloupka, G. Jackeli, G. Khaliullin, Zigzag magnetic order in the iridium oxide Na_2IrO_3, Phys. Rev. Lett. 110 (2013) 097204.
[120] I. Kimchi, A. Vishwanath, Kitaev-heisenberg models for iridates on the triangular, hyperkagome, kagome, fcc, and pyrochlore lattices, Phys. Rev. B 89 (2014) 014414.
[121] J. Reuther, R. Thomale, S. Trebst, Finite-temperature phase diagram of the Heisenberg-Kitaev model, Phys. Rev. B 84 (2011) 100406.
[122] M. Gohlke, R. Verresen, R. Moessner, F. Pollmann, Dynamics of the Kitaev-Heisenberg model, Phys. Rev. Lett. 119 (2017) 157203.
[123] I. Kimchi, Y.-Z. You, Kitaev-Heisenberg-J_2-J_3 model for the iridates A_2IrO_3, Phys. Rev. B 84 (2011) 180407.
[124] I. Rousochatzakis, J. Reuther, R. Thomale, S. Rachel, N.B. Perkins, Phase diagram and quantum order by disorder in the Kitaev K_1-K_2 honeycomb magnet, Phys. Rev. X 5 (2015) 041035.
[125] R. Schaffer, S. Bhattacharjee, Y.B. Kim, Quantum phase transition in Heisenberg-Kitaev model, Phys. Rev. B 86 (2012) 224417.
[126] X.-Y. Song, Y.-Z. You, L. Balents, Low-energy spin dynamics of the honeycomb spin liquid beyond the Kitaev limit, Phys. Rev. Lett. 117 (2016) 037209.
[127] J. Knolle, S. Bhattacharjee, R. Moessner, Dynamics of a quantum spin liquid beyond integrability: The Kitaev-Heisenberg-Γ model in an augmented parton mean-field theory, Phys. Rev. B 97 (2018) 134432.
[128] S.-S. Zhang, G.B. Halász, W. Zhu, C.D. Batista, Variational study of the Kitaev-Heisenberg-Gamma model, Phys. Rev. B 104 (2021) 014411.
[129] J. Nasu, Y. Kato, J. Yoshitake, Y. Kamiya, Y. Motome, Spin-liquid–to–spin-liquid transition in Kitaev magnets driven by fractionalization, Phys. Rev. Lett. 118 (2017) 137203.
[130] M. Laubach, J. Reuther, R. Thomale, S. Rachel, Three-band Hubbard model for Na_2IrO_3: Topological insulator, zigzag antiferromagnet, and Kitaev-Heisenberg material, Phys. Rev. B 96 (2017) 121110.
[131] C.C. Price, N.B. Perkins, Critical properties of the Kitaev-Heisenberg model, Phys. Rev. Lett. 109 (2012) 187201.
[132] C. Price, N.B. Perkins, Finite-temperature phase diagram of the classical Kitaev-Heisenberg model, Phys. Rev. B 88 (2013) 024410.
[133] L. Janssen, E.C. Andrade, M. Vojta, Honeycomb-lattice Heisenberg-Kitaev model in a magnetic field: Spin canting, metamagnetism, and vortex crystals, Phys. Rev. Lett. 117 (2016) 277202.
[134] G.-W. Chern, Y. Sizyuk, C. Price, N.B. Perkins, Kitaev-Heisenberg model in a magnetic field: Order-by-disorder and commensurate-incommensurate transitions, Phys. Rev. B 95 (2017) 144427.
[135] P. McClarty, Topological magnons: A review, Annual Review of Condensed Matter Physics 13 (2022).
[136] D.G. Joshi, Topological excitations in the ferromagnetic Kitaev-Heisenberg model, Phys. Rev. B 98 (2018) 060405.
[137] L. Chen, J.-H. Chung, B. Gao, T. Chen, M.B. Stone, A.I. Kolesnikov, Q. Huang, P. Dai, Topological spin excitations in honeycomb ferromagnet CrI_3, Phys. Rev. X 8 (2018) 041028.
[138] I. Rousochatzakis, N.B. Perkins, Classical spin liquid instability driven by off-diagonal exchange in strong spin-orbit magnets, Phys. Rev. Lett. 118 (2017) 147204.
[139] P. Saha, Z. Fan, D. Zhang, G.-W. Chern, Hidden plaquette order in a classical spin liquid stabilized by strong off-diagonal exchange, Phys. Rev. Lett. 122 (2019) 257204.
[140] A. Catuneanu, Y. Yamaji, G. Wachtel, Y.B. Kim, H.-Y. Kee, Path to stable quantum spin liquids in spin-orbit coupled correlated materials, Npj Quant. Mater. 3 (1) (2018) 23.
[141] M. Gohlke, G. Wachtel, Y. Yamaji, F. Pollmann, Y.B. Kim, Quantum spin liquid signatures in Kitaev-like frustrated magnets, Phys. Rev. B 97 (2018) 075126.
[142] Q. Luo, J. Zhao, H.-Y. Kee, X. Wang, Gapless quantum spin liquid in a honeycomb Γ magnet, npj Quantum Mater. 6 (2021) 57.
[143] D.A. Tennant, T.G. Perring, R.A. Cowley, S.E. Nagler, Unbound spinons in the S=1/2 antiferromagnetic chain $KCuF_3$, Phys. Rev. Lett. 70 (1993) 4003–4006.
[144] B. Lake, D.A. Tennant, J.-S. Caux, T. Barthel, U. Schollwöck, S.E. Nagler, C.D. Frost, Multispinon continua at zero and finite temperature in a near-ideal heisenberg chain, Phys. Rev. Lett. 111 (2013) 137205.
[145] A.K. Bera, B. Lake, F.H.L. Essler, L. Vanderstraeten, C. Hubig, U. Schollwöck, A.T.M.N. Islam, A. Schneidewind, D.L. Quintero-Castro, Spinon confinement in a quasi-one-dimensional anisotropic heisenberg magnet, Phys. Rev. B 96 (2017) 054423.
[146] A. Banerjee, C.A. Bridges, J.Q. Yan, A.A. Aczel, L. Li, M.B. Stone, G.E. Granroth, M.D. Lumsden, Y. Yiu, J. Knolle, S. Bhattacharjee, D.L. Kovrizhin, R. Moessner, D.A. Tennant, D.G. Mandrus, S.E. Nagler, Proximate Kitaev quantum spin liquid behaviour in a honeycomb magnet, Nat. Mater. 15 (2016) 733–740.
[147] A. Banerjee, J. Yan, J. Knolle, C.A. Bridges, M.B. Stone, M.D. Lumsden, D.G. Mandrus, D.A. Tennant, R. Moessner, S.E. Nagler, Neutron scattering in the proximate quantum spin liquid α-$RuCl_3$, Science 356 (6342) (2017) 1055–1059.
[148] H. Takagi, Private communication, 2009.
[149] Y. Singh, P. Gegenwart, Antiferromagnetic Mott insulating state in single crystals of the honeycomb lattice material Na_2IrO_3, Phys. Rev. B 82 (2010) 064412.
[150] A. Shitade, H. Katsura, J. Kuneš, X.-L. Qi, S.-C. Zhang, N. Nagaosa, Quantum spin hall effect in a transition metal oxide Na_2IrO_3, Phys. Rev. Lett. 102 (2009) 256403.
[151] F. Ye, S. Chi, H. Cao, B.C. Chakoumakos, J.A. Fernandez-Baca, R. Custelcean, T.F. Qi, O.B. Korneta, G. Cao, Direct evidence of a zigzag spin-chain structure in the honeycomb lattice: A neutron and x-ray diffraction investigation of single-crystal na_2iro_3, Phys. Rev. B 85 (2012) 180403.
[152] R. Comin, G. Levy, B. Ludbrook, Z.-H. Zhu, C.N. Veenstra, J.A. Rosen, Y. Singh, P. Gegenwart, D. Stricker, J.N. Hancock, D. van der Marel, I.S. Elfimov, A. Damascelli, Na_2IrO_3 as a novel relativistic mott insulator with a 340-meV Gap, Phys. Rev. Lett. 109 (2012) 266406.
[153] Y. Singh, S. Manni, J. Reuther, T. Berlijn, R. Thomale, W. Ku, S. Trebst, P. Gegenwart, Relevance of the Heisenberg-Kitaev model for the honeycomb lattice iridates A_2IrO_3, Phys. Rev. Lett. 108 (2012) 127203.

[154] C.H. Sohn, H.-S. Kim, T.F. Qi, D.W. Jeong, H.J. Park, H.K. Yoo, H.H. Kim, J.-Y. Kim, T.D. Kang, D.-Y. Cho, G. Cao, J. Yu, S.J. Moon, T.W. Noh, Mixing between $J_{\text{eff}} = \frac{1}{2}$ and $\frac{3}{2}$ orbitals in Na_2IrO_3: A spectroscopic and density functional calculation study, Phys. Rev. B 88 (2013) 085125.

[155] H. Gretarsson, J.P. Clancy, X. Liu, J.P. Hill, E. Bozin, Y. Singh, S. Manni, P. Gegenwart, J. Kim, A.H. Said, D. Casa, T. Gog, M.H. Upton, H.-S. Kim, J. Yu, V.M. Katukuri, L. Hozoi, J. van den Brink, Y.-J. Kim, Crystal-field splitting and correlation effect on the electronic structure of A_2IrO_3, Phys. Rev. Lett. 110 (2013) 076402.

[156] H. Gretarsson, J.P. Clancy, Y. Singh, P. Gegenwart, J.P. Hill, J. Kim, M.H. Upton, A.H. Said, D. Casa, T. Gog, Y.-J. Kim, Magnetic excitation spectrum of Na_2IrO_3 probed with resonant inelastic x-ray scattering, Phys. Rev. B 87 (2013) 220407.

[157] B. Andlauer, J. Schneider, W. Tolksdorf, Optical absorption, fluorescence, and electron spin resonance of Ir4+ on octahedral sites in Y3ga5o12, Phys. Status Solidi (B) 73 (1976) 533–540.

[158] K. Blazey, F. Levy, EPR of rhodium, osmium and iridium-doped rutile, Solid State Commun. 59 (1986) 335–338.

[159] X. Liu, T. Berlijn, W.-G. Yin, W. Ku, A. Tsvelik, Y.-J. Kim, H. Gretarsson, Y. Singh, P. Gegenwart, J.P. Hill, Long-range magnetic ordering in Na_2IrO_3, Phys. Rev. B 83 (2011) 220403.

[160] S.K. Choi, R. Coldea, A.N. Kolmogorov, T. Lancaster, I.I. Mazin, S.J. Blundell, P.G. Radaelli, Y. Singh, P. Gegenwart, K.R. Choi, S.-W. Cheong, P.J. Baker, C. Stock, J. Taylor, Spin waves and revised crystal structure of honeycomb iridate Na_2IrO_3, Phys. Rev. Lett. 108 (2012) 127204.

[161] Y. Sizyuk, C. Price, P. Wölfle, N.B. Perkins, Importance of anisotropic exchange interactions in honeycomb iridates: Minimal model for zigzag antiferromagnetic order in Na_2IrO_3, Phys. Rev. B 90 (2014) 155126.

[162] Y. Sizyuk, P. Wölfle, N.B. Perkins, Selection of direction of the ordered moments in Na_2IrO_3 and $\alpha - RuCl_3$, Phys. Rev. B 94 (2016) 085109.

[163] I.I. Mazin, H.O. Jeschke, K. Foyevtsova, R. Valentí, D.I. Khomskii, Na_2IrO_3 as a molecular orbital crystal, Phys. Rev. Lett. 109 (2012) 197201.

[164] K. Foyevtsova, H.O. Jeschke, I.I. Mazin, D.I. Khomskii, R. Valentí, *Ab initio* analysis of the tight-binding parameters and magnetic interactions in Na_2IrO_3, Phys. Rev. B 88 (2013) 035107.

[165] I.I. Mazin, S. Manni, K. Foyevtsova, H.O. Jeschke, P. Gegenwart, R. Valentí, Origin of the insulating state in honeycomb iridates and rhodates, Phys. Rev. B 88 (2013) 035115.

[166] J. Yoshitake, J. Nasu, Y. Motome, Fractional spin fluctuations as a precursor of quantum spin liquids: Majorana dynamical mean-field study for the Kitaev model, Phys. Rev. Lett. 117 (2016) 157203.

[167] S. Hwan Chun, J.-W. Kim, J. Kim, H. Zheng, C.C. Stoumpos, C.D. Malliakas, J.F. Mitchell, K. Mehlawat, Y. Singh, Y. Choi, T. Gog, A. Al-Zein, M.M. Sala, M. Krisch, J. Chaloupka, G. Jackeli, G. Khaliullin, B.J. Kim, Direct evidence for dominant bond-directional interactions in a honeycomb lattice iridate Na_2IrO_3, Nat. Phys. 11 (2015) 462–466.

[168] J. Kim, J.c.v. Chaloupka, Y. Singh, J.W. Kim, B.J. Kim, D. Casa, A. Said, X. Huang, T. Gog, Dynamic spin correlations in the honeycomb lattice Na_2IrO_3 measured by resonant inelastic x-ray scattering, Phys. Rev. X 10 (2020) 021034.

[169] A. Revelli, M. Moretti Sala, G. Monaco, C. Hickey, P. Becker, F. Freund, A. Jesche, P. Gegenwart, T. Eschmann, F.L. Buessen, S. Trebst, P.H.M. van Loosdrecht, J. van den Brink, M. Grüninger, Fingerprints of Kitaev physics in the magnetic excitations of honeycomb iridates, Phys. Rev. Res. 2 (2020) 043094.

[170] Y. Yamaji, T. Suzuki, T. Yamada, S.-i. Suga, N. Kawashima, M. Imada, Clues and criteria for designing a Kitaev spin liquid revealed by thermal and spin excitations of the honeycomb iridate Na_2IrO_3, Phys. Rev. B 93 (2016) 174425.

[171] S.M. Winter, Y. Li, H.O. Jeschke, R. Valentí, Challenges in design of Kitaev materials: Magnetic interactions from competing energy scales, Phys. Rev. B 93 (2016) 214431.

[172] T. Takayama, A. Kato, R. Dinnebier, J. Nuss, H. Kono, L.S.I. Veiga, G. Fabbris, D. Haskel, H. Takagi, Hyperhoneycomb iridate β—Li_2IrO_3 as a platform for Kitaev magnetism, Phys. Rev. Lett. 114 (2015) 077202.

[173] K.A. Modic, T.E. Smidt, I. Kimchi, N.P. Breznay, A. Biffin, S. Choi, R.D. Johnson, R. Coldea, P. Watkins-Curry, G.T. McCandless, J.Y. Chan, F. Gandara, Z. Islam, A. Vishwanath, A. Shekhter, R.D. McDonald, J.G. Analytis, Realization of a three-dimensional spin–anisotropic harmonic honeycomb iridate, Nature Commun. 5 (2014) 4203.

[174] M. Jenderka, R. Schmidt-Grund, M. Grundmann, M. Lorenz, Electronic excitations and structure of Li2IrO3 thin films grown on ZrO_2:Y (001) substrates, J. Appl. Phys. 117 (2015) 025304.

[175] F. Freund, S.C. Williams, R.D. Johnson, R. Coldea, P. Gegenwart, A. Jesche, Single crystal growth from separated educts and its application to lithium transition-metal oxides, Sci. Rep. 6 (2016) 35362.

[176] S.C. Williams, R.D. Johnson, F. Freund, S. Choi, A. Jesche, I. Kimchi, S. Manni, A. Bombardi, P. Manuel, P. Gegenwart, R. Coldea, Incommensurate counterrotating magnetic order stabilized by Kitaev interactions in the layered honeycomb α—Li_2IrO_3, Phys. Rev. B 93 (2016) 195158.

[177] J. Reuther, R. Thomale, S. Rachel, Spiral order in the honeycomb iridate Li_2IrO_3, Phys. Rev. B 90 (2014) 100405.

[178] S. Nishimoto, V.M. Katukuri, V. Yushankhai, H. Stoll, U.K. Rößler, L. Hozoi, I. Rousochatzakis, J. van den Brink, Strongly frustrated triangular spin lattice emerging from triplet dimer formation in honeycomb Li2IrO3, Nature Commun. 7 (2016) 10273.

[179] I. Kimchi, R. Coldea, A. Vishwanath, Unified theory of spiral magnetism in the harmonic-honeycomb iridates α, β, and γ Li_2IrO_3, Phys. Rev. B 91 (2015) 245134.

[180] E.K.-H. Lee, Y.B. Kim, Theory of magnetic phase diagrams in hyperhoneycomb and harmonic-honeycomb iridates, Phys. Rev. B 91 (2015) 064407.

[181] E.K.-H. Lee, J.G. Rau, Y.B. Kim, Two iridates, two models, and two approaches: A comparative study on magnetism in three-dimensional honeycomb materials, Phys. Rev. B 93 (2016) 184420.

[182] L. Binotto, I. Pollini, G. Spinolo, Optical and transport properties of the magnetic semiconductor α-$RuCl_3$, Phys. Status Solidi (B) 44 (1971) 245–252.

[183] I. Pollini, Electronic properties of the narrow-band material $\alpha - RuCl_3$, Phys. Rev. B 53 (1996) 12769–12776.

[184] K.W. Plumb, J.P. Clancy, L.J. Sandilands, V.V. Shankar, Y.F. Hu, K.S. Burch, H.-Y. Kee, Y.-J. Kim, $\alpha - RuCl_3$: A spin-orbit assisted Mott insulator on a honeycomb lattice, Phys. Rev. B 90 (2014) 041112.

[185] X. Zhou, H. Li, J.A. Waugh, S. Parham, H.-S. Kim, J.A. Sears, A. Gomes, H.-Y. Kee, Y.-J. Kim, D.S. Dessau, Angle-resolved photoemission study of the Kitaev candidate $\alpha - RuCl_3$, Phys. Rev. B 94 (2016) 161106.

[186] L.J. Sandilands, Y. Tian, A.A. Reijnders, H.-S. Kim, K.W. Plumb, Y.-J. Kim, H.-Y. Kee, K.S. Burch, Spin-orbit excitations and electronic structure of the putative Kitaev magnet $\alpha - RuCl_3$, Phys. Rev. B 93 (2016) 075144.

[187] B.N. Figgis, J. Lewis, F.E. Mabbs, G.A. Webb, Magnetic properties of some iron(III) and ruthenium(III) low-spin complexes, J. Chem. Soc. A (1966) 422–426.

[188] Y. Kobayashi, T. Okada, K. Asai, M. Katada, H. Sano, F. Ambe, Moessbauer spectroscopy and magnetization studies of .alpha.- and .beta.-ruthenium trichloride, Inorg. Chem. 31 (1992) 4570–4574.

[189] J.M. Fletcher, W.E. Gardner, A.C. Fox, G. Topping, X-Ray, infrared, and magnetic studies of α- and β-ruthenium trichloride, J. Chem. Soc. A (1967) 1038–1045.

[190] A. Koitzsch, C. Habenicht, E. Müller, M. Knupfer, B. Büchner, H.C. Kandpal, J. van den Brink, D. Nowak, A. Isaeva, T. Doert, J_{eff} Description of the honeycomb mott insulator α—$RuCl_3$, Phys. Rev. Lett. 117 (2016) 126403.

[191] S. Sinn, C.H. Kim, B.H. Kim, K.D. Lee, C.J. Won, J.S. Oh, M. Han, Y.J. Chang, N. Hur, H. Sato, B.-G. Park, C. Kim, H.-D. Kim, T.W. Noh, Electronic structure of the Kitaev material α-$RuCl_3$ probed by photoemission and inverse photoemission spectroscopies, Sci. Rep. 6 (2016) 39544.

[192] M. Ziatdinov, A. Banerjee, A. Maksov, T. Berlijn, W. Zhou, H.B. Cao, J.Q. Yan, C.A. Bridges, D.G. Mandrus, S.E. Nagler, A.P. Baddorf, S.V. Kalinin, Atomic-scale observation of structural and electronic orders in the layered compound α-$RuCl_3$, Nature Commun. 7 (2016) 13774.

[193] M. Majumder, M. Schmidt, H. Rosner, A.A. Tsirlin, H. Yasuoka, M. Baenitz, Anisotropic $Ru^{3+}4d^5$ magnetism in the $\alpha-RuCl_3$ honeycomb system: Susceptibility, specific heat, and zero-field NMR, Phys. Rev. B 91 (2015) 180401.

[194] H.B. Cao, A. Banerjee, J.-Q. Yan, C.A. Bridges, M.D. Lumsden, D.G. Mandrus, D.A. Tennant, B.C. Chakoumakos, S.E. Nagler, Low-temperature crystal and magnetic structure of $\alpha-RuCl_3$, Phys. Rev. B 93 (2016) 134423.

[195] J.A. Sears, M. Songvilay, K.W. Plumb, J.P. Clancy, Y. Qiu, Y. Zhao, D. Parshall, Y.-J. Kim, Magnetic order in $\alpha-RuCl_3$: A honeycomb-lattice quantum magnet with strong spin-orbit coupling, Phys. Rev. B 91 (2015) 144420.

[196] C. Ritter, Zigzag type magnetic structure of the spin J_{eff}=1/2 compound α-RuCl 3 as determined by neutron powder diffraction, J. Phys. Conf. Ser. 746 (2016) 012060.

[197] R.D. Johnson, S.C. Williams, A.A. Haghighirad, J. Singleton, V. Zapf, P. Manuel, I.I. Mazin, Y. Li, H.O. Jeschke, R. Valentí, R. Coldea, Monoclinic crystal structure of $\alpha-RuCl_3$ and the zigzag antiferromagnetic ground state, Phys. Rev. B 92 (2015) 235119.

[198] F. Lang, P.J. Baker, A.A. Haghighirad, Y. Li, D. Prabhakaran, R. Valentí, S.J. Blundell, Unconventional magnetism on a honeycomb lattice in $\alpha-RuCl_3$ studied by muon spin rotation, Phys. Rev. B 94 (2016) 020407.

[199] H.-S. Kim, V.S. V., A. Catuneanu, H.-Y. Kee, Kitaev magnetism in honeycomb $RuCl_3$ with intermediate spin-orbit coupling, Phys. Rev. B 91 (2015) 241110.

[200] H.-S. Kim, H.-Y. Kee, Crystal structure and magnetism in $\alpha-RuCl_3$: An *ab initio* study, Phys. Rev. B 93 (2016) 155143.

[201] R. Yadav, N.A. Bogdanov, V.M. Katukuri, S. Nishimoto, J. van den Brink, L. Hozoi, Kitaev exchange and field-induced quantum spin-liquid states in honeycomb α-$RuCl_3$, Sci. Rep. 6 (2016) 37925.

[202] J. Chaloupka, G. Khaliullin, Magnetic anisotropy in the Kitaev model systems Na_2IrO_3 and $RuCl_3$, Phys. Rev. B 94 (2016) 064435.

[203] S.M. Winter, K. Riedl, P.A. Maksimov, A.L. Chernyshev, A. Honecker, R. Valentí, Breakdown of magnons in a strongly spin-orbital coupled magnet, Nature Commun. 8 (1) (2017) 1152.

[204] J.A. Sears, L.E. Chern, S. Kim, P.J. Bereciartua, S. Francoual, Y.B. Kim, Y.-J. Kim, Ferromagnetic Kitaev interaction and the origin of large magnetic anisotropy in $\alpha-RuCl_3$, Nat. Phys. 16 (8) (2020) 837–840.

[205] S.M. Winter, A.A. Tsirlin, M. Daghofer, J. van den Brink, Y. Singh, P. Gegenwart, R. Valentí, Models and materials for generalized Kitaev magnetism, 29 (49) (2017) 493002.

[206] Y. Wang, G.B. Osterhoudt, Y. Tian, P. Lampen-Kelley, A. Banerjee, T. Goldstein, J. Yan, J. Knolle, H. Ji, R.J. Cava, J. Nasu, Y. Motome, S.E. Nagler, D. Mandrus, K.S. Burch, The range of non-Kitaev terms and fractional particles in α-$RuCl_3$, Npj Quant. Mater. 5 (1) (2020) 14.

[207] L.J. Sandilands, Y. Tian, K.W. Plumb, Y.-J. Kim, K.S. Burch, Scattering continuum and possible fractionalized excitations in $\alpha-RuCl_3$, Phys. Rev. Lett. 114 (2015) 147201.

[208] J. Nasu, J. Knolle, D.L. Kovrizhin, Y. Motome, R. Moessner, Fermionic response from fractionalization in an insulating two-dimensional magnet, Nat. Phys. 12 (2016) 912–915.

[209] L.J. Sandilands, C.H. Sohn, H.J. Park, S.Y. Kim, K.W. Kim, J.A. Sears, Y.-J. Kim, T.W. Noh, Optical probe of Heisenberg-Kitaev magnetism in $\alpha-RuCl_3$, Phys. Rev. B 94 (2016) 195156.

[210] Y. Kubota, H. Tanaka, T. Ono, Y. Narumi, K. Kindo, Successive magnetic phase transitions in $\alpha-RuCl_3$: XY-like frustrated magnet on the honeycomb lattice, Phys. Rev. B 91 (2015) 094422.

[211] S.-H. Baek, S.-H. Do, K.-Y. Choi, Y.S. Kwon, A.U.B. Wolter, S. Nishimoto, J. van den Brink, B. Büchner, Evidence for a field-induced quantum spin liquid in α-$RuCl_3$, Phys. Rev. Lett. 119 (2017) 037201.

[212] J.A. Sears, Y. Zhao, Z. Xu, J.W. Lynn, Y.-J. Kim, Phase diagram of $\alpha-RuCl_3$ in an in-plane magnetic field, Phys. Rev. B 95 (2017) 180411.

[213] K.A. Modic, R.D. McDonald, J.P.C. Ruff, M.D. Bachmann, Y. Lai, J.C. Palmstrom, D. Graf, M.K. Chan, F.F. Balakirev, J.B. Betts, G.S. Boebinger, M. Schmidt, M.J. Lawler, D.A. Sokolov, P.J.W. Moll, B.J. Ramshaw, A. Shekhter, Scale-invariant magnetic anisotropy in $RuCl_3$ at high magnetic fields, Nat. Phys. 17 (2) (2021) 240–244.

[214] C. Balz, L. Janssen, P. Lampen-Kelley, A. Banerjee, Y. Liu, J. Yan, D. Mandrus, M. Vojta, S.E. Nagler, Field-induced intermediate ordered phase and anisotropic interlayer interactions in α-$rucl_3$, Phys. Rev. B 103 (2021) 174417.

[215] A.U.B. Wolter, L.T. Corredor, L. Janssen, K. Nenkov, S. Schönecker, S.-H. Do, K.-Y. Choi, R. Albrecht, J. Hunger, T. Doert, M. Vojta, B. Büchner, Field-induced quantum criticality in the Kitaev system $\alpha-RuCl_3$, Phys. Rev. B 96 (2017) 041405.

[216] I.A. Leahy, C.A. Pocs, P.E. Siegfried, D. Graf, S.-H. Do, K.-Y. Choi, B. Normand, M. Lee, Anomalous thermal conductivity and magnetic torque response in the honeycomb magnet $\alpha-RuCl_3$, Phys. Rev. Lett. 118 (2017) 187203.

[217] R. Hentrich, A.U.B. Wolter, X. Zotos, W. Brenig, D. Nowak, A. Isaeva, T. Doert, A. Banerjee, P. Lampen-Kelley, D.G. Mandrus, S.E. Nagler, J. Sears, Y.-J. Kim, B. Büchner, C. Hess, Unusual phonon heat transport in $\alpha-RuCl_3$: Strong Spin-Phonon Scattering and Field-Induced Spin Gap, Phys. Rev. Lett. 120 (2018) 117204.

[218] Y.J. Yu, Y. Xu, K.J. Ran, J.M. Ni, Y.Y. Huang, J.H. Wang, J.S. Wen, S.Y. Li, Ultralow-temperature thermal conductivity of the Kitaev honeycomb magnet $\alpha-RuCl_3$ across the field-induced phase transition, Phys. Rev. Lett. 120 (2018) 067202.

[219] A.N. Ponomaryov, E. Schulze, J. Wosnitza, P. Lampen-Kelley, A. Banerjee, J.-Q. Yan, C.A. Bridges, D.G. Mandrus, S.E. Nagler, A.K. Kolezhuk, S.A. Zvyagin, Unconventional spin dynamics in the honeycomb-lattice material $\alpha-RuCl_3$: High-field electron spin resonance studies, Phys. Rev. B 96 (2017) 241107.

[220] Z. Wang, S. Reschke, D. Hüvonen, S.-H. Do, K.-Y. Choi, M. Gensch, U. Nagel, T. Rõ om, A. Loidl, Magnetic excitations and continuum of a possibly field-induced quantum spin liquid in $\alpha-RuCl_3$, Phys. Rev. Lett. 119 (2017) 227202.

[221] A. Sahasrabudhe, D.A.S. Kaib, S. Reschke, R. German, T.C. Koethe, J. Buhot, D. Kamenskyi, C. Hickey, P. Becker, V. Tsurkan, A. Loidl, S.H. Do, K.Y. Choi, M. Grüninger, S.M. Winter, Z. Wang, R. Valentí, P.H.M. van Loosdrecht, High-field quantum disordered state in $\alpha-RuCl_3$: Spin flips, bound states, and multiparticle continuum, Phys. Rev. B 101 (2020) 140410.

[222] A. Banerjee, P. Lampen-Kelley, J. Knolle, C. Balz, A.A. Aczel, B. Winn, Y. Liu, D. Pajerowski, J. Yan, C.A. Bridges, A.T. Savici, B.C. Chakoumakos, M.D. Lumsden, D.A. Tennant, R. Moessner, D.G. Mandrus, S.E. Nagler, Excitations in the field-induced quantum spin liquid state of α-$RuCl_3$, Npj Quant. Mater. 3 (1) (2018) 8.

[223] S. Bachus, D.A.S. Kaib, Y. Tokiwa, A. Jesche, V. Tsurkan, A. Loidl, S.M. Winter, A.A. Tsirlin, R. Valentí, P. Gegenwart, Thermodynamic perspective on field-induced behavior of $\alpha-RuCl_3$, Phys. Rev. Lett. 125 (2020) 097203.

[224] S. Bachus, D.A.S. Kaib, A. Jesche, V. Tsurkan, A. Loidl, S.M. Winter, A.A. Tsirlin, R. Valentí, P. Gegenwart, Angle-dependent thermodynamics of α-$RuCl_3$, Phys. Rev. B 103 (2021) 054440.

[225] D. Wulferding, Y. Choi, S.-H. Do, C.H. Lee, P. Lemmens, C. Faugeras, Y. Gallais, K.-Y. Choi, Magnon bound states versus anyonic Majorana excitations in the Kitaev honeycomb magnet α-$RuCl_3$, Nature Commun. 11 (1) (2020) 1603.

[226] J. Zheng, K. Ran, T. Li, J. Wang, P. Wang, B. Liu, Z.-X. Liu, B. Normand, J. Wen, W. Yu, Gapless spin excitations in the field-induced quantum spin liquid phase of $\alpha-RuCl_3$, Phys. Rev. Lett. 119 (2017) 227208.

[227] Y. Nagai, T. Jinno, J. Yoshitake, J. Nasu, Y. Motome, M. Itoh, Y. Shimizu, Two-step gap opening across the quantum critical point in the Kitaev honeycomb magnet $\alpha-RuCl_3$, Phys. Rev. B 101 (2020) 020414.

[228] Y. Kasahara, T. Ohnishi, Y. Mizukami, O. Tanaka, S. Ma, K. Sugii, N. Kurita, H. Tanaka, J. Nasu, Y. Motome, T. Shibauchi, Y. Matsuda, Majorana quantization and half-integer thermal quantum Hall effect in a Kitaev spin liquid, Nature 559 (2018) 227.
[229] M. Banerjee, M. Heiblum, V. Umansky, D. Feldman, Y. Oreg, A. Stern, Observation of half-integer thermal Hall conductance, Nature 559 (2018) 205.
[230] T. Yokoi, S. Ma, Y. Kasahara, S. Kasahara, T. Shibauchi, N. Kurita, H. Tanaka, J. Nasu, Y. Motome, C. Hickey, S. Trebst, Y. Matsuda, Half-integer quantized anomalous thermal Hall effect in the Kitaev material candidate α-$RuCl_3$, SCIENCE 373 (6554) (2020).
[231] J. Cookmeyer, J.E. Moore, Spin-wave analysis of the low-temperature thermal hall effect in the candidate Kitaev spin liquid $\alpha - RuCl_3$, Phys. Rev. B 98 (2018) 060412.
[232] P.A. McClarty, X.-Y. Dong, M. Gohlke, J.G. Rau, F. Pollmann, R. Moessner, K. Penc, Topological magnons in Kitaev magnets at high fields, Phys. Rev. B 98 (2018) 060404.
[233] L.E. Chern, E.Z. Zhang, Y.B. Kim, Sign structure of thermal Hall conductivity and Topological Magnons for in-plane-field polarized Kitaev magnets, Phys. Rev. Lett. 126 (2020) 147201.
[234] Y. Vinkler-Aviv, A. Rosch, Approximately quantized thermal hall effect of chiral liquids coupled to phonons, Phys. Rev. X 8 (2018) 031032.
[235] M. Ye, G.B. Halász, L. Savary, L. Balents, Quantization of the thermal hall conductivity at small hall angles, Phys. Rev. Lett. 121 (2018) 147201.
[236] A. Go, J. Jung, E.-G. Moon, Vestiges of topological phase transitions in Kitaev quantum spin liquids, Phys. Rev. Lett. 122 (2019) 147203.
[237] S.M. Winter, K. Riedl, D. Kaib, R. Coldea, R. Valentí, Probing $\alpha - \mathrm{RuCl_3}$ beyond magnetic order: Effects of temperature and magnetic field, Phys. Rev. Lett. 120 (2018) 077203.
[238] A.P. Joy, A. Rosch, Dynamics of visons and thermal Hall effect in perturbed Kitaev models, 2021, http://arxiv.org/abs/2109.00250.
[239] G.-W. Chern, Y. Sizyuk, C. Price, N.B. Perkins, Kitaev-Heisenberg model in a magnetic field: Order-by-disorder and commensurate-incommensurate transitions, Phys. Rev. B 95 (2017) 144427.
[240] K. Kitagawa, T. Takayama, Y. Matsumoto, A. Kato, R. Takano, Y. Kishimoto, S. Bette, R. Dinnebier, G. Jackeli, H. Takagi, A spin–orbital-entangled quantum liquid on a honeycomb lattice, Nature 554 (7692) (2018) 341–345.
[241] V. Todorova, A. Leineweber, L. Kienle, V. Duppel, M. Jansen, On agrho2, and the new quaternary delafossites $AgLi1/3M_2/3O_2$, syntheses and analyses of real structures, J. Solid State Chem. 184 (5) (2011) 1112–1119.
[242] J.H. Roudebush, K.A. Ross, R.J. Cava, Iridium containing honeycomb Delafossites by topotactic cation exchange, Dalton Trans. 45 (2016) 8783–8789.
[243] M. Abramchuk, C. Ozsoy-Keskinbora, J.W. Krizan, K.R. Metz, D.C. Bell, F. Tafti, Cu_2IrO_3: A new magnetically frustrated honeycomb iridate, J. Am. Chem. Soc. 139 (43) (2017) 15371–15376.
[244] S. Bette, T. Takayama, K. Kitagawa, R. Takano, H. Takagi, R.E. Dinnebier, Solution of the heavily stacking faulted crystal structure of the honeycomb iridate $H_3LiIr_2O_6$, Dalton Trans. 46 (2017) 15216–15227.
[245] R. Yadav, R. Ray, M.S. Eldeeb, S. Nishimoto, L. Hozoi, J. van den Brink, Strong effect of hydrogen order on magnetic Kitaev interactions in $H_3LiIr_2O_6$, Phys. Rev. Lett. 121 (2018) 197203.
[246] Y. Li, S.M. Winter, R. Valentí, Role of hydrogen in the spin-orbital-entangled quantum liquid candidate $H_3LiIr_2O_6$, Phys. Rev. Lett. 121 (2018) 247202.
[247] R. Yadav, M.S. Eldeeb, R. Ray, S. Aswartham, M.I. Sturza, S. Nishimoto, J. van den Brink, L. Hozoi, Engineering Kitaev exchange in stacked iridate layers: impact of inter-layer species on in-plane magnetism, Chem. Sci. 10 (2019) 1866–1872.
[248] K. Geirhos, P. Lunkenheimer, M. Blankenhorn, R. Claus, Y. Matsumoto, K. Kitagawa, T. Takayama, H. Takagi, I. Kézsmárki, A. Loidl, Quantum paraelectricity in the Kitaev quantum spin liquid candidates $H_3LiIr_2O_6$ and $D_3LiIr_2O_6$, Phys. Rev. B 101 (2020) 184410.
[249] J. Knolle, R. Moessner, N.B. Perkins, Bond-disordered spin liquid and the honeycomb iridate $H_3LiIr_2O_6$: Abundant low-energy density of states from random majorana hopping, Phys. Rev. Lett. 122 (2019) 047202.
[250] W.-H. Kao, J. Knolle, G.B. Halász, R. Moessner, N.B. Perkins, Vacancy-induced low-energy density of states in the Kitaev spin liquid, Phys. Rev. X 11 (2021) 011034.
[251] F. Bahrami, W. Lafargue-Dit-Hauret, O.I. Lebedev, R. Movshovich, H.-Y. Yang, D. Broido, X. Rocquefelte, F. Tafti, Thermodynamic evidence of proximity to a Kitaev spin liquid in $Ag_3LiIr_2O_6$, Phys. Rev. Lett. 123 (2019) 237203.
[252] S. Bette, T. Takayama, V. Duppel, A. Poulain, H. Takagi, R.E. Dinnebier, Crystal structure and stacking faults in the layered honeycomb, delafossite-type materials $Ag_3LiIr_2O_6$ and $Ag_3LiRu_2O_6$, Dalton Trans. 48 (2019) 9250–9259.
[253] Y.S. Choi, C.H. Lee, S. Lee, S. Yoon, W.-J. Lee, J. Park, A. Ali, Y. Singh, J.-C. Orain, G. Kim, J.-S. Rhyee, W.-T. Chen, F. Chou, K.-Y. Choi, Exotic low-energy excitations emergent in the random Kitaev magnet Cu_2IrO_3, Phys. Rev. Lett. 122 (2019) 167202.
[254] E.M. Kenney, C.U. Segre, W. Lafargue-Dit-Hauret, O.I. Lebedev, M. Abramchuk, A. Berlie, S.P. Cottrell, G. Simutis, F. Bahrami, N.E. Mordvinova, G. Fabbris, J.L. McChesney, D. Haskel, X. Rocquefelte, M.J. Graf, F. Tafti, Coexistence of static and dynamic magnetism in the Kitaev spin liquid material Cu_2IrO_3, Phys. Rev. B 100 (2019) 094418.
[255] S.K. Takahashi, J. Wang, A. Arsenault, T. Imai, M. Abramchuk, F. Tafti, P.M. Singer, Spin excitations of a proximate Kitaev quantum spin liquid realized in Cu_2IrO_3, Phys. Rev. X 9 (2019) 031047.
[256] S. Pal, A. Seth, P. Sakrikar, A. Ali, S. Bhattacharjee, D.V.S. Muthu, Y. Singh, A.K. Sood, Probing signatures of fractionalisation in candidate quantum spin liquid Cu_2IrO_3 via anomalous Raman scattering, Phys. Rev. B 104 (2021) 184420.
[257] L. Viciu, Q. Huang, E. Morosan, H. Zandbergen, N. Greenbaum, T. McQueen, R. Cava, Structure and basic magnetic properties of the honeycomb lattice compounds $Na_2Co_2TeO_6$ and $Na_3Co_2SbO_6$, J. Solid State Chem. 180 (3) (2007) 1060–1067.
[258] R. Berthelot, W. Schmidt, A. Sleight, M. Subramanian, Studies on solid solutions based on layered honeycomb-ordered phases P2-Na2M2TeO6 (M=Co, Ni, Zn), J. Solid State Chem. 196 (2012) 225–231.
[259] E. Lefrançois, M. Songvilay, J. Robert, G. Nataf, E. Jordan, L. Chaix, C.V. Colin, P. Lejay, A. Hadj-Azzem, R. Ballou, V. Simonet, Magnetic properties of the honeycomb oxide **$Na_2Co_2TeO_6$**, Phys. Rev. B 94 (2016) 214416.
[260] C. Wong, M. Avdeev, C.D. Ling, Zig-zag magnetic ordering in honeycomb-layered $Na_3Co_2SbO_6$, J. Solid State Chem. 243 (2016) 18–22.
[261] M. Songvilay, J. Robert, S. Petit, J.A. Rodriguez-Rivera, W.D. Ratcliff, F. Damay, V. Balédent, M. Jiménez-Ruiz, P. Lejay, E. Pachoud, A. Hadj-Azzem, V. Simonet, C. Stock, Kitaev interactions in the Co honeycomb antiferromagnets $Na_3Co_2SbO_6$ and $Na_2Co_2TeO_6$, Phys. Rev. B 102 (2020) 224429.
[262] C. Kim, J. Jeong, G. Lin, P. Park, T. Masuda, S. Asai, S. Itoh, H.-S. Kim, H. Zhou, J. Ma, J.-G. Park, Antiferromagnetic Kitaev interaction in $J_{eff} = 1/2$ cobalt honeycomb materials $Na_3Co_2SbO_6$ and $Na_2Co_2TeO_6$, Journal of Physics: Condensed Matter 34 (4) (2020).
[263] G. Lin, J. Jeong, C. Kim, Y. Wang, Q. Huang, T. Masuda, S. Asai, S. Itoh, G. Günther, M. Russina, Z. Lu, J. Sheng, L. Wang, J. Wang, G. Wang, Q. Ren, C. Xi, W. Tong, L. Ling, Z. Liu, L. Wu, J. Mei, Z. Qu, H. Zhou, J.-G. Park, Y. Wan, J. Ma, Field-induced quantum spin disordered state in spin-1/2 honeycomb magnet $Na_2Co_2TeO_6$ with small Kitaev interaction, Nature Communications 12 (2021) 5559.
[264] X. Hong, M. Gillig, R. Hentrich, W. Yao, V. Kocsis, A.R. Witte, T. Schreiner, D. Baumann, N. Perez, A.U. Wolter, Y. Li, B. Büchner, C. Hess, Unusual heat transport of the Kitaev material $Na_2Co_2TeO_6$: putative quantum spin liquid and low-energy spin excitations, 2021.
[265] H. Yao, S.A. Kivelson, Exact chiral spin liquid with non-abelian anyons, Phys. Rev. Lett. 99 (2007) 247203.
[266] V. Kalmeyer, R.B. Laughlin, Equivalence of the resonating-valence-bond and fractional quantum hall states, Phys. Rev. Lett. 59 (1987) 2095–2098.
[267] B. Bauer, L. Cincio, B.P. Keller, M. Dolfi, G. Vidal, S. Trebst, A.W.W. Ludwig, Chiral spin liquid and emergent anyons in a Kagome lattice Mott insulators, Nat. Commun. 5 (2014) 5137.

[268] Y.-C. He, D.N. Sheng, Y. Chen, Chiral spin liquid in a frustrated anisotropic kagome Heisenberg model, Phys. Rev. Lett. 112 (2014) 137202.
[269] S.-S. Gong, W. Zhu, D.N. Sheng, Emergent chiral spin liquid: Fractional quantum hall effect in a kagome heisenberg model, Sci. Rep. May (2014) 6317.
[270] S.-S. Gong, W. Zhu, L. Balents, D.N. Sheng, Global phase diagram of competing ordered and quantum spin-liquid phases on the kagome lattice, Phys. Rev. B 91 (2015) 075112.
[271] S. Ryu, Three-dimensional topological phase on the diamond lattice, Phys. Rev. B 79 (2009) 075124.
[272] T. Si, Y. Yu, Exactly soluble spin-1/2 models on three-dimensional lattices and non-abelian statistics of closed string excitations, preprint arXiv:0709.1302.
[273] T. Si, Y. Yu, Anyonic loops in three-dimensional spin liquid and chiral spin liquid, Nuclear Phys. B 803 (2008) 428–449.
[274] S. Mandal, N. Surendran, Exactly solvable Kitaev model in three dimensions, Phys. Rev. B 79 (2009) 024426.
[275] K. O'Brien, M. Hermanns, S. Trebst, Classification of gapless $\mathbb{Z}_2$ spin liquids in three-dimensional Kitaev models, Phys. Rev. B 93 (2016) 085101.
[276] T. Eschmann, P.A. Mishchenko, K. O'Brien, T.A. Bojesen, Y. Kato, M. Hermanns, Y. Motome, S. Trebst, Thermodynamic classification of three-dimensional Kitaev spin liquids, Phys. Rev. B 102 (2020) 075125.
[277] A.F. Wells, Three-Dimensional Nets and Polyhedra, Wiley, New York, 1977.
[278] E.H. Lieb, Flux phase of the half-filled band, Phys. Rev. Lett. 73 (1994) 2158–2161.
[279] M. Hermanns, S. Trebst, Quantum spin liquid with a Majorana Fermi surface on the three-dimensional hyperoctagon lattice, Phys. Rev. B 89 (2014) 235102.
[280] M.G. Yamada, V. Dwivedi, M. Hermanns, Crystalline Kitaev spin liquids, Phys. Rev. B 96 (2017) 155107.
[281] M. Hermanns, K. O'Brien, S. Trebst, Weyl spin liquids, Phys. Rev. Lett. 114 (2015) 157202.
[282] R. Schaffer, E.K.-H. Lee, Y.-M. Lu, Y.B. Kim, Topological spinon semimetals and gapless boundary states in three dimensions, Phys. Rev. Lett. 114 (2015) 116803.
[283] M. Hermanns, S. Trebst, A. Rosch, Spin-Peierls instability of three-dimensional spin liquids with majorana Fermi surfaces, Phys. Rev. Lett. 115 (2015) 177205.
[284] A.P. Schnyder, S. Ryu, A. Furusaki, A.W.W. Ludwig, Classification of topological insulators and superconductors in three spatial dimensions, Phys. Rev. B 78 (2008) 195125.
[285] A. Kitaev, Periodic table for topological insulators and superconductors, AIP Conf. Proc. 1134 (2009) 22–30.
[286] S. Ryu, A.P. Schnyder, A. Furusaki, A.W.W. Ludwig, Topological insulators and superconductors: tenfold way and dimensional hierarchy, New J. Phys. 12 (2010) 065010.
[287] A. Altland, M.R. Zirnbauer, Nonstandard symmetry classes in mesoscopic normal-superconducting hybrid structures, Phys. Rev. B 55 (1997) 1142–1161.
[288] J. Nasu, M. Udagawa, Y. Motome, Vaporization of Kitaev spin liquids, Phys. Rev. Lett. 113 (2014) 197205.
[289] T. Eschmann, Thermodynamics of Kitaev spin liquids, (Ph.D. thesis), University of Cologne, 2020.
[290] P.A. Mishchenko, Y. Kato, Y. Motome, Finite-temperature phase transition to a Kitaev spin liquid phase on a hyperoctagon lattice: A large-scale quantum Monte Carlo study, Phys. Rev. B 96 (2017) 125124.
[291] T. Eschmann, P.A. Mishchenko, T.A. Bojesen, Y. Kato, M. Hermanns, Y. Motome, S. Trebst, Thermodynamics of a gauge-frustrated Kitaev spin liquid, Phys. Rev. Res. 1 (2019) 032011.
[292] P.A. Mishchenko, Y. Kato, K. O'Brien, T.A. Bojesen, T. Eschmann, M. Hermanns, S. Trebst, Y. Motome, Chiral spin liquids with crystalline $\mathbb{Z}_2$ gauge order in a three-dimensional Kitaev model, Phys. Rev. B 101 (2020) 045118.
[293] A. Smith, J. Knolle, D.L. Kovrizhin, J.T. Chalker, R. Moessner, Neutron scattering signatures of the 3D hyperhoneycomb Kitaev quantum spin liquid, Phys. Rev. B 92 (2015) 180408.
[294] B. Perreault, J. Knolle, N.B. Perkins, F.J. Burnell, Theory of Raman response in three-dimensional Kitaev spin liquids: Application to β- and $\gamma - Li_2IrO_3$ compounds, Phys. Rev. B 92 (2015) 094439.
[295] G.B. Halász, B. Perreault, N.B. Perkins, Probing spinon nodal structures in three-dimensional Kitaev spin liquids, Phys. Rev. Lett. 119 (2017) 097202.
[296] G.J. Sreejith, S. Bhattacharjee, R. Moessner, Vacancies in Kitaev quantum spin liquids on the three-dimensional hyperhoneycomb lattice, Phys. Rev. B 93 (2016) 064433.
[297] E.K.-H. Lee, R. Schaffer, S. Bhattacharjee, Y.B. Kim, Heisenberg-Kitaev model on the hyperhoneycomb lattice, Phys. Rev. B 89 (2014) 045117.
[298] I. Kimchi, J.G. Analytis, A. Vishwanath, Three-dimensional quantum spin liquids in models of harmonic-honeycomb iridates and phase diagram in an infinite-*D* approximation, Phys. Rev. B 90 (2014) 205126.
[299] S. Lee, E.K.-H. Lee, A. Paramekanti, Y.B. Kim, Order-by-disorder and magnetic field response in the Heisenberg-Kitaev model on a hyperhoneycomb lattice, Phys. Rev. B 89 (2014) 014424.
[300] C. Castelnovo, R. Moessner, S. Sondhi, Spin ice, fractionalization, and topological order, Ann. Rev. Condens. Matter Phys. 3 (1) (2012) 35–55.
[301] M. Udagawa, L. Jaubert, Spin Ice, Springer International Publishing, Cham, 2021, pp. 1–18,
[302] A. Biffin, R.D. Johnson, S. Choi, F. Freund, S. Manni, A. Bombardi, P. Manuel, P. Gegenwart, R. Coldea, Unconventional magnetic order on the hyperhoneycomb Kitaev lattice in $\beta - Li_2IrO_3$: Full solution via magnetic resonant x-ray diffraction, Phys. Rev. B 90 (2014) 205116.
[303] A. Biffin, R.D. Johnson, I. Kimchi, R. Morris, A. Bombardi, J.G. Analytis, A. Vishwanath, R. Coldea, Noncoplanar and counterrotating incommensurate magnetic order stabilized by Kitaev Interactions in $\gamma - Li_2IrO_3$, Phys. Rev. Lett. 113 (2014) 197201.
[304] H.-S. Kim, E.K.-H. Lee, Y.B. Kim, Predominance of the Kitaev interaction in a three-dimensional honeycomb iridate: From ab initio to spin model, Europhys. Lett. 112 (2015) 67004.
[305] V.M. Katukuri, R. Yadav, L. Hozoi, S. Nishimoto, J. van den Brink, The vicinity of hyper-honeycomb β-Li2IrO3 to a three-dimensional Kitaev spin liquid state, Sci. Rep. 6 (2016) 29585.
[306] Y. Li, S.M. Winter, H.O. Jeschke, R. Valentí, Electronic excitations in $\gamma - Li_2IrO_3$, Phys. Rev. B 95 (2017) 045129.
[307] J.P. Hinton, S. Patankar, E. Thewalt, A. Ruiz, G. Lopez, N. Breznay, A. Vishwanath, J. Analytis, J. Orenstein, J.D. Koralek, I. Kimchi, Photoexcited states of the harmonic honeycomb iridate $\gamma - Li_2IrO_3$, Phys. Rev. B 92 (2015) 115154.
[308] I. Kimchi, R. Coldea, Spin dynamics of counterrotating Kitaev spirals via duality, Phys. Rev. B 94 (2016) 201110.
[309] A. Glamazda, P. Lemmens, S.H. Do, Y.S. Choi, K.Y. Choi, Raman spectroscopic signature of fractionalized excitations in the harmonic-honeycomb iridates β- and γ-Li_2IrO_3, Nature Commun. 7 (2016) 12286.
[310] K.A. Modic, B.J. Ramshaw, J.B. Betts, N.P. Breznay, J.G. Analytis, R.D. McDonald, A. Shekhter, Robust spin correlations at high magnetic fields in the harmonic honeycomb iridates, Nature Commun. 8 (1) (2017).
[311] A. Ruiz, A. Frano, N.P. Breznay, I. Kimchi, T. Helm, I. Oswald, J.Y. Chan, R.J. Birgeneau, Z. Islam, J.G. Analytis, Correlated states in γ-Li2IrO3 driven by applied magnetic fields, Nature Commun. 8 (1) (2017).
[312] I. Rousochatzakis, N.B. Perkins, Magnetic field induced evolution of intertwined orders in the Kitaev magnet $\beta - Li_2IrO_3$, Phys. Rev. B 97 (2018) 174423.
[313] M. Li, I. Rousochatzakis, N.B. Perkins, Unconventional magnetic field response of the hyperhoneycomb Kitaev magnet $\beta - Li_2IrO_3$, Phys. Rev. Res. 2 (2020) 013065.

[314] M. Majumder, F. Freund, T. Dey, M. Prinz-Zwick, N. Büttgen, Y. Skourski, A. Jesche, A.A. Tsirlin, P. Gegenwart, Anisotropic temperature-field phase diagram of single crystalline $\beta - Li_2IrO_3$: Magnetization, specific heat, and ^{7}Li NMR study, Phys. Rev. Mater. 3 (2019) 074408.
[315] M. Majumder, M. Prinz-Zwick, S. Reschke, A. Zubtsovskii, T. Dey, F. Freund, N. Büttgen, A. Jesche, I. Kézsmárki, A.A. Tsirlin, P. Gegenwart, Field evolution of low-energy excitations in the hyperhoneycomb magnet $\beta - Li_2IrO_3$, Phys. Rev. B 101 (2020) 214417.
[316] A. Ruiz, N.P. Breznay, M. Li, I. Rousochatzakis, A. Allen, I. Zinda, V. Nagarajan, G. Lopez, Z. Islam, M.H. Upton, J. Kim, A.H. Said, X.-R. Huang, T. Gog, D. Casa, R.J. Birgeneau, J.D. Koralek, J.G. Analytis, N.B. Perkins, A. Frano, Magnon-spinon dichotomy in the Kitaev hyperhoneycomb β−Li_2IrO_3, Phys. Rev. B 103 (2021) 184404.
[317] H.-S. Kim, Y.B. Kim, H.-Y. Kee, Revealing frustrated local moment model for pressurized hyperhoneycomb iridate: Paving the way toward a quantum spin liquid, Phys. Rev. B 94 (2016) 245127.
[318] L.S.I. Veiga, K. Glazyrin, G. Fabbris, C.D. Dashwood, J.G. Vale, H. Park, M. Etter, T. Irifune, S. Pascarelli, D.F. McMorrow, T. Takayama, H. Takagi, D. Haskel, Pressure-induced structural dimerization in the hyperhoneycomb iridate β−Li_2IrO_3 at low temperatures, Phys. Rev. B 100 (2019) 064104.
[319] N.P. Breznay, A. Ruiz, A. Frano, W. Bi, R.J. Birgeneau, D. Haskel, J.G. Analytis, Resonant x-ray scattering reveals possible disappearance of magnetic order under hydrostatic pressure in the Kitaev candidate $\gamma - Li_2IrO_3$, Phys. Rev. B 96 (2017) 020402.
[320] T. Takayama, A. Krajewska, A.S. Gibbs, A.N. Yaresko, H. Ishii, H. Yamaoka, K. Ishii, N. Hiraoka, N.P. Funnell, C.L. Bull, H. Takagi, Pressure-induced collapse of the spin-orbital Mott state in the hyperhoneycomb iridate $\beta - Li_2IrO_3$, Phys. Rev. B 99 (2019) 125127.
[321] S. Choi, H.-S. Kim, H.-H. Kim, A. Krajewska, G. Kim, M. Minola, T. Takayama, H. Takagi, K. Haule, D. Vanderbilt, B. Keimer, Lattice dynamics and structural transition of the hyperhoneycomb iridate $\beta - Li_2IrO_3$ investigated by high-pressure Raman scattering, Phys. Rev. B 101 (2020) 054102.
[322] A. Revelli, C.C. Loo, D. Kiese, P. Becker, T. Fröhlich, T. Lorenz, M. Moretti Sala, G. Monaco, F.L. Buessen, J. Attig, M. Hermanns, S.V. Streltsov, D.I. Khomskii, J. van den Brink, M. Braden, P.H.M. van Loosdrecht, S. Trebst, A. Paramekanti, M. Grüninger, Spin-orbit entangled $j = \frac{1}{2}$ moments in Ba_2CeIrO_6: A frustrated fcc quantum magnet, Phys. Rev. B 100 (2019) 085139.
[323] A.M. Cook, S. Matern, C. Hickey, A.A. Aczel, A. Paramekanti, Spin-orbit coupled $j_{\text{eff}} = 1/2$ iridium moments on the geometrically frustrated fcc lattice, Phys. Rev. B 92 (2015) 020417.
[324] A.A. Aczel, A.M. Cook, T.J. Williams, S. Calder, A.D. Christianson, G.-X. Cao, D. Mandrus, Y.-B. Kim, A. Paramekanti, Highly anisotropic exchange interactions of $j_{\text{eff}} = \frac{1}{2}$ iridium moments on the fcc lattice in $La_2BIrO_6 (B = Mg, Zn)$, Phys. Rev. B 93 (2016) 214426.
[325] N. Khan, D. Prishchenko, Y. Skourski, V.G. Mazurenko, A.A. Tsirlin, Cubic symmetry and magnetic frustration on the fcc spin lattice in K_2IrCl_6, Phys. Rev. B 99 (2019) 144425.
[326] A.A. Aczel, J.P. Clancy, Q. Chen, H.D. Zhou, D. Reig-i Plessis, G.J. MacDougall, J.P.C. Ruff, M.H. Upton, Z. Islam, T.J. Williams, S. Calder, J.-Q. Yan, Revisiting the Kitaev material candidacy of Ir^{4+} double perovskite iridates, Phys. Rev. B 99 (2019) 134417.
[327] A. Revelli, M. Moretti Sala, G. Monaco, P. Becker, L. Bohatý, M. Hermanns, T.C. Koethe, T. Fröhlich, P. Warzanowski, T. Lorenz, S.V. Streltsov, P.H.M. van Loosdrecht, D.I. Khomskii, J. van den Brink, M. Grüninger, Resonant inelastic x-ray incarnation of Young's double-slit experiment, Sci. Adv. 5 (1) (2019).
[328] M.G. Yamada, H. Fujita, M. Oshikawa, Designing Kitaev spin liquids in metal-organic frameworks, Phys. Rev. Lett. 119 (2017) 057202.
[329] Y. Okamoto, M. Nohara, H. Aruga-Katori, H. Takagi, Spin-liquid state in the $S = 1/2$ hyperkagome antiferromagnet $Na_4Ir_3O_8$, Phys. Rev. Lett. 99 (2007) 137207.
[330] R. Shindou, Nature of the possible magnetic phases in a frustrated hyperkagome iridate, Phys. Rev. B 93 (2016) 094419.
[331] T. Mizoguchi, K. Hwang, E.K.-H. Lee, Y.B. Kim, Generic model for the hyperkagome iridate $Na_4Ir_3O_8$ in the local-moment regime, Phys. Rev. B 94 (2016) 064416.
[332] M. Becker, M. Hermanns, B. Bauer, M. Garst, S. Trebst, Spin-orbit physics of $j = \frac{1}{2}$ Mott insulators on the triangular lattice, Phys. Rev. B 91 (2015) 155135.
[333] T. Dey, A.V. Mahajan, P. Khuntia, M. Baenitz, B. Koteswararao, F.C. Chou, Spin-liquid behavior in $J_{\text{eff}} = \frac{1}{2}$ triangular lattice compound $Ba_3IrTi_2O_9$, Phys. Rev. B 86 (2012) 140405.
[334] T. Sakamoto, Y. Doi, Y. Hinatsu, Crystal structures and magnetic properties of 6H-perovskite-type oxides $Ba_3MIr_2O_9$ (M=Mg, Ca, Sc, Ti, Zn, Sr, Zr, Cd and In), J. Solid State Chem. 179 (2006) 2595–2601.
[335] I. Rousochatzakis, U.K. Rössler, J. van den Brink, M. Daghofer, Kitaev anisotropy induces mesoscopic $\mathbb{Z}_2$ vortex crystals in frustrated hexagonal antiferromagnets, Phys. Rev. B 93 (2016) 104417.
[336] S. Wang, Z. Qi, B. Xi, W. Wang, S.-L. Yu, J.-X. Li, Comprehensive study of the global phase diagram of the $J - K - \Gamma$ model on a triangular lattice, Phys. Rev. B 103 (2021) 054410.
[337] R. Kumar, D. Sheptyakov, P. Khuntia, K. Rolfs, P.G. Freeman, H.M. Rønnow, T. Dey, M. Baenitz, A.V. Mahajan, $Ba_3M_xTi_{3-x}O_9$ (M = Ir, Rh): A family of 5d/4d-based diluted quantum spin liquids, Phys. Rev. B 94 (2016) 174410.
[338] W.-J. Lee, S.-H. Do, S. Yoon, S. Lee, Y.S. Choi, D.J. Jang, M. Brando, M. Lee, E.S. Choi, S. Ji, Z.H. Jang, B.J. Suh, K.-Y. Choi, Putative spin liquid in the triangle-based iridate $Ba_3IrTi_2O_9$, Phys. Rev. B 96 (2017) 014432.
[339] A. Catuneanu, J.G. Rau, H.-S. Kim, H.-Y. Kee, Magnetic orders proximal to the Kitaev limit in frustrated triangular systems: Application to $Ba_3IrTi_2O_9$, Phys. Rev. B 92 (2015) 165108.
[340] E. Seabrook, M.L. Baez, J. Reuther, $\mathbb{Z}_2$ vortices in the ground states of classical Kitaev-Heisenberg models, Phys. Rev. B 101 (2020) 174443.
[341] P. Kos, M. Punk, Quantum spin liquid ground states of the Heisenberg-Kitaev model on the triangular lattice, Phys. Rev. B 95 (2017) 024421.
[342] K. Shinjo, S. Sota, S. Yunoki, K. Totsuka, T. Tohyama, Density-matrix renormalization group study of Kitaev–Heisenberg model on a triangular lattice, J. Phys. Soc. Japan 85 (2016) 114710.
[343] P.A. Maksimov, Z. Zhu, S.R. White, A.L. Chernyshev, Anisotropic-exchange magnets on a triangular lattice: Spin waves, accidental degeneracies, and dual spin liquids, Phys. Rev. X 9 (2019) 021017.
[344] K. Morita, T. Tohyama, Finite-temperature properties of the Kitaev-Heisenberg models on kagome and triangular lattices studied by improved finite-temperature Lanczos methods, Phys. Rev. Res. 2 (2020) 013205.
[345] M. Li, N.B. Perkins, I. Rousochatzakis, Collective spin dynamics of $\mathbb{Z}_2$ vortex crystals in triangular Kitaev-Heisenberg antiferromagnets, Phys. Rev. Res. 1 (2019) 013002.
[346] T. Okubo, S. Chung, H. Kawamura, Multiple-q states and the skyrmion lattice of the triangular-lattice heisenberg antiferromagnet under magnetic fields, Phys. Rev. Lett. 108 (2012) 017206.
[347] H.D. Rosales, D.C. Cabra, P. Pujol, Three-sublattice skyrmion crystal in the antiferromagnetic triangular lattice, Phys. Rev. B 92 (2015) 214439.
[348] S.A. Osorio, M.B. Sturla, H.D. Rosales, D.C. Cabra, From skyrmions to $\mathbb{Z}_2$ vortices in distorted chiral antiferromagnets, Phys. Rev. B 100 (2019) 220404.
[349] T. Dey, A.V. Mahajan, R. Kumar, B. Koteswararao, F.C. Chou, A.A. Omrani, H.M. Ronnow, Possible spin-orbit driven spin-liquid ground state in the double perovskite phase of $Ba_3YIr_2O_9$, Phys. Rev. B 88 (2013) 134425.
[350] T. Dey, R. Kumar, A.V. Mahajan, S.D. Kaushik, V. Siruguri, Unconventional magnetism in the spin-orbit-driven mott insulators $Ba_3MIr_2O_9$ ($M = Sc, Y$), Phys. Rev. B 89 (2014) 205101.
[351] T. Dey, CRC 1238 colloquium, Cologne (October 2016).

[352] I. Terasaki, T. Igarashi, T. Nagai, K. Tanabe, H. Taniguchi, T. Matsushita, N. Wada, A. Takata, T. Kida, M. Hagiwara, K. Kobayashi, H. Sagayama, R. Kumai, H. Nakao, Y. Murakami, Absence of magnetic long range order in $Ba_3ZnRu_2O_9$: A spin-liquid candidate in the S=3/2 dimer lattice, J. Phys. Soc. Japan 86 (3) (2017) 033702.
[353] H. Takagi, Opening colloquium of CRC 1283 "control and dynamics of quantum materials", university of cologne, 2016.
[354] Y. Luo, C. Cao, B. Si, Y. Li, J. Bao, H. Guo, X. Yang, C. Shen, C. Feng, J. Dai, G. Cao, Z.-a. Xu, Li_2RhO_3: A spin-glassy relativistic Mott insulator, Phys. Rev. B 87 (2013) 161121.
[355] C. Cao, Y. Luo, Z. Xu, J. Dai, Electronic structure of relativistic Mott insulator Li_2RhO_3, preprint arXiv:1303.4675.
[356] P. Khuntia, S. Manni, F.R. Foronda, T. Lancaster, S.J. Blundell, P. Gegenwart, M. Baenitz, Local magnetism and spin dynamics of the frustrated honeycomb rhodate Li_2RhO_3, Phys. Rev. B 96 (2017) 094432.
[357] P. Khuntia, S. Manni, F.R. Foronda, T. Lancaster, S.J. Blundell, P. Gegenwart, M. Baenitz, Local magnetism and spin dynamics of the frustrated honeycomb rhodate Li_2RhO_3, Phys. Rev. B 96 (2017) 094432.
[358] V. Hermann, S. Biswas, J. Ebad-Allah, F. Freund, A. Jesche, A.A. Tsirlin, M. Hanfland, D. Khomskii, P. Gegenwart, R. Valentí, C.A. Kuntscher, Pressure-induced formation of rhodium zigzag chains in the honeycomb rhodate Li_2RhO_3, Phys. Rev. B 100 (2019) 064105.
[359] F.-Y. Li, Y.-D. Li, Y. Yu, A. Paramekanti, G. Chen, Kitaev materials beyond iridates: Order by quantum disorder and weyl magnons in rare-earth double perovskites, Phys. Rev. B 95 (2017) 085132.
[360] B. Zhou, J. Balgley, P. Lampen-Kelley, J.-Q. Yan, D.G. Mandrus, E.A. Henriksen, Evidence for charge transfer and proximate magnetism in graphene–$\alpha-RuCl_3$ heterostructures, Phys. Rev. B 100 (2019) 165426.
[361] S. Mashhadi, Y. Kim, J. Kim, D. Weber, T. Taniguchi, K. Watanabe, N. Park, B. Lotsch, J.H. Smet, M. Burghard, K. Kern, Spin-split band hybridization in graphene proximitized with α-$RuCl_3$ nanosheets, Nano Lett. 19 (7) (2019) 4659–4665.
[362] D.J. Rizzo, B.S. Jessen, Z. Sun, F.L. Ruta, J. Zhang, J.-Q. Yan, L. Xian, A.S. McLeod, M.E. Berkowitz, K. Watanabe, T. Taniguchi, S.E. Nagler, D.G. Mandrus, A. Rubio, M.M. Fogler, A.J. Millis, J.C. Hone, C.R. Dean, D.N. Basov, Charge-transfer plasmon polaritons at graphene/α-$RuCl_3$ interfaces, Nano Lett. 20 (12) (2020) 8438–8445.
[363] S. Biswas, Y. Li, S.M. Winter, J. Knolle, R. Valentí, Electronic properties of $\alpha-RuCl_3$ in proximity to graphene, Phys. Rev. Lett. 123 (2019) 237201.
[364] V. Leeb, K. Polyudov, S. Mashhadi, S. Biswas, R. Valentí, M. Burghard, J. Knolle, Anomalous quantum oscillations in a heterostructure of graphene on a proximate quantum spin liquid, Phys. Rev. Lett. 126 (2021) 097201.
[365] H.-K. Jin, J. Knolle, Flat and correlated plasmon bands in *graphene*/$\alpha - RuCl_3$ heterostructures, Phys. Rev. B 104 (2021) 045140.